Available online at www.sciencedirect.com

ScienceDirect

Journal of Magnesium and Alloys 10 (2022) 863–898

www.elsevier.com/locate/jma

Review

Research advances of magnesium and magnesium alloys worldwide in 2021

Jiangfeng Song[a,*], Jing Chen[a], Xiaoming Xiong[a], Xiaodong Peng[a,*], Daolun Chen[b], Fusheng Pan[a,*]

[a] National Engineering Research Center for Magnesium Alloys, Chongqing University, Chongqing 400044, China
[b] Department of Mechanical and Industrial Engineering, Ryerson University, Toronto, Ontario M5B 2K3, Canada

Received 21 March 2022; received in revised form 12 April 2022; accepted 21 April 2022
Available online 29 April 2022

Abstract

More than 4000 papers in the field of Mg and Mg alloys were published and indexed in Web of Science (WoS) Core Collection database in 2021. The bibliometric analyses indicate that the microstructure, mechanical properties, and corrosion of Mg alloys still are the main research focus. Mg ion batteries and hydrogen storage Mg materials have attracted much attention. Significant contributions to the research and development of magnesium alloys were made by Chongqing University, Shanghai Jiaotong University, and Chinese Academy of Sciences in China, Helmholtz Zentrum Hereon in Germany, Ohio State University in the United States, the University of Queensland in Australia, Kumanto University in Japan, and Seoul National University in Korea, University of Tehran in Iran, etc.. This review is aimed to summarize the progress in the development of structural and functional Mg and Mg alloys in 2021. Based on the issues and challenges identified here, some future research directions are suggested.

Keywords: Magnesium alloys; Cast magnesium alloys; Wrought magnesium alloys; Bio-magnesium alloys; Mg based energy storage materials; Processing technologies; Corrosion and protection.

1. Introduction

In September 2020, China proposed the 'carbon neutrality' and 'emission peak' strategies, which have attracted worldwide attention. Extensive application of magnesium (Mg) and magnesium alloys is one of the best solutions to achieve the goal. Mg alloys are the lightest structural materials, which have a great potential for weight-saving and CO_2 emission reduction. Besides, Mg alloys have high specific strength and stiffness, superior damping performance, good biocompatibility, large hydrogen storage capacity, and high theoretical specific capacity for battery, etc. [1–6]. Hence, magnesium and its alloys have been applied in the field of aerospace, automotive, 3C (computers, communications, and consumer electronics) etc. in the world. In addition, the application of Mg and Mg alloy in biomedical and energy sectors has recently attracted increasing attention. However, a lot of difficulties still need to be overcome to expand the further applications of magnesium alloys [7–12]. The relatively low strength, poor plasticity, and inferior corrosion resistance of magnesium alloys impede the structural applications, while the problems on the fast degradation rate of Mg alloys and narrow hydrogen charging and discharging window need to be solved in functional materials to broaden the future application of Mg alloys [13–20].

In the past year of 2021, more than 4000 papers in the field of Mg and Mg alloys were published and indexed in the authoritative database of "Web of Science Core Collection". Based on such a literature search, the research trends and hotspots of magnesium alloys were analyzed. The present

* Corresponding authors.
E-mail addresses: jiangfeng.song@cqu.edu.cn (J. Song), pxd@cqu.edu.cn (X. Peng), fspan@cqu.edu.cn (F. Pan).

https://doi.org/10.1016/j.jma.2022.04.001

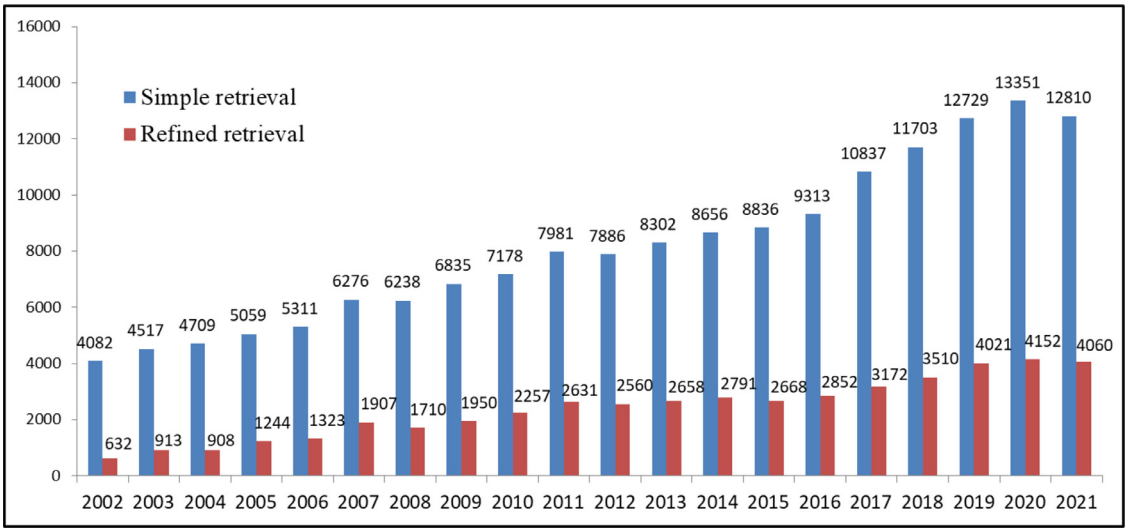

Fig. 1. Published Mg-related papers in the past 20 years in the Web of Science (WoS) Core Collection database.

work aims to review the important advances of magnesium and its alloys worldwide in 2021, in order to boost the multi-faceted scientific research of magnesium alloys and promote the development and application of magnesium alloys globally.

2. Overview of Mg research in 2021

2.1. Overall status of Mg research

The published Mg-related papers in 2021 were searched in the Web of Science (WoS) Core Collection database on February 10, 2022. Fig. 1 presents a simple search results in the past 20 years using 'Magnesium or Mg alloy' as the topic (blue comlumn). To reveal more precisely the publications on Mg and Mg alloys, a more sophisticate retrieval strategy is applied. Briefly, 'Mg alloy', 'Magnesium hydrogen', 'Magnesium battery', 'Magnesium biodegradable', 'Magnesium corrosion', 'Magnesium mechanical' were used as topics with a certain rule in the WoS Core Collection database. After the duplicates are automatically eliminated, the results are shown with red comlumn in Fig. 1. It is seen from both the simple and refined searches that the number of publications gradually increases from 2002 to 2020 and the number of publications in 2021 is slightly lower than that of 2020. The slight decrease in 2021 would mainly be due to the fact that some publications in 2021 have not yet been indexed in WoS by February 10, 2022. It is expected that the total number of publications in 2021 would be higher than that of 2020 in the WoS database. The gradual increase in publications illustrates that the research on Mg and Mg alloys is a hot spot in the field of materials science and engineering in the past 20 years and has attracted more and more attention.

With the refined or more precise retrieval, 4060 papers on Mg and Mg alloys in total were collected by February 10, 2022. Statistical analysis was conducted via the VOSviewer software. The distributions of countries and regions and organizations that published Mg papers were analyzed on the basis of the above-mentioned literature. 88 countries and regions in total have published Mg and Mg alloys in 2021. Fig. 2 shows a statistical analysis result of the distribution of countries and regions with at least 5 Mg publications in 2021. Fig. 2(a) shows a distribution of countries and regions, where China

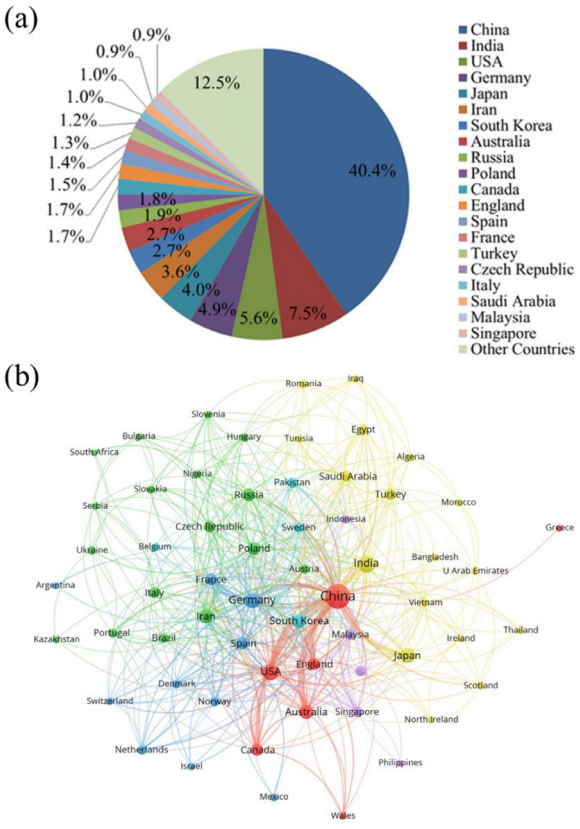

Fig. 2. Statistical analysis of the distribution of countries with at least 5 Mg papers published in 2021: (a) Paper percentage in different countries and regions; (b) network visualization among different countries.

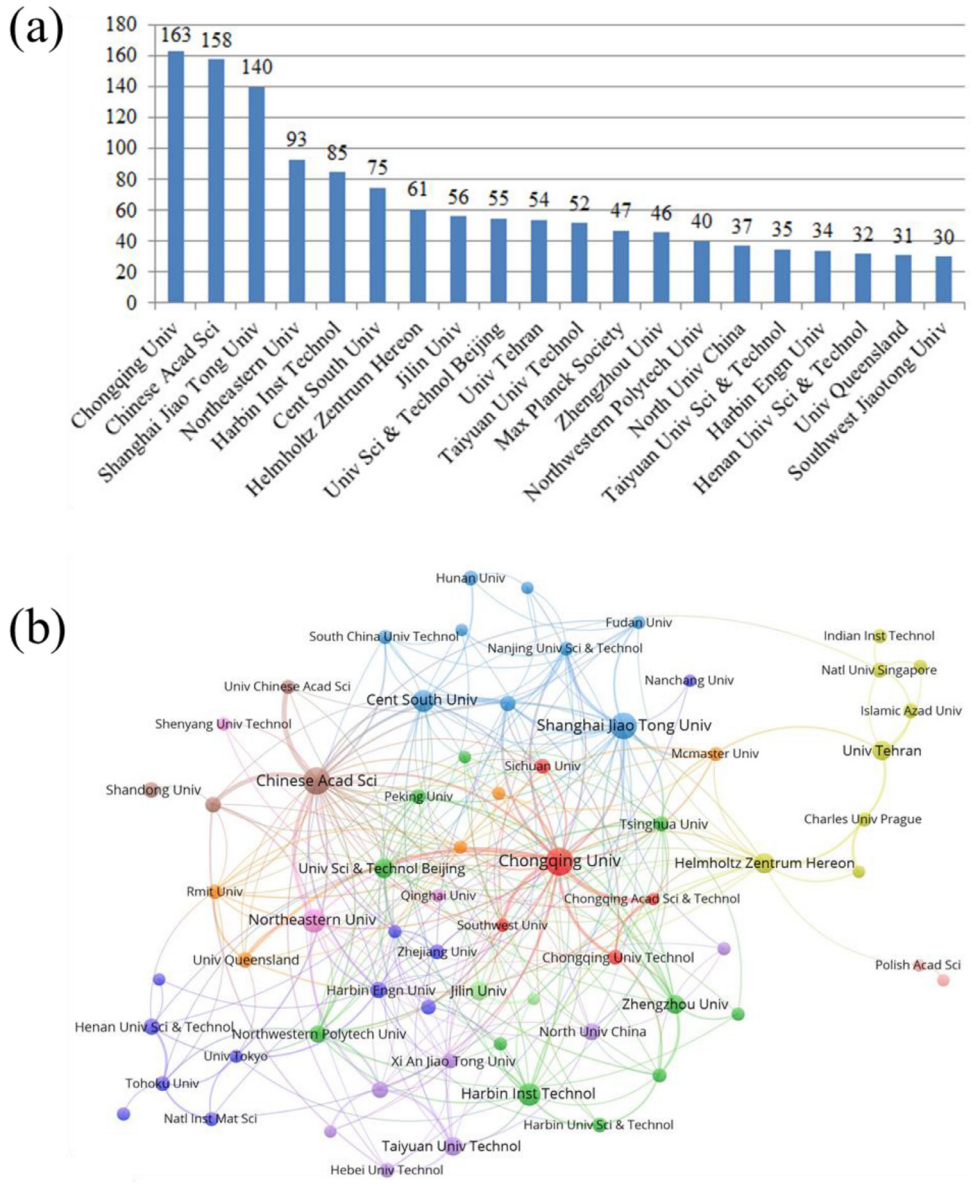

Fig. 3. Statistical analysis of organizations publishing at least 15 Mg papers in 2021: (a) top 20 organizations; (b) network visualization among different organizations.

remains the country that publishes the most Mg papers with a contribution of 40.38%, followed successively by India, the USA, Germany, and Japan, etc. Fig. 2(b) shows the network visualization among different countries and regions. The size of circle represents the number of published papers while the width of the link lines among different countries and regions indicates the collaboration intensity. About 23.81% of Mg papers were published based on international collaborations in 2021. Intensive international collaborations are seen among China, the USA, Germany, Australia, England and India.

Fig. 3 shows the statistical analysis result of organizations that published at least 15 Mg papers in 2021. The top 20 organizations are shown in Fig. 3(a). Chongqing University has published 163 Mg papers, remains the top spot in 2021 like 2020, followed by Chinese Academy of Sciences, Shanghai Jiaotong University, Northeastern University, and Harbin Institute of Technology. Helmholtz Zentrum Hereon and Max Plank Society from Germany, University of Tehran from Iran, and University of Queensland from Australia are also positioned in the top 20 spots in 2021. Fig. 3(b) shows the network visualization among different organizations. Similarly, the circle area or size represents the number of published papers, while the width of the link lines among different organizations indicates the collaboration activities. 65.76% of Mg papers are published based on collaborations, which suggests that collaborations among different organizations can significantly accelerate Mg research.

2.2. Statistics and analysis of journals publishing Mg papers

According to the number of magnesium papers published in 2021, the top 20 journals are listed in Table 1. *Journal of*

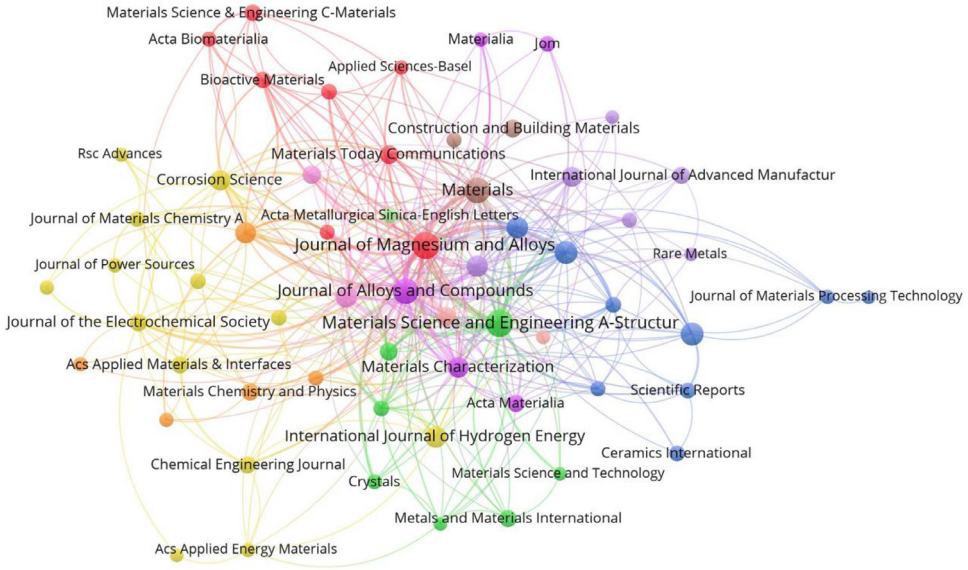

Fig. 4. Network visualization among different journals published at least 10 Mg papers in 2021.

Table 1
Top 20 journals with Mg papers worldwide in 2021.

Journals	Impact factor	Number of magnesium papers
Journal of Magnesium and Alloys	10.088	161
Materials Science and Engineering A	5.234	157
Materials	3.623	127
Journal of Alloys and Compounds	5.316	122
Metals	2.351	82
Journal of Materials Research and Technology	5.039	66
Journal of Materials Engineering and Performance	1.819	65
International Journal of Hydrogen Energy	5.816	61
Journal of Materials Science & Technology	8.067	59
Materials Characterization	4.342	58
Surface & Coatings Technology	4.158	55
Corrosion Science	7.205	50
Materials Letters	3.423	50
Materials Research Express	1.62	40
Transactions of Nonferrous Metals Society of China	2.917	35
Materials Today Communications	3.383	34
Advanced Engineering Materials	3.862	32
Construction and Building Materials	6.141	29
Journal of the Electrochemical Society	4.316	28
Acs Applied Materials & Interfaces	9.229	27

Magnesium and Alloys publishes the most papers, followed by *Materials Science and Engineering A* and *Materials*. The network visualization among different journals that published at least 10 Mg papers in 2021 is shown in Fig. 4. Similarly, the wider links between two journals reveal more citations between them. The results indicate that the correlations among the *Journal of Magnesium and Alloys, Materials Science and Engineering A, and Journal of Alloys and Compounds* are quite close.

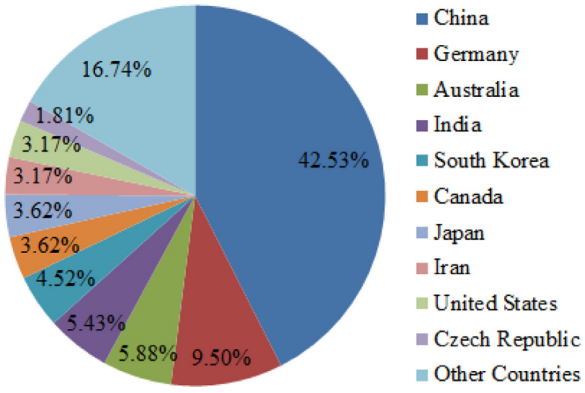

Fig. 5. Statistical analysis of county (region) distribution of Mg papers published in the *Journal of Magnesium and Alloys* in 2021.

Journal of Magnesium and Alloys (JMA) published 161 papers in 2021, with an increase of 45% from 2020. The impact factor (IF) of JMA increases rapidly from 7.115 in 2019 to 10.088 in 2020, ranking No. 1 among the 80 journals in Metallurgy & Metallurgical Engineering category (JCR Q1). Fig. 5 shows the statistical analysis result of country (region) distribution of Mg papers published in the JMA in 2021. The number of collaborations among different institutions is 108, accounting for 67%. More than half of the articles in the JMA involved institutional collaborations, which is also similar to the whole trend. The statistical results confirm that the JMA enjoys collaborative academic achievements.

2.3. Research hotspots in 2021 based on bibliometric analysis

The top 150 keywords by relevance, based on the Mg and Mg alloy articles published in 2021 are shown in Fig. 6. The larger size of the circle reflects the more times of keywords

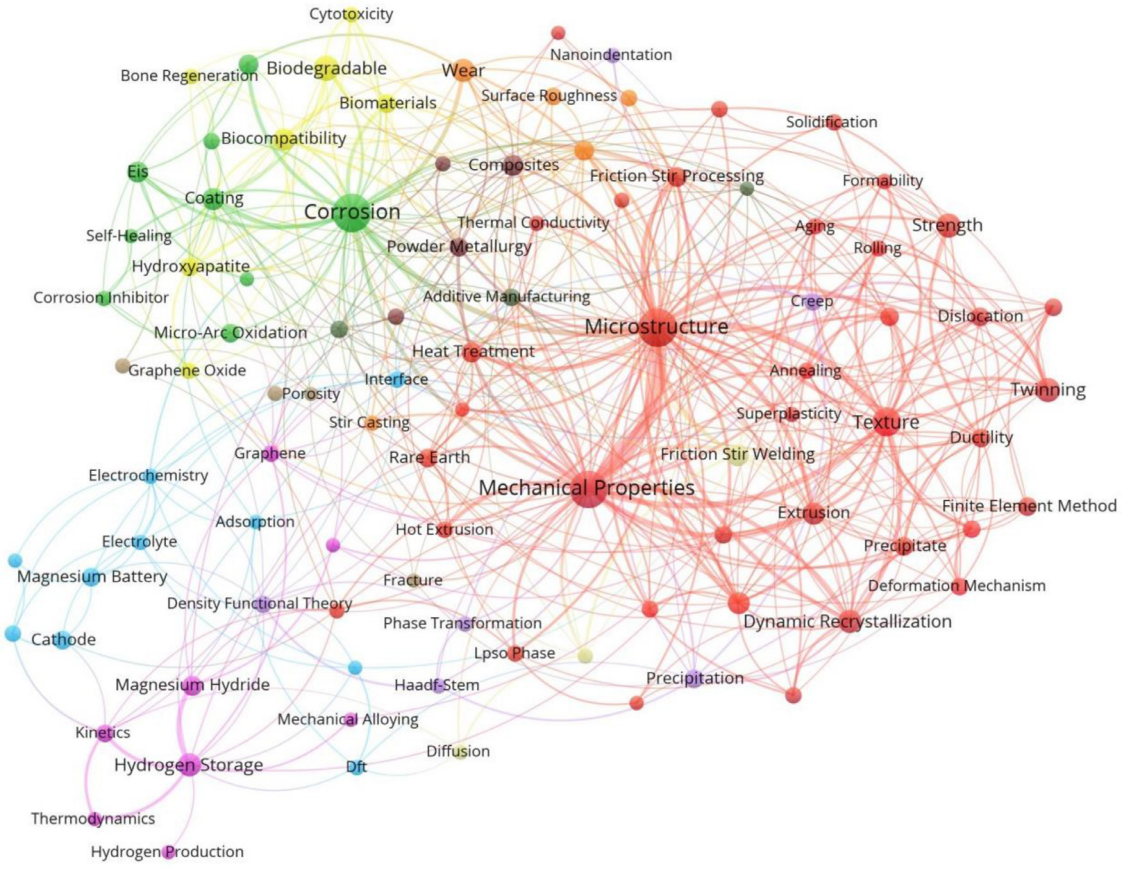

Fig. 6. Network visualization among different keywords in Mg-related papers.

used. For instance, ‘Microstructure’, ‘Mechanical properties’, and ‘Corrosion’ are the top three keywords, which implies that the microstructure, mechanical properties and corrosion of magnesium alloys continue to be the research hot areas.

In addition, the similar color of circles indicates a high relevance of the keywords. There are mainly four colors in Fig. 6, i.e., red for ‘microstructure’ and ‘mechanical properties’ group, green for ‘corrosion’ group, purple for ‘hydrogen storage’ group, and blue for ‘magnesium battery’. The largest group is the red ‘microstructure’ and ‘mechanical properties’, suggests that the mechanical properties and microstructures of structural Mg alloys as well as their processing technologies in 2021 still attracted much attention in the R&D of Mg and Mg alloys. Research in the second largest green group of ‘corrosion’ is very near to the yellow ‘bio-Mg’ group, indicating that bio-Mg alloys have attracted increasing attention and are closely related to the corrosion properties.

Interestingly, in each color group, the interconnected keywords are identified as the sub-hot spots in each hot field, as listed in Table 2. From the listed keywords, the sub-hot spots are revealed.

In short, the bibliometric analysis of keywords is capable of showing both the hot fields and the hot spots in each hot field, which could be used to guide the research directions and topics. Based on the bibliometric analysis results, the research fields on Mg and Mg alloys could be generally grouped into four main categories: (1) traditional structural cast and wrought Mg alloys that focused mainly on microstructure and mechanical properties, (2) functional materials including Mg battery, hydrogen storage Mg materials, and bio-Mg materials, (3) processing technologies of Mg and Mg alloys, and (4) corrosion and protection of Mg and Mg alloys.

Table 2
Keywords in each research group.

Color region	Research groups	Keywords
Red	Microstructure and mechanical properties group	strength, ductility, texture, twinning, dynamic recrystallization, heat treatment, extrusion, rolling, friction stir processing, etc.
Green and light yellow	Corrosion group	coating, corrosion inhibitor, micro arc oxidation, biomaterials, biodegradable, hydroxyapatite, etc.
Purple	Hydrogen storage group	magnesium hydride, hydrogen production, kinetics, and density functional theory, etc.
Blue	Magnesium battery group	cathode, electrolyte, and electrochemistry, etc.

Table 3
Mechanical properties of RE-containing cast magnesium alloys.

Alloys (wt.%)	Cast method	Heat treatment	YS(MPa)	UTS(MPa)	EL(%)	Ref.
Mg-3Nd-4.5Gd-0.2Zn-0.5Zr	permanent mold cast	peak aged @ 200 °C 16 h	200	343	5.4	[21]
Mg-3Nd-2.6Gd-0.2Zn-0.5Zr	sand cast	solution @ 535 °C 10 h +aged @ 200 °C 14 h	220	303	4.1	[22]
Mg-3Nd-3Gd-0.5Zn-0.5Zr	permanent mold cast	peak aged @ 200 °C 16 h	179	301	5.3	[23]
Mg-4Al-4RE-0.3Mn	HPDC	peak aged @ 200 °C 32 h	192	284	11.4	[24]
Mg-9Gd-1Yb-0.5Zn-0.2Zr	permanent mold cast	peak aged @ 225 °C 256 h	229	283	1.2	[25]
Mg-6Y-3Zn-1Al	HPDC	–	175	281	9.5	[26]
Mg-4Al-3La-1Ca-0.3Mn	HPDC	peak aged @ 200 °C 144 h	220	274	6.3	[27]
Mg-4La-2.5Al-0.5Mn	HPDC	–	149	253	11.5	[28]

3. Structural Mg alloys

Light weighting of structural materials is one of the most efficient ways to save energy and reduce CO_2 emission, which has become a main strategy of most countries in the world. For instance, as stated in the 'Energy-saving and new energy vehicle technology roadmap' released by China, the weight of vehicles should reduce 10% in 2020, 20% in 2025, and 35% in 2035, compared to that in 2015. The application of Mg structural materials provides a potential solution since the density of Mg alloys is the lowest among the metallic structural materials. Hence, investigation on structual Mg alloys is still a hot spot.

3.1. Cast Mg alloys

3.1.1. Rare-earth containing high strength cast Mg alloys

The mechanical properties of RE-containing cast Mg alloys developed in 2021 with an ultimate tensile strength (UTS) above 250 MPa are listed in Table 3 [21–28].

Guohua Wu's group [21] investigated the role of Gd on the mechanical properties of Mg-3Nd-4.5Gd-0.2Zn-0.5Zr alloy under permanent mold casting. The peak-aged Mg-3Nd-4.5Gd-0.2Zn-0.5Zr alloy exhibited a relatively good combination of strength and ductility (YS = 200 MPa, UTS = 343 MPa, (elongation) EL = 5.4%) due to the dense distribution of β'' phases with a higher aspect ratio. They also developed a permanent cast alloy Mg-9Gd-1Yb-0.5Zn-0.2Zr with a high YS of 229 MPa in the peak-aged condition [25]. The high YS of this peak-aged alloy is attributed to the dense co-precipitation of thin γ'' plates and prismatic β' and β_1 precipitates.

In addition, some high pressure die cast (HPDC) Mg alloys were developed. Suming Zhu et al. [24] found that an addition of 0.3 wt.% Mn to AE44 (Mg-4Al-4RE) alloy resulted in the precipitation of nanoscale Al-Mn particles. The UTS, YS and EL of the T5 treated HPDC AE44–0.3Mn alloy were obtained to be 284 MPa, 192 MPa and 11.4%, respectively, which exhibited a better strength-ductility combination than most die-cast Mg alloys and A380 alloy. Bai et al. [26] developed a novel HPDC WZA631 (Mg-6Y-3Zn-1Al) alloy showing YS, UTS, and EL of 175 MPa, 281 MPa, and 9.8%, respectively. The strength was enhanced due to the solute atoms Y and Zn into the matrix inhibiting the dynamic recovery by migrating dislocations, and the formed LPSO phase hindering dislocation movement along with increased dislocation storage. Furthermore, the coherent interface of LPSO phase with Mg matrix weakens the occurrence of interfacial cracking and twinning, thus promoting the ductility.

3.1.2. Rare earth-free high strength cast Mg alloys

Some newly developed RE-free cast Mg alloys were reported in 2021, with the mechanical properties of these alloys listed in Table 4. Cui et al. [29] found that Mg-6Al-4Zn-1.2Sn alloy exhibited a high UTS of 240 MPa, YS of 136 MPa and EL of 14%. The high UTS and EL were due to the low amount of shrinkage and the high YS was attributed to the decreased grain size.

3.1.3. Heat-resistant cast magnesium alloys

Mg alloy castings used in heat-resistant aerospace components have recently attracted a lot of attention. The mechanical properties of some newly-developed heat-resistant alloys are listed in Table 5.

Shouxun Ji's group [32] developed a new HPDC Mg-RE-Al alloy with superior mechanical properties at elevated temperatures. The YS of the alloy was 94 ± 1.8 MPa at 300 °C, which was 42% and 20% higher than that of AE44 and Mg-4 wt.% RE (La, Ce, Nd) at 300 °C. The UTS of the Mg-RE-Al alloy was the highest among the three alloys at 150 °C, 250 °C and 300 °C. The strengthening of Mg-RE-Al was attributed to the enhanced affinity of Nd and Gd to Al atoms. Jung et al. [33] reported that a T6-treated Mg-6.0Zn-1.2Y-0.7Zr-0.7Ca (ZWK611+0.7Ca) alloy showed the highest strength at 150 °C (the YS was 143 ± 2.6 MPa, the UTS was 179 ± 10.7 MPa and the EL was 8.2 ± 0.9%) and the lowest creep strain (0.22%) at 150 °C/100 MPa among all the tested alloys. The addition of Ca led to the formation of uniformly distributed τ-($Ca_2Mg_6Zn_3$) phase and I-phase. Yang et al. [34] revealed that Mg-8Al-1.0Gd-1.0Nd (T6 heat treatment) exhibited an excellent tensile creep resistance which was superior to AZ91 alloy. The steady-state creep rate and creep strain of Mg-8Al-1.0Gd-1.0Nd at 150 °C/60 MPa were $1.03 \times 10^{-8} s^{-1}$ and 0.31%, respectively.

3.2. Wrought Mg alloys

3.2.1. Traditional commercial wrought Mg alloys

In 2021, many researchers used special processing technology to control the microstructure in order to enhance the

Table 4
Mechanical properties of some RE-free cast Mg alloys.

Alloy (wt.%)	Cast method	Heat treatment	YS(MPa)	UTS(MPa)	EL(%)	Ref.
Mg-6Al-4Zn-1.2Sn	permanent mold cast	–	136	240	14	[29]
Mg-5Zn-0.2Ca-0.3Mn	permanent mold cast	homogenize @ 400 °C 12 h	151	205	1	[30]
Mg-0.87Al-0.05Ca-0.57Mn	permanent mold cast	–	130	183	–	[31]

Table 5
Mechanical properties of some newly-developed heat-resistant Mg alloys.

Alloys (wt.%)	Cast method	Heat treatment	Test temperature (°C)	YS(MPa)	UTS(MPa)	EL(%)	Creep rate(s^{-1})	Ref.
Mg–RE–Al	HPDC	–	150	141	160	8	–	[32]
			250	113	126	27	–	
			300	94	98	27	–	
Mg-6.0Zn-1.2Y-0.7Zr-0.7Ca	permanent mold cast	T6	150	143	179	8	4.547E-09 (150 °C/100 MPa/>100 h)	[33]
Mg-8Al-1.0Gd-1.0Nd	permanent mold cast	T6	–	–	–	–	1.03E-08 (150 °C/60 MPa/50 h)	[34]

Table 6
Mechanical properties of traditional commercial wrought Mg alloys at room temperature reported in 2021.

Alloys	Process	YS(MPa)	UTS(MPa)	EL(%)	Ref.
Mg-6Al-1Zn	ECAP+EPT	330	448	15	[38]
Mg-9Al-1Zn	Hard-plate rolling	314	381	11	[39]
Mg-8.46Al-0.66Zn-0.23Mn	Multi-directional forging	298	402	17.7	[40]
Mg-8.0Al-0.5Zn-0.11Mn	Repetitive upsetting-extrusion	230	335	12.7	[41]
ZK60	Radial forging	192	341	27.1	[42]

mechanical properties of commercial wrought magnesium alloys [35–37]. Table 6 summarizes the mechanical properties of traditional commercial wrought magnesium alloys.

Shan et al. [38] developed a technology of combining equal channel angular pressing (ECAP) with electropulsing treatment (EPT) to enhance the mechanical property of commercial AZ61 magnesium alloy. 'ECAP+EPT' technology can optimize the microstructure and largely improve the YS, UTS, EL of AZ61 alloy to 330 MPa, 448 MPa, and 15%, respectively. The AZ80 prepared by Zhang et al. [40] by multi-directional forging exhibited excellent mechanical performance. The UTS reached 402 MPa with the EL above 17%. In addition, Zou et al. [42] found that ZK60 alloy rods after radial forging at 300 °C showed a high tensile strength of 341 MPa and a high elongation of 27.1%.

3.2.2. High strength wrought Mg alloys

Table 7 summarizes the mechanical properties of ultra-high strength rare-earth based wrought magnesium alloys developed in 2021.

Adding rare earth elements is one of the effective methods to enhance the mechanical properties of wrought magnesium alloys [54–57]. Ma et al. [43] found that with the addition of 0.5 wt.% La, the YS of Mg-9Gd-3Y-0.5La-0.5Zr can reach 480 MPa and the EL is close to 6%. The addition of La leads to more precipitates and results in finer grains. Su et al. [44] optimized Gd and Y content and obtained high mechanical properties. The extruded Mg-1.75Gd-0.75Y-0.5Zn-Mn (at.%, Mg-14.5Gd-2.3Y-1.1Zn-0.3Mn (wt.%)) alloy exhibited a high UTS of 520 MPa. The alloy with Y/Gd atomic ratio of 0.4 has high peak hardness and mechanical properties. Furthermore, the addition of Ag [49] and Sm [58] can also improve the mechanical properties of magnesium alloys.

The high strength of materials is often at the expense of plasticity, which is a well-known dilemma in materials science and engineering. Some researchers have developed materials with both high strength and good ductility. Zhen et al. [46] improved the comprehensive mechanical properties of Mg-9.5Gd-4Y-2.2Zn-0.5Zr (wt.%) alloy through an alternating aging process, so that its YS reaches 425 MPa and its UTS reaches 493 MPa, and the elongation (EL) is 11.2%. Furthermore, Tong et al. [47] obtained Mg-8.2Gd-3.8Y-1.0Zn-0.4Zr (wt.%) alloy with ultra-high yield strength (417 MPa) and high plasticity (12.9%) by multi-directional forging (MDF) and aging treatment. Li et al. [48] achieved a simultaneous increase in the strength and plasticity of the extruded Mg-13Gd alloy through aging treatment. The YS of 400 MPa and EL of 15% are mainly attributed to the formation of high-density nano-sized β' precipitates and a certain proportion of precipitation-free areas in the structure dominated by dynamic recrystallization and fine grains. S. Kamado's group [50] developed a Mg-8.0Gd-4.0Y-1.0Mn-0.4Sc alloy with an UTS of 425 MPa and an EL of 10.6%.

Rare earth elements can effectively improve the mechanical properties of wrought magnesium alloys, but the cost is generally very high. Some researchers have also developed wrought magnesium alloys with low-cost and high performance, which are listed in Table 8.

Table 7
Mechanical properties of high strength rare-earth wrought Mg alloys at room temperature developed in 2021.

Alloys (wt.%)	Process	YS(MPa)	UTS(MPa)	EL(%)	Ref.
Mg-9Gd-3Y-0.5La-0.5Zr	Extrusion+aged	480	496	5.8	[43]
Mg-14.5Gd-2.3Y-1.1Zn-0.3Mn	Extrusion+aged	448	520	3.5	[44]
Mg-1.5Zn-0.25Gd	Semi-solid treatment + extrusion	444	408	12.5	[45]
Mg-9.5Gd-4Y-2.2Zn-0.5Zr	Extrusion+aged	425	494	11.2	[46]
Mg-8.2Gd-3.8Y-1.0Zn-0.4Zr	Multi-directional forging	417	434	12.9	[47]
Mg-13Gd	Extrusion+aged	408	433	15.3	[48]
Mg-11Gd-2Ag	Rolling+aged	393	435	5.2	[49]
Mg-8.0Gd-4.0Y-1.0Mn-0.4Sc	Extrusion	352	425	10.6	[50]
Mg-2Y-0.5Zn-0.5Ni	Extrusion	336	389	12.6	[51]
Mg-13Gd-4Y-2Zn-0.5Zr	Multi-directional forging + intermediate thermo-mechanical treatment	332	356	8	[52]
Mg-9Gd-2Nd-1.6Zn-1Zr	ECAP	321	378	14.4	[53]

Table 8
Mechanical properties of high strength and low-cost wrought Mg alloys at room temperature reported in 2021.

Alloys (wt.%)	Process	YS(MPa)	UTS(MPa)	EL(%)	Ref.
Mg-1Ca-1Al-0.3Zn-0.4Mn	Extrusion	435	449	4.2	[59]
Mg-6Zn-1Mn-2Sn-0.5Ca	Extrusion+aged	379	407	7.5	[60]
Mg-0.8Zn-0.2Zr	Extrusion	330	345	15.5	[61]
Mg-5Zn-0.6Sr	Rolling	305	359	20	[62]
Mg-6Zn-0.2Ca	Rolling+annealing+pre-strain+aging	267	333	18	[63]

Hucheng Pan's group [59] developed an ultra-high strength wrought Mg-1Ca-1Al-0.3Zn-0.4Mn (wt.%) alloy. The YS, UTS, and EL of this alloy through conventional extrusion reach 435 MPa, 449 MPa, and 4.2%, respectively. This is mainly because the nano-precipitates are formed, i.e., a large number of nanoscale second phase precipitates can be observed. Dingfei Zhang's group [60] found that during the aging treatment, the addition of Sn refines the precipitates and increases the density of the precipitates. The YS, UTS, and EL of the peak-aged Mg-6Zn-1Mn-2Sn-0.5Ca alloy can reach 379 MPa, 407 MPa and 7.5%, respectively. Yan et al. [62] prepared Mg-5Zn-xSr alloy (x = 0, 0.2, 0.6, 1.0 wt.%) by high strain rate rolling. The rolled Mg-5Zn-0.6Sr alloy has the best UTS of 359 MPa and EL of 20%.

3.2.3. High plasticity wrought Mg alloys

Magnesium alloy with hexagonal close-packed (HCP) crystal structure does not have sufficient independent slip systems and thus exhibits poor ductility. Recently, there have been many reports on microalloying [64,65] or heat treatment to obtain high-plasticity magnesium alloys [66–69]. Table 9 summarizes the mechanical properties of typical high plasticity magnesium alloys developed in 2021.

Bin Jiang' group [70] found that extruded Mg-4Gd-0.5Zr-0.5Nd alloy showed a plasticity of 42.3%, Mg-4Gd-0.5Zr-1.5Nd alloy has excellent strength of 224 MPa and plasticity of 39.3%. Mg-4Zn-1Gd alloy developed by K. S. Shin's group [71] exhibited good comprehensive mechanical properties with a UTS of 336 MPa and an EL of 33.9%. Due to the low content of RE, this Mg-4Zn-1Gd alloy shows good industrialization potential. Xiaoqin Zeng's group [73] developed a RE free Mg-1.8Zn-0.2Ca alloy exhibited high elongation of ~30% and strength of 265 MPa. The Mg-1Gd-0.5Zn-0.3Ce alloy developed by Bin Jiang's group [72] and the Mg-2Zn-0.3Ca-0.2Ce-0.1Mn (ZXEM2000) alloy developed by Zhao et al. [75] have high plasticity of about 30%. In addition, The high-plasticity Mg-Zn-Ca-Mn alloys were developed through adding Ca and Mn elements into Mg-Zn alloy by Xianhua Chen's group [74]. It was found that Mg-4Zn-0.3Ca-0.2Mn alloy exhibited the highest EL of 30%, Mg-4Zn-0.3Ca-0.7Mn alloy has excellent strength of 289 MPa and plasticity of 26%.

More slip systems can be activated in Mg alloys at high temperature than at room temperature. Thus, some Mg alloys with superplasticity were reported in 2021. Table 10 summarizes the developed wrought Mg alloys with superplasticity at high temperatures in 2021. Sun et al. [83] reported the highest plasticity of 782% of peak aged Mg-10Gd-3Y-1.5Zn-1Zr (wt.%) alloy at 450 °C at a strain rate of $5 \times 10^{-3} s^{-1}$. The precipitation of the new 14H LPSO phase and $Mg_{24}Y_5$ delays the separation of grain boundaries and improves the bearing capacity of strain accumulation, which accounts for the superplasticity. Malik Abdul et al. [84] studied the superplasticity of fine-grained extruded ZK61 alloy. At a tensile strain rate of 1×10^{-3} s^{-1} and a temperature of 673 K, an elongation at break (FE) of 400% can be obtained. Liu et al. [85] studied the effect of the isothermal repeated upsetting and extrusion process (RUE) on the superplasticity of ZK60 magnesium alloy. The optimized superplasticity is 142% at 653 K. Chen et al. [86] found that the two-phase Mg-Li alloy exhibits superplasticity of 307% at 623 K.

3.2.4. Superlight wrought Mg alloys

Ultra-light wrought magnesium alloys are mainly magnesium-lithium alloys with a density of 1.4–1.65 g/cm^3. Table 11 summarizes the mechanical properties of the ultra-light wrought magnesium-lithium alloy developed in 2021.

Table 9
The mechanical properties of typical high plasticity wrought Mg alloys at room temperature reported in 2021.

Alloys	Process	YS(MPa)	UTS(MPa)	EL(%)	Ref.
Mg-4Gd-0.5Zr-0.5Nd	Extrusion	97	196	42.3	[70]
Mg-4Gd-0.5Zr-1.5Nd	Extrusion	160	224	39.3	[70]
Mg-4Zn-1Gd	Extrusion	241	336	33.9	[71]
Mg-1Gd-0.5Zn-0.3Ce	Extrusion	107	323	33.6	[72]
Mg-1.8Zn-0.2Ca	Extrusion	–	265	~30	[73]
Mg-4Zn-0.3Ca-0.7Mn	Extrusion	206	289	26	[74]
Mg-2Zn-0.3Ca-0.2Ce-0.1Mn	Rolling	154	231	29	[75]
Mg-0.5Ca	Extrusion	224	244	25.6	[76]
Mg-Zn-Ca-Mn	ECAP	270	324	22.7	[77]
Mg-7Ga	Extrusion	166	268	22.2	[78]
Mg-7.2Y-2.8Ni	Extrusion+annealing	154	280	21.8	[79]
Mg-5Sn-1Ga	Extrusion	217	279	21.7	[80]
Mg-1.0Zn-0.45Ca-0.35Sn-0.2Mn	SRS+Rolling	270	305	21	[81]
Mg-3Sn-5Zn-1Al	Extrusion	188	340	20.1	[82]

Table 10
The mechanical properties of wrought Mg alloys with superplasticity at high temperatures reported in 2021.

Alloys	Process	EL at room temperature (%)	Temperature(K)	EL at high temperature (%)	Ref.
Mg-10Gd-3Y-1.5Zn-1Zr	Extrusion	23.1%	723	782	[83]
ZK61	Extrusion	–	673	400	[84]
Mg-5.5Zn-0.5Zr	RUE	21.6%	653	142	[85]
Mg-10.73Li-4.49Al-0.52Y	ECAP	–	623	307	[86]

Table 11
Mechanical properties of the superlight wrought Mg-Li alloys developed in 2021.

Alloys	Process	Specific strength(kN m kg^{-1})	YS(MPa)	UTS(MPa)	EL(%)	Ref.
Mg-14Li-7Al	Cast +quenching	~350	~470*	~475*	~2.5*	[87]
Mg-4Li-3Al-3Zn	Rotary die forging	–	360	409	6.5	[88]
Mg-2.76Li-3Al-2.6Zn-0.39Y	Forging+rolling	185.58	207	275	29	[89]
Mg-14Li-6Sn	Rolling	–	131	142	42	[90]

Note: * denotes the data is estimated from the tensile curve shown in [87].

Michael Ferry's group [87] prepared a body-centered cubic Mg-14Li-7Al alloy with high specific strength of ~350 kN m kg^{-1} by cast +quenching. They proposed a spinodal decomposition strengthening mechnism for ultralightweight Mg alloy with specific yield strengths surpassing almost every other engineering alloy. The compelling morphological, chemical, structural, and thermodynamic evidence for the spinodal decomposition were provided. Yang et al. [88] used rotary die forging to introduce a large number of twins and stacking faults into the coarse grains. The bulk Mg-4Li-3Al-3 Zn alloy with a UTS of 409 MPa has been successfully prepared. Cao et al. [89] developed a new Mg-2.76Li-3Al-2.6Zn-0.39Y alloy by multi-directional forging (MDF) and rolling process, which also has excellent mechanical properties. Ruizhi Wu's group [90] prepared Mg-14Li-xSn alloys and reported that the strength and ductility of Mg-14Li-6Sn alloy after 50% cold rolling have been improved.

3.2.5. Laminated composite sheets of wrought Mg alloys

In order to overcome some shortcomings of magnesium alloys, such as low mechanical properties, low formability at room temperature and corrosion resistance, laminated composites of magnesium alloy have been developed greatly in recent years. Table 12 presents the mechanical properties of laminated composites of Mg alloys reported in 2021.

Wang et al. [91] fabricated Ti6Al4V/AA6061/AZ31 laminated composites by hot rolling. It was found that the UTS and YS of the Ti/Al/Mg laminated composites increased, and the elongation decreased with increasing rolling reduction. The highest UTS of 476 MPa was achieved when the rolling reduction was 50%. When a rolling temperature of 350 °C was employed, comprehensive tensile properties (UTS = 384 MPa, elongation = 15.5%) of AZ31/5052 laminated composites were achieved [93]. AZX611 [94] and ZK60 [95] were also used to prepare laminated composites and good mechanical properties were obtained. In addition, laminated composite sheets of the same magnesium alloy were also developed to improve the mechanical properties. For example, Wei et al. [97] prepared four-layer Mg-14Li-3Al-2Gd sheets by accumulative roll bonding (ARB). With increasing ARB paths, both the strength and interfacial bonding strength increased, and the elongation decreased constantly. Bai et al. [99] investigated the atomic diffusion at the interface during the extrusion bonding of pure magnesium and Mg-Al-Zn-RE alloy. The results confirmed that atomic diffusion indeed occurred across the interface during extrusion. The gradients in

Table 12
Mechanical properties of the mechanical properties of laminated composites of Mg alloys reported in 2021.

Laminated composites	Process	Specific strength(kN m kg^{-1})	YS(MPa)	UTS(MPa)	EL(%)	Ref.
Ti6Al4V/AA6061/AZ31	Rolling	–	420	476	6.7	[91]
1060/AZ31/1060	Rolling	–	72	315	5	[92]
AZ31/5052	Corrugated-Flat Rolling	–	–	384	15.5	[93]
AZX611/A6005C	Explosive-welded+ Rolling	–	237	281	16	[94]
6061/ZK60/6061	Rolling	–	208	268	6.8	[95]
Mg-Li-Zn-Gd/MWCNTs	Heat treatment +Electrophoretic deposition +Accumulative roll bonding	–	264	280	–	[96]
Mg-14Li-3Al-2Gd	Accumulative roll bonding	–	240	254	27.4	[97]
AZ91	Extrusion	–	–	386	19.8	[98]

element concentration, local stresses, and hydrostatic pressure were considered to be the necessary conditions for extensive atomic diffusion to occur.

3.3. Microstrutures

Guohua Wu's group [100] successfully refined the grain size of GW83 from 832 μm to 229 μm by applying $ZrCl_4$ instead of Zr. They verified the feasibility of $ZrCl_4$ alloying at low temperature for grain refinement of sand-cast GW83 alloy. Shu-Qing Yang et al. [101] found that the adding of $MgAl_2O_4$ + Ca has better refining effect on Mg-3 wt.%Al alloy than adding $MgAl_2O_4$ only. The grain size of Mg-3 wt.%Al was hugely refined from 660 ± 55 μm to 178 ± 12 μm by adding of 2 wt.% $MgAl_2O_4$ and 0.2 wt.% Ca, due to Ca significantly promotes Mg adsorption on $MgAl_2O_4$(110) surface.

Yuansheng Yang's group [102,103] investigated the microstructure and microsegregation evolution of Mg–6Al–4Zn–1.2Sn (wt.%) cast magnesium alloy with sub-rapidly solidification, which provides essential information for the application of Mg alloy in the thin-wall castings. It is found that the microsegregation of Al, Zn, and Sn in the alloy decreases with the increase in cooling rate.

HAADF-STEM was extentively used to reveal the precipitation behavior of Mg alloys. Guohua Wu's group [21] revealed that the matrix precipitation of Mg-3Nd-4.5Gd-0.2Zn-0.5Zr was dense distribution of β'' and few β'. The EDS results indicated that Gd incorporated into β" precipitates and is likely to be substituting for Nd atoms, leading to the strongly enhanced precipitation kinetics and greatly augmented volume fraction of p" phase. Therefore, the dense distribution of β'' phases with higher aspect radio lead to substantial enhancements of alloy strength. In the case of peak aged Mg-9Gd-1Yb-0.5Zn-0.2Zr alloy, there was a specific mutually perpendicular dense distribution between the fine-scale basal γ'' and prismatic β' and β_1 phases [104]. The dense co-precipitation of thin γ'' plates and prismatic $\beta'$and β_1 precipitates with different contrasts lead to high YS of Mg-9Gd-1Yb-0.5Zn-0.2Zr alloy. Mingzhe Bian's group [105] revealed that the heterogeneously nucleated $AgMg_4$ at the grain boundaries resulted in microvoid formation in the general high misorientation angle grain boundaries. Therefore, the ductility in precipitation hardenable Mg–12Ag–0.1Ca alloy decreased significantly.

To sum up, much progress has been made in cast and wrought Mg alloys in 2021 compare to that in 2020 [106]. In the case of high strength RE containing cast Mg alloys, the UTS, YS, EL of Mg-Nd-Gd-Zn-Zr alloy developed in 2021 was reported as 343 MPa, 200 MPa, and 5.4%. The mechanical properties are comparable to those of Mg-6Gd-3Y-0.5Zr alloy reported in 2020 with an UTS of 340 MPa and EL of 6.2% [106]. However, as reviewed by Song et al. [107], Chongqing University has reported a permanent mold cast Mg-10Gd-2Y-1Zn-0.5Zr alloy which exhibited an UTS of 351 MPa and an EL of 10.2%. Due to such a high content of RE, the high cost of Mg-10Gd-2Y-1Zn-0.5Zr alloy limits its wide application to some extent. In the case of HPDC Mg alloys, the UTS of Mg-4Al-4RE-0.3Mn alloy developed in 2021 exceeded 280 MPa, and the elongation maintained at 11% [24,26]. The UTS and EL of HPDC Mg-4Al-3La-0.3Mn-2Gd alloy developed in 2020 were reported as 284 MPa and 14% [106], which is slightly higher due to the higher RE content.

In the case of commercial wrought Mg alloys, excellent mechanical properties (UTS= 448 MPa, EL=15%) of the commercial AZ61 alloys achieved by 'ECAP+EPT' technology were reported in 2021. It is of great importance to commercialize such technology for the industrialization of Mg and Mg alloys. In the case of ultra-high strength RE containing wrought Mg alloys in 2021, the highest UTS was 520 MPa obtained for extruded and aged Mg-14.5Gd-2.3Y-1.1Zn-0.3Mn alloy. However, it was reported that the highest UTS of wrought Mg-8Gd-3Y-0.4Zr alloy developed in 2020 was 710 MPa, which was prepared by rotary swaging technology and aging. In the case of low cost wrought Mg alloys in 2021, the highest UTS reaches 449 MPa for a Mg-1Ca-1Al-0.3Zn-0.4Mn alloy, the EL is 4.2%. In 2020, the same research group reported a similar low-cost Mg-1.0Ca-1.0Al-0.2Zn-0.1Mn alloy having an UTS of 425 MPa and an EL of 11%. Thus, the enhanced UTS is at the expense of EL. In addition, a new spinodal decomposition strengthening mechanism was reported in ultralight Mg-14Li-7Al alloy in 2021.

In the future, low-cost and high performance cast and wrought Mg alloys with high industrilization potential are still in demand.

4. Functional Mg materials

In addition to the high specific strength and stiffness of structural Mg alloys, Mg and Mg alloys also exhibited good biocompatibility, large hydrogen storage capacity, and high theoretical specific capacity for battery, damping properties, fast dissolve properties, electromagnetic shielding properties. Consequently, Mg and Mg alloys have great potential in energetic and biomedical applications. However, the fast degradability of bio-Mg alloys presents the biggest challenge for the biomedical application. The massive application of Mg based hydrogen materials was mainly restricted by the high thermodynamic stability and poor kinetics of hydrogen absorption and desorption. In the case of rechargeable Mg batteries (RMBs), although Mg has ultrahigh theoretical capacity and high safety, RMBs still fall short of their potential meritdue to the lack of practical electrolytes and cathodes [108].

4.1. Bio-magnesium alloys

Mg alloy as a type of metallic biomaterials possesses the advantage of degradability, but its degradation process produces various complex changes in the material and the organism [109,110]. The development of new bio-Mg alloys has consistently been a research hotspot. Investigation on bio-Mg alloys mainly focuses on improving the biodegradation or biological responses via alloying and surface coating.

Alloying elements, such as Zn, Ca, Cu, Mn, and Zr, with good biocompatibility are the primary considerations in the composition design of Mg alloys [111–114]. The *in-vitro* results show that Mg-5Sn-4In alloy has a minimum corrosion rate of 0.36 mm/y [115]. Bulk amorphous materials developed in the Mg-Zn-Ca system also show good mechanical properties, with strengths reaching 700 MPa [116]. Rare earth elements Y, Ce, Pr, Gd, Dy, Yb, Sm, and Eu were evaluated before being used as biomedical Mg alloys [117]. Sc appears to be suitable from a biological perspective. Given the paucity of data, Tb and Ho may have some potential, the applicability of Tm, Lu, and Er remains unclear. Further investigations are needed to determine the physiological effect of each rare earth element.

Surface modification, including coating, chemical transformation, and surface treatment, is applied to control the biodegradation of bio-Mg alloys. For example, MAO/CS composite coatings have been generated on the surface of Mg-1.75Zn-0.56Ca alloys to protect the matrix and improve biocompatibility in physiological environments [118]. Biocompatible Ti has also been coated on the Mg surface via the physical vapor deposition (PVD) technique to improve the corrosion resistance. nontoxic, non-allergic, β Ti-29Nb-13Ta-4.6Zr (TNTZ) has been deposited on pure Mg and AZ31 Mg alloys [119], *in-vitro* corrosion tests show that the E_{corr} of the coated sample is about 400 mV, being higher than that of the uncoated Mg sample.

In terms of biological responses, only a few studies have examined the metabolism of typical alloying elements in living organisms, whereas numerous studies have been conducted on the implantation of Mg alloys in animals. For example, Willumeit-Römer Regine's group [120] evaluated Mg-10Gd alloy in implantation and conducted in-vivo fluorescence molecular tomography to measure the initial increase in the fluorescence signal at the implantation site. The results revealed cellular stress at the implantation site, and the signal did not diminish until day 42. The Mg-10Gd alloy affected the connective tissue on the implant side.

In addition to the regular improvement of biodegradation of bio-Mg alloys, the new Resoloy rare earth Mg-Dy alloy for bioresorbable vascular implant is developed [121] as an alternative to WE43 scaffolds developed by Biotronik, Inc., which received CE approval in 2016. *In-vitro* degradation tests have shown that the combination of MgF_2 passivation and PLLA surface coating on the Resoloy Mg backbone results in slower degradation and longer support times (40+ days), compared with WE43 alloy. This finding sheds light on the industrialization of bio-Mg alloys for the bioresorbable vascular implant application. Hess et al. [122] revealed the anti-tumor mechanism of extracellular Mg^{2+}, Mg^{2+} enhances T cell effect or function by raising LFA-1 outside-in signaling, thereby increasing the efficiency of T cells immunotherapies.

4.2. Mg battery

4.2.1. Mg-air battery

Magnesium has been considered as a good anode material for metal-air batteries because of its high specific capacity (2200 mAh), high discharge voltage (3.03 V), relatively low-cost and abundant global reserves. In 2021, the anode materials of magnesium air battery mainly include the following magnesium alloys, such as AZ31, Mg-Li, Mg-Bi, Mg-Ca-Zn, Mg-Gd-Zn alloys, etc. The average discharge voltage and anode efficiency of these alloys are listed in Table 13. Among these alloys, Mg-0.7Sn-1.4Y alloy shows the highest anode efficiency of 53.1% at a current of 10 mA•cm^{-2}.

The discharge performance of magnesium-air battery is mainly improved by microalloying and processing modification. In Wu's work [123], the discharge characteristics of two α-Mg-based lithium alloys (LAZ131 and LAZ531) were studied. It was observed that grain boundaries are easier to be corroded than grains, thus accelerating the corrosion process of alloy materials. Jiang et al. [127] adopted a powder metallurgy technique to prepare a modified AZ31 anode with extremely fine grains (667 $\pm$ 291 nm). Compared with the coarse AZ31 alloy with a grain size of 473 $\pm$ 154 μm, the modified AZ31 alloy shows significantly higher activity and higher capacity as the anode material of magnesium-air battery during discharge. In addition, Chen et al. [124] found that the discharge voltage and anode efficiency of magnesium-air battery with extruded Mg-xBi (x = 0.5, 1.0, 2.0 wt.%) as anode decrease with increasing bismuth alloying element under

Table 13
Average discharge voltage and anode efficiency of Mg alloys for Mg-air battery.

Alloys	Current(mA•cm^{-2})	Average discharge voltage(V)	Anode efficiency(%)	Ref.
LAZ131	10	1.3037	44.3	[123]
LAZ531	10	1.3742	48.7	[123]
Mg-0.5Bi	2.5	1.4789	41.41	[124]
M-Gd-Zn	2.5	1.3900	–	[125]
Mg-0.7Sn-1.4Y	10	1.4151	53.1	[126]
Modified AZ31	10	1.2110	–	[127]

constant current discharge. The magnesium-air battery shows good anode discharge activity and stable discharge process when the anode material is Mg-0.5Bi due to the thin and loose film of discharge products.

In terms of cathode material of magnesium-air battery, Dong et al. [128] synthesized copper disulfide nanosheets by one-step hydrothermal method. The half-wave potential of $CuMnO_2$ was achieved at 0.63 V, along with a limiting diffusion current density of 5.60 mA•cm^{-2} at 1600 rpm in 0.1 M KOH electrolyte. Besides, the half-wave potential shows only a small change of 22 mV after 5000 CV cycles, suggesting the outstanding stability and durability. Liu et al. [129] found that MnO_2/reduced graphene oxide (rGO) layered hybrids have a high BET surface area for synergistic effects on the introduction of rGO and the morphological transformation of anchor MnO_2.

In the case of electrolyte, Leong et al. proved that the bi-electrolyte acid salts can significantly improve the voltage and power performance of magnesium air batteries [130], which provides spread of electrochemical windows and a decrease in passivation, doubling the peak power density and having an open voltage of 46%. In Ye's work, Mg-air batteries (pure Mg as an anode material) with ultrahigh average specific capacity of 2190 mAhg^{-1} and high energy density of 2282 Wh kg^{-1} had been achieved by designing a dual-layer gel electrolyte. Organic gel protects magnesium anode from corrosion, and chloride ions in hydrogel are helpful to produce unique needle-like discharge products, instead of the dense passivation layer commonly reported [131].

4.2.2. Rechargeable Mg batteries

Rechargeable Mg batteries (RMBs) are considered as highly promising candidates for next-generation large-scale energy storage systems, owing to the ultrahigh theoretical capacity (3833 mAh cm^{-3} or 2205 mAh g^{-1}) of Mg having the abundant resource, and its high safety (no obvious dendrite morphology during Mg plating process) [132]. However, although tremendous breakthroughs (including free-chlorine electrolyte designs, and the development of high-capacity conversion-type cathodes, availably artificial solid electrolyte interphase (SEI) on Mg metal (Fig. 7)) were obtained two decades ago, RMBs still fall short of their potential merit [108]. The main bottlenecks still originated from a lack of practical electrolytes and cathodes that would enable high energy density and power density [133].

(1) Anode of rechargeable Mg batteries

The Mg metal is currently an ideal anode for RMBs, owing to the high theoretical mass and volume capacities, and low redox potential (−2.37 V vs. H^+/H). But the formation of passive layers on the surface of the Mg anode in most conventional electrolytes (e.g., $Mg(ClO_4)_2$, $Mg(PF_6)_2$ or $Mg(TFSI)_2$ salts in carbonate or ether solvents) restricts the reversible plating/stripping of Mg^{2+}. Thus, some effective strategies, such as designing the protective layer on Mg metal, developing the Mg alloy anodes, or searching the insertion-type or conversion-type metal compound anodes, have been proposed to promote the development of RMBs anodes [134].

Zhao et al. designed a bismuth (Bi)-based artificial protective layer on Mg metal by the displacement reaction between Mg and $BiCl_3$ in solution [135]. The Mg-Mg symmetric cell assembled by the modified Mg anode exhibited a relatively lower overpotential of ∼0.6 V and maintained cycling stability over 4000 h in $Mg(TFSI)_2$/DME electrolyte. Zhang et al. prepared an artificial interlayer made of amorphous $MgCl_2$@polymer on Mg metal surface by *in-situ* chemical reaction of metallic Mg with H_3PO_4 and $SiCl_4$ in sequence [136], the corresponding symmetric Mg cell exhibited a low overpotential of ∼0.25 V and stable cycles over 700 h in $Mg(TFSI)_2$/DME electrolyte. Dou et al. constructed a "MgF_2-rich" SEI on Mg metal surface with high electronic insulation though the electrolyte modification [137]. The symmetric cell exhibited superior cycling performances of over 1150 h with low polarization. In addition, introducing the sodium cations [138] or $Mg(BH_4)_2$ [139] in Mg-based electrolytes could also decrease the interface impedance and reduce the passive layer.

The deposition behavior of Mg is still controversial. Most researchers demonstrated that there was no Mg dendrite formation during Mg plating/stripping process in most conventional electrolytes. Recently, Kwak et al. observed that the spherical Mg seeds covered the substrate in APC electrolytes at the relatively low rate of 2 mA cm^{-2} [140]. When current density was increased to 10 mA cm^{-2}, needle-like dendritic growth could be observed. Moreover, they introduced Au magnesiophilic sites in the substrate, which effectively suppressed the Mg dendritic growth. Bae et al. designed an amorphous MgO-wrapped Zn-skeleton as a unique current collector for anode-free Mg battery [141]. This MgO/Zn interlayer behaves as a mixed ionic-electronic conductor, ren-

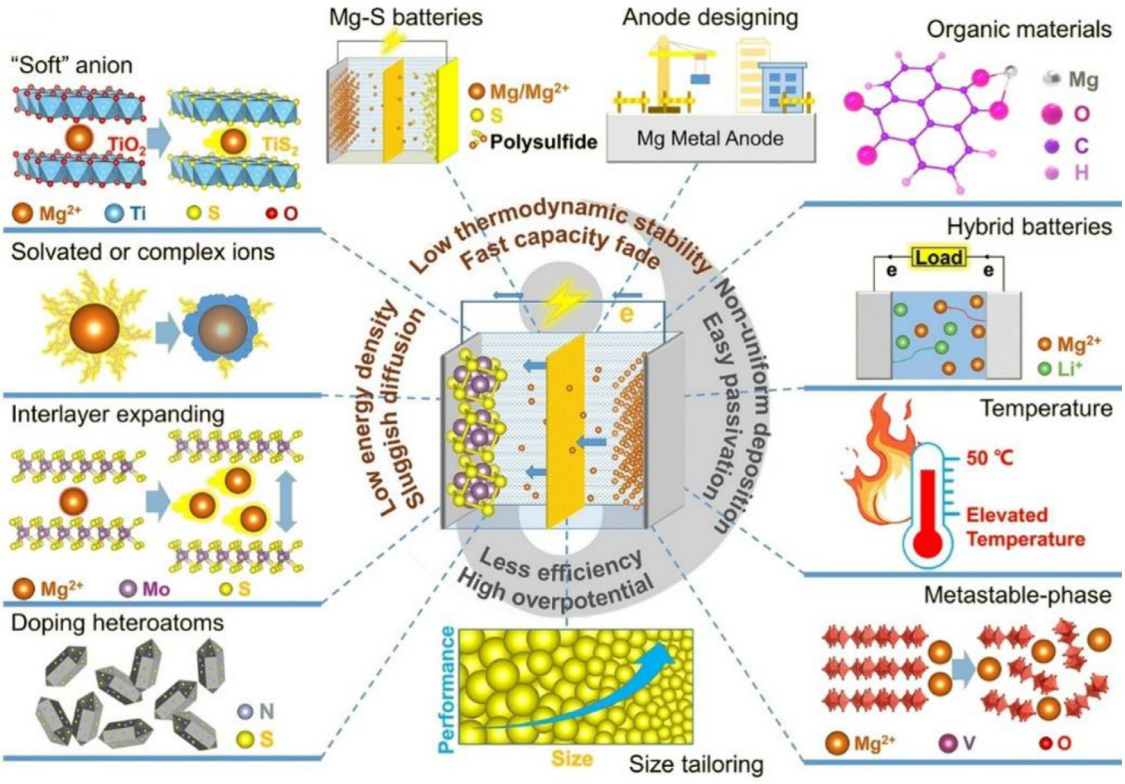

Fig. 7. Current design strategies for rechargeable Mg-based batteries [108].

dering uniform Mg nanoparticles upon electroplating. It also improved the charge transfer kinetics and lowered the cell impedance. Song et al. proposed vertically aligned N- and O-doped carbon nanofiber arrays on carbon cloth (VNCA@C) as current collector for Mg battery [142]. The evenly nanoarray was favorable to homogenize the surface current density, and the microchannels built in this 3D host promoted the uniform nucleation of Mg. Under a high current density of 10 mA cm^{-2}, the carbon host delivered a reduced nucleation overpotential of 429 mV and an elongated Mg plating/stripping cycle life (110 cycles).

The alloy-type anodes usually avoid the passivation reaction from the conventional electrolytes, but the huge volume expansion/shrinkage during Mg^{2+} alloying and de-alloying leads to a serious capacity fading. Song et al. focused on liquid gallium (Ga) electrodes owing to the self-healing properties [143]. In order to improve the poor wettability of liquid Ga on stainless steel (SS) mesh, they constructed a $CuGa_2$ layer on the surface of SS mesh and the wettability of liquid Ga was significantly enhanced. The liquid Ga electrode also exhibited good compatibility with $Mg(TFSI)_2$.

(2) Cathode of rechargeable Mg batteries

For cathode, the high-polarization of Mg^{2+} leads to strong electrostatic interactions between Mg^{2+} and anion lattices, further resulting in serious voltage polarization and low magnesiation degree [144]. In 2021, some high-performance sulfide or selenide cathode materials were reported, as listed in Table 14. Among these materials, the reversible specific capacity of defect-rich $Cu_{7.2}S_4$ nanotubes could reach 314 mAh g^{-1} at 0.1 A g^{-1} [145]. Meanwhile, it also exhibited excellent rate capability of 91.7 mAh g^{-1} at 1.0 A g^{-1} and cycling stability over 1600 cycles with capacity decay of 0.0109% per cycle at 1.0 A g^{-1}. Shen et al. reported a high-performance FeS_2 cathode using a copper current collector [146]. They found that the formation of copper nanowires during discharge could activate the redox reactions of FeS_2 to realize the four-electron transfer, thus delivering a significantly enhanced reversible capacity of 679 mAh g^{-1} at 50 mAh g^{-1}.

The high-voltage RMBs cathode is of great interest but rarely reported. Fluorophosphates with the inserted magnesium ion channels and high discharge voltages (>3 V) have been studied to some extent [155]. Rubio et al. [154] found that $Na_3V(PO_4)_2F_2$ cathode could perform the reversible multi-electron storage through the V^{4+}/V^{3+} and V^{5+}/V^{4+} redox couples for RMBs, thus the specific capacity of 136 mAh g^{-1} could be obtained.

(3) Electrolyte for rechargeable Mg batteries

The chloride-free magnesium battery electrolyte with wide electrochemical stable windows, high ionic conductivity, and good compatibility with electrode materials are significant for developing high-performance RMBs.

Sun et al. introduced an effective additive, reduced perylene diimide-ethylene diamine (rPDI), in simple $Mg(TFSI)_2$/DME electrolyte [156]. A high power den-

Table 14
Summary of the electrochemical performance of cathode materials for RMBs reported in 2021.

Cathode	Reversible capacity(mAh g^{-1})	Average dischargepotential (V vs. Mg/Mg^{2+})	Cycles	Ref.
Defect-rich $Cu_{7.2}S_4$ nanotubes	314 (at 100 mA g^{-1})	~1.0	1600	[145]
CuS microspheres	252 (at 100 mA g^{-1})	~1.0	500	[147]
FeS_2 on Cu current collector	679 (at 50 mA g^{-1})	~1.1	1000	[146]
$CuCo_2S_4$/CuS@MWCNTs	214.79 (at 10 mA g^{-1})	~0.8	1000	[148]
Mo-doped VS_4	120 (at 50 mA g^{-1})	~0.75	350	[149]
CuSe nanoflakes	204 (at 200 mA g^{-1})	~0.9	700	[150]
Defect-spinel-type $ZnMnO_3$	100 (at 10 mA g^{-1})	~2.5	120	[151]
Spinal $Mg(Mg_{0.5}V_{1.5})O_4$	250 (at 100 mA g^{-1})	~2.0	500	[152]
Vanadium oxide@PANI superlattices	275 (at 100 mA g^{-1})	~1.8	500	[153]
$Na_3V(PO_4)_2F_2$	136 (at 100 mA g^{-1})	~1.4	-	[154]

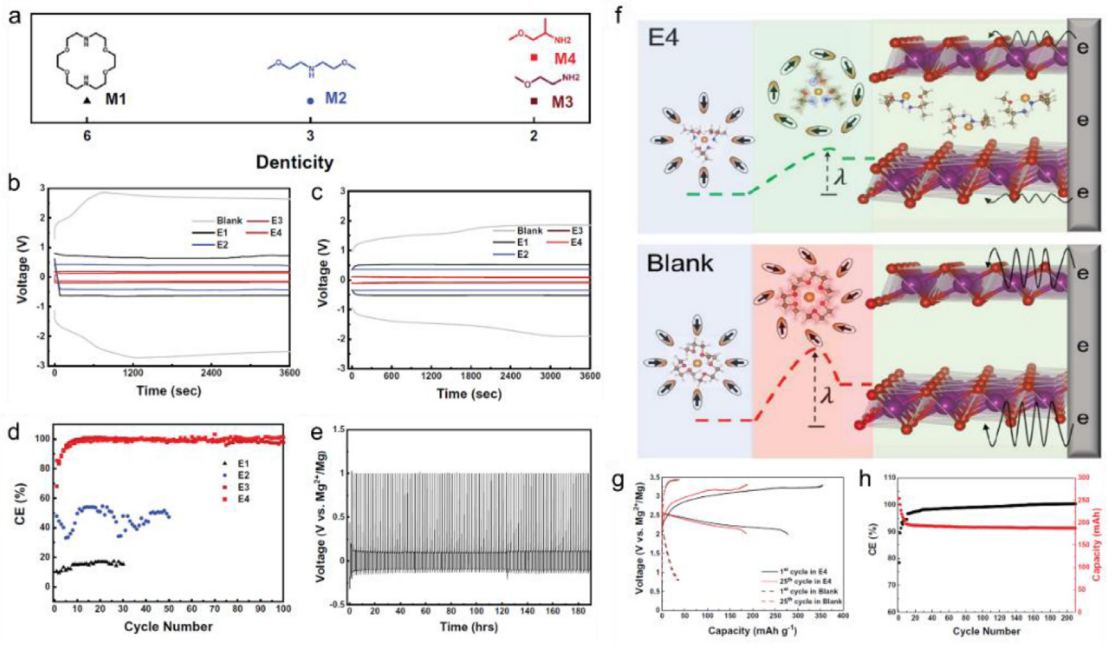

Fig. 8. (a) The molecular structure and denticity of the methoxyethyl-amine chelants. The overpotentials at the 10th cycle of Mg‖Mg cells at (b) 1.5 mA cm^{-2} for 1.5 mAh cm^{-2} and (c) 0.1 mA cm^{-2} for 0.1 mAh cm^{-2}. (d) CEs of Mg//SS cells cycled at 0.1 mA cm^{-2}. (e) Long-term cycling of the Mg//SS cell. (f) Scheme of solvated Mg^{2+} and electron transfer in $Mg_{0.15}MnO_2$ host. (g) Charge-discharge curve of Mg//$Mg_{0.15}MnO_2$ cell at 0.5 C. (h) Cycling performance and CE of Mg//$Mg_{0.15}MnO_2$ at 0.5 C [158].

sity (2.0 mW cm^{-2}) and a stable cycle life (>200 cycles) in an Mg-organic full cell could be achieved. Horia et al. used tetrabutylammonium borohydride as a moisture scavenger to control the moisture content in chloride-free $Mg(HMDS)_2$/DME electrolyte [157]. This electrolyte demonstrated a low polarization voltage of 0.25 V over 1000 cycles, an average coulombic efficiency of 98.3% over 150 cycles in asymmetrical cell and no obvious corrosive reaction to current collectors.

Very interestingly, Hou et al. found a family of methoxyethyl-amine chelants (Fig. 8a) that could tune solvation structure of simple $Mg(TFSI)_2$/DME electrolyte, improving the interfacial charge transfer kinetics and suppressing the passivation reaction [158]. This electrolyte demonstrated low polarization voltage of ~0.1 V (Fig. 8b, c) and a high coulombic efficiency of over 99.5% (Fig. 8d, e). Moreover, this electrolyte system provided an excellent compatibility for layered $Mg_{0.15}MnO_2$ cathode, enabling a fast diffusion kinetics of the solvated Mg^{2+} in the interlamination (Fig. 8f). Thus, a high average discharge voltage of ~2.3 V and a reversible capacity of 190 mAh g^{-1} after 200 cycles in Mg//$Mg_{0.15}MnO_2$ cell could be achieved (Fig. 8g, h).

The high-voltage boron-based electrolytes also exhibit large potential in RMBs due to high oxidation stability, high ionic conductivity, and weak corrosion to current collectors [159]. But the complex synthesis process and expensive raw materials hinder their widespread application. Ren et al. reported a magnesium tetra(trifluoroethanoloxy)borate ($Mg[B(Otfe)_4]_2$) electrolye by two methods of microcrystal redissolution and *in-situ* reaction [160]. First, a stoichiomet-

ric reaction between $Mg(Bu)_2$ and BH_3•THF was performed with 2,2,2-trifluoroethanol (HOtfe) under ambient conditions. Then, the Otfe- from $Mg(Otfe)_2$ was subsequently separated and transferred to $B(Otfe)_3$ via the transmetalation reaction, generating Mg-B complex product separated by solvent vacuum extraction. This electrolyte exhibited an average coulombic efficiency of ~99% and low overpotential of 0.2 V and an oxidation stability over 3 V vs. Mg^{2+}/Mg at SS.

(4) Mg-S batteries

Magnesium-sulfur batteries with high mass/volumetric energy density, great safety and low cost have been considered as one of most potential RMBs [161]. Nowadays, these issues including insulating nature of elemental sulfur, sluggish redox kinetics between S and Mg^{2+}, severe volume changes, low conductivity and low utilization of polysulfides, etc., still extremely limit the electrochemical performance [162]. The results reported to date are still far from the expected performance indicators.

In order to improve the redox kinetics, Xu et al. introduced the Ag current collector in S cathode [163]. The composited S cathode delivered an improved specific capacity of ~1200 mAh g^{-1} and a long cycling life of 100 cycles. Zhao et al. designed a Co_3S_4@MXene heterostructure sulfur host to improve the electrochemical redox kinetics [164]. The Co_3S_4@MXene-S cathode could display a high sulfur utilization with a specific capacity of 1220 mAh g^{-1} and retain a capacity of 528 mAh g^{-1} after 100 cycles.

The sulfur conversion reaction is also associated with the properties of electrolyte solvent, such as permittivity, viscosity and chemical stability. Zou et al. found that the Mg-S reactions in the commonly used DME-based electrolyte was "solid-solid" reactions due to the low polysulfide solubility of MgS_x in DME, thus leading to sluggish kinetics and poor reversibility [165]. The polysulfide solubility could be increased by using high-donor-number solvents (e.g., dimethyl sulfoxide, dimethyl formamide), which increases the discharge capacity from 660 to ~1500 mAh g^{-1} and decreases the sulfur overpotential from >600 to ~200 mV at 0.1 C. This work provided critical insights into the electrolyte design for Mg-S batteries. In addition, Mg-S batteries suffer from serious self-discharge behavior. Ford and Schaefer et al. revealed that the decreased self-discharge capacity could reach to 32% of the first cycle discharge capacity in 0.5 M MgFPB/DEG electrolyte [166]. In response, preventing contacts of S_8 and polysulfide with the Mg anode will prevent the first step of self-discharge. The electrolyte modification, the optimization of sulfur host and artificial Mg SEI design may be effective to improve this issue.

In 2021, the practical matching between the available cathode, anode and electrolyte, and the manufacture of large-capacity soft-package RMBs are still absent. Chongqing University successfully produced the soft-package RMBs as a result of extensive fundamental studies on high-capacity sulfide/oxide cathodes, magnesium alloy anodes and low-cost electrolytes. It is expected to facilitate the commercialization of RMBs and the revolution of energy storage market.

4.3. Hydrogen storage Mg materials

Among many metal hydrides, Mg-based hydrogen storage materials have attracted wide attention due to the high theoretical hydrogen storage density of 7.6 wt.% and bulk hydrogen storage density of 110 kg/L. However, due to the high thermodynamic stability and poor kinetics of hydrogen absorption and desorption, it is difficult to apply Mg-based hydrogen storage materials on a large scale commercially. To this end, researchers around the world continue to investigate on alloying, nanostructuring, mixing with additives and changing reaction path and so on.

The first-principle calculations are commonly used to predict the structure and properties of materials and explore the mechanism of hydrogen storage. Ding et al. [167] found that $Mg_{14}Ti_4H_{36}$ system shows the best hydrogen storage performance in complex indexes such as substitution energy, desorption temperature and bulk modulus. Magnesium hydrides can obtain excellent hydrogen storage performance through the substitution of transition metal elements and adjustment of substitution concentration and configuration, which provide a new idea for the performance improvement of Mg-based hydrogen storage materials.

Alloying, as the most effective method to improve the absorption/desorption performance of Mg-based hydrogen storage materials, is usually optimized by adjusting the internal structure of the alloy. As a common means of alloying modification, element substitution has been widely concerned by researchers. For example, Zhang et al. [168] studied the hydrogen storage performance of $Mg_{98}Ni_{2-x}La_x$ alloy (x = 0, 0.33, 0.67 and 1) in which lanthanum replaced part of nickel. He et al. [169] investigated the hydrogen storage properties of $La_{10-x}Re_xMg_{80}Ni_{10}$ (x = 0 or 3; RE = Sm or Ce) alloys, which was prepared by vacuum induction casting with elements Ce and Sm replacing part of lanthanum. It has been proved that the thermodynamics and kinetics of hydrogen storage in Mg-based hydrogen storage alloys have been greatly improved by the element substitution.

In recent years, some studies have shown that the existence of LPSO phase in Mg-based hydrogen storage alloys will significantly affect the hydrogen storage properties. Nano-sized rare earth hydrides (REHx) generated by *in-situ* decomposition of LPSO phase can be evenly distributed at the grain boundary of Mg matrix, thus effectively reducing the catalytic dead zone and improving the catalytic efficiency. In addition, these nanosized REHx hydrides can also be fixed on the grain boundaries of Mg nanocrystals to inhibit the growth of Mg/MgH_2 grains, thus improving the stability of the nanophase structure. Mao et al. [170] studied the hydrogen storage performance and catalytic mechanism of $Mg_{98.5}Gd_{0.5}Y_{0.5}Zn_{0.5}$ by adding Gd to $Mg_{98.5}Y_1Zn_{0.5}$ alloy. The *in-situ* generated RE(Gd/Y)Hx(x = 2,3) nano-hydride by the LPSO phase decomposition can not only promote the hydrogen absorption/desorption of Mg matrix as *in-situ* cat-

Table 15
Information on nanostructured systems.

Sample	Preparation methods	De/Rehydrogenation kinetics	Ref.
Nano-MgH_2	liquid-solid phase driven by ultrasound	6.7 wt.%H_2/2500 min/30°C/De	[174]
Mg/GO	chemical reduction method	~6.5 wt.% H_2/180 min/300°C/De	[175]
MgNi/NG	chemical reduction method	5.4 wt.% H_2/3 MPa/25°C/*Re*	[176]
Mg-Nb@C	reactive gas evaporation method	4.8 wt.% H_2/60 min/300°C/De	[177]

Table 16
Information on catalyst doping systems.

Sample	Activation energy	Dehydrogenation kinetics	Ref.
MgH_2+10 wt.%TiFe	56.6 ± 5.8 KJ/mol	6.5 wt.%H_2/10 min/300°C	[179]
MgH_2+5 wt.% Mg(Nb)O	84.1 KJ/mol	5 wt.% H_2/120 min/280°C	[180]
MgH_2+5 wt.%Ti_3C_2	57.5 KJ/mol	4.8 wt.% H_2/10 min/300°C	[64]
MgH_2+10 wt.%V_2C/Ti_3C_2	79.7 ± 1.9 KJ/mol	5.1 wt.% H_2/60 min/225°C	[181]
MgH_2+5 wt.%Ni/Ti_3C_2-WE	91.64 KJ/mol	6.25 wt.% H_2/600 s/275°C	[178]

alysts, but also inhibit the growth of Mg/ MgH_2 grains via pinning effect during hydrogenation and dehydrogenation.

In addition, besides the conventional casting method to obtain Mg-based hydrogen storage alloy, researchers have also developed other special preparation methods, such as DC arc plasma method [171], mechanical alloying [172], and melt spinning method [173] and so on. The alloys obtained by these special preparation processes not only solve the problem that cannot be prepared by conventional casting methods, but also have special structure, which opens a new field of study on the hydrogen storage properties of Mg-based hydrogen storage alloys.

Nanostructuring and catalyst doping, as the most rapid and effective methods to improve the dynamic properties of Mg-based hydrogen storage materials, have also attracted the attention of researchers all over the world. Tables 15 and 16 list some relevant information of nanostructures and catalyst doping systems, respectively, reported in recent years. Studies have shown that nanostructures can have profound effects on the hydrogen storage properties of Mg-based hydrogen storage materials by increasing the specific surface area, enriching grain boundaries/defects, and shortening hydrogen transport paths. Xin Zhang's team [174] successfully prepared ultrafine-sized MgH_2 nanoparticles with a major size of 4–5 nm for the first time through a novel metathesis process of liquid-solid phase driven by ultrasound, and achieved 6.7 wt.% reversible storage of hydrogen at 30 °C.

In recent years, a family of two-dimensional layered MXenes materials has shown great potential in catalysis, sensors, conversion, energy storage, gas absorption and electronic devices due to their layered structure, relatively large surface area, significant chemical durability and high electrical conductivity. Therefore, MXenes materials came into the attention of researchers of Mg-based hydrogen storage materials. They mixed the MXenes materials into MgH_2 by ball milling, and greatly improved the hydrogen absorption and desorption performance of MgH_2. For example, Zhihui Tian et al. [64] mixed 5 wt.% Ti_3C_2 into MgH_2, which not only led to a significant reduction in activation energy of MgH_2 ($\Delta H = 57.5$ kJ/mol), but also achieved hydrogen desorption of 4.8 wt.% within 10 min at 300 °C. Based on this result, Hou et al. [178] successfully realized Ni particles loaded on Ti_3C_2 by hydrothermal method, which further improved the hydrogen absorption/desorption kinetics of MgH_2. The MgH_2+5 wt.% Ni/Ti_3C_2-WE can desorb 6.25 wt.% hydrogen within 600 s at 275 °C and absorb 4.55 wt.% hydrogen within 1200 s at 100 °C. Obviously, the full contact between Ni nanoparticles and Ti_3C_2 matrix and the rich electronic interaction brought by the interface can significantly improve the ab/desorption performance of MgH_2. In addition, the electron transfer and the unique structure of Ni/Ti_3C_2-WE in multivalent Ti (Ti^0, Ti^{2+}, Ti^{3+}, Ti^{4+}) are also the key factors for superior catalytic activity of Ni/Ti_3C_2-WE.

In addition to the application of Mg-based materials in solid hydrogen storage, they can also be used in the field of hydrolytic hydrogen production. Pang et al. [182] investigated the effect of monovalent alkali metal cations in seawater on hydrogen production behavior of $(Mg_{10}Ni)_{10}Ce$ alloy. The results show that the $(Mg_{10}Ni)_{10}Ce$ alloy has the shortest hydrolysis induction time within 20 min in KCl solution at 25 °C, and the highest H_2 yield is 173.4 mL g^{-1}. The results of this study lay a solid foundation for the development of green portable hydrogen generators and the popularization of clean hydrogen energy and emission reduction.

Based on the thermodynamics and kinetics of de/hydriding reactions, catalyst addition is an effective method to enhance the properties of Mg-based hydrogen storage materials [5]. Liu et al. [183] synthesized smaller and uniform graphene-supported TiO_2 nanoparticles (TiO_2@rGO) via solvothermal method and found that the MgH_2–70TiO_2@rGO composite exhibited superior kinetic properties. The composite can desorb 6.0 wt.% hydrogen within 6 min at 300 °C and absorb 5.9 wt.% hydrogen within 2 min at 200 °C. Besides, Mg is also a vital substitution element for the property improvement of La-Y-Ni hydrogen storage alloys. For example, the $LaY_{1.25}Mg_{0.75}Ni_9$ alloy exhibited good overall electrochemical properties with the maximum discharge capacity of 308.4 mAh/g and capacity retention of 69.0% after 100 cycles,

which were 10.7% and 47.1% higher than those of the original LaY_2Ni_9 alloy, respectively [184].

To achieve the practical application of hydrogen, the metal hydride tank (MHT) is a widely used device for the safe storage and delivery of hydrogen. However, due to the highly complex hydrogen reaction and transport, the design of a MHT with desired properties is difficult. Lin et al. [185] developed a numerical model that can accurately simulate the absorption and desorption processes in a double-layered annulus MHT and optimized the parameters of the MHT with desired properties. This physical model based and numerical simulation guided strategy is of general value for the design of MHT in hydrogen-related applications.

Chongqing University has investigated Mg-based hydrogen storage materials, and successfully discovered novel Mg-Ni-Y and Mg-Ni-Nd systems, which show high hydrogen storage capacity, low operating temperature, and robust recyclability. Moreover, Chongqing University also established an integrated hydrogen storage system, including light-weight tanks, solar-power-based hydrolysis systems and fuel-cell, demonstrating their capability for potential applications.

4.4. High modulus and high damping Mg alloys

It is difficult for Mg alloy to maintain high elastic modulus and high damping capacity simultaneously, which hinders the further development and application of magnesium alloys. Wang et al. [186] prepared Mg-8Li-4Y-2Er-2Zn-0.6Zr alloy with high damping capacity, high elastic modulus (E) through heat treatment and cold rolling. With the presence of 18R LPSO and later formed twins and kinks, the damping capacity increases from 0.01 to 0.02. In addition, the modulus of elasticity of the cold-rolled alloy reaches 48.9 GPa.

Xianhua Chen's group develops magnesium alloys with both high modulus and high strength. They found that the addition of Ge element to the matrix Mg-Gd-Ag-Mn alloy could improve the elastic modulus and strength of the alloy at the same time [187]. Among the alloys containing Ge, Mg-10Gd-1.5Ag-0.2Mn-3.5Ge alloy exhibited the best comprehensive mechanical properties, with E, UTS and EL of 51 GPa, 423 MPa and 10%, respectively. In addition, they designed a new as-cast Mg-Y-Zn-Al-Li alloy with a high elastic modulus of 52.9 GPa [188].

4.5. Dissoluble magnesium alloys

In recent years, dissoluble magnesium alloys have broad application prospects because of their strength to bear high pressure and controllable degradation rate. However, it is key to enhance the degradation rate and simultaneously maintain good mechanical properties. Many researchers have found that Ni has a great influence on the mechanical properties and degradation rate of soluble magnesium alloys, the developed Mg alloys in 2021 are summarized in Table 17.

Liu et al. [189] added Ni to hollow glass microsphere/Mg alloy composites. The results show that adding Ni leads to the formation of Al_3Ni_2 intermetallic, refines the matrix and reduces the function of corrosion barrier of the β-phase. As a result, the UCS increases to 393 MPa, and the average degradation rate dramatically increases to 95.6 mg cm^{-2} h^{-1} at 93 °C. Wang et al. [190] developed a high strength Mg-10Gd-3Y-0.3Zr-0.8Ni alloy with a moderate degradation rate. The UCS is as high as 597 MPa and the degradation rate is 24 mg cm^{-2} h^{-1} at 93 °C. Wang et al. [193] rationally designed Mg-Y-Ni dissoluble magnesium alloys with a combination of high strength and rapid degradation with the help of the special structure of LPSO phase. This suggested that the Ni-containing LPSO structure could not only improve the mechanical properties, but also accelerate the corrosion of magnesium alloys. In addition, Wang et al. [194] investigated the effect of compositions, contents and morphologies of Ni-containing LPSO phase on the mechanical and degradation properties and their corrosion mechanisms. The higher potential difference between the Ni-containing LPSO and the magnesium matrix promotes the occurrence of galvanic corrosion and enhances the degradation rate. Thus, the degradation rate is accelerated with increasing Ni-containing LPSO content. However, the continuous distribution of LPSO phase can act as a corrosion barrier to prevent corrosion expansion and reduce the degradation rate. Moreover, Ma et al. [191] proposed novel Mg-7.2Y-2.8Ni alloys containing rod-shaped LPSO phase. The average degradation rate increases by 27% and the UCS increases to 456 MPa in an annealed state.

4.6. Electromagnetic shielding Mg alloys

Current studies on the electromagnetic shielding performance of Mg alloys have become increasingly extensive and thorough. Some new shielding Mg alloy materials, such as low-RE content Mg-Sn series alloys, RE-free Mg-Li series alloys and Mg-based composite materials, have been developed.

Xianhua Chen's group has successfully developed Mg–Sn–Zn alloys with minor amounts of Ca and Ce, which exhibit superior shielding effectiveness (SE) and high strength [195]. When the Sn content is 3 wt.%, the Mg–Sn–Zn–Ca–Ce alloy possesses SE value of 91–114 dB at 30–1500 MHz, which is mainly attributed to the regular arrangement of Mg_2Sn precipitates. Zhang et al. have studied the SE and corrosion resistance of Mg alloys fabricated by electro-pulsing [196]. The SE of the alloys (~87 dB) at a high frequency (1500 MHz) increases by 109.4%. The enhanced SE is attributed to the dissolution and refinement of precipitates. At present the shielding properties of Mg-based composites have become a research hotspot. Wang et al. have found a novel Mg–Li–Zn–Gd/MWCNTs composite with high SE and mechanical strength (X-band) [68]. The EMI SE of the ARB5 (five accumulative roll bonding cycles) sheet in the X-band frequency range is increased up to 77–96 dB.

To sum up, a new Resoloy rare earth Mg–Dy alloy with excellent mechanical properties and biocorrosion behavior as an alternative to WE43 scaffolds for bioresorbable vascular implant is developed, which helps promote the industrializa-

Table 17
Compressive and degradation properties of dissoluble Mg alloys developed in 2021.

Alloys	State	UCS (MPa)	CYS (MPa)	Degradation rate(mg cm^{-2} h^{-1})	Ref.
HGM/Mg+2Ni	As-cast	393	–	95.6(93°C,3.5%KCl)	[189]
Mg-10 Gd-3Y-0.3Zr-0.8Ni	As-extruded	597	297	24.4(93°C,3.0%KCl)	[190]
Mg-7.2Y-2.8Ni	As-annealed	456	168	12.7(25°C,3.0%KCl)	[191]
Mg-7.2Y-2.8Ni	As-extruded	500	245	~10.0(25°C,3.0%KCl)	[191]
$MgGd_1Ni_{0.75}$	As-cast	355	126	43.6(25°C, 3.0%KCl)	[192]

tion of bio-Mg alloys for bioresorbable vascular implant application. A simple low-cost $Mg(TFSI)_2$/DME electrolyte in $Mg//Mg_{0.15}MnO_2$ cell with a high average discharge voltage of ~2.3 V and a reversible capacity of 190 mAh g^{-1} after 200 cycles is developed. In addition, Chongqing University successfully produced the soft-package RMBs by virtue of extensive fundamental studies on high-capacity sulfide/oxide cathodes, magnesium alloy anodes and low-cost electrolytes. An ultrafine-sized MgH_2 nanoparticles with a major size of 4–5 nm led to 6.7 wt.% reversible storage of hydrogen at 30 °C. Chongqing University also established an integrated hydrogen storage system, including light-weight tanks, solar-power-based hydrolysis systems and fuel-cell, demonstrating their capability for potential applications.

In the future, controlling the fast degradability of bio-Mg alloys remains to be a hot topic. In the case of rechargeable Mg batteries (RMBs), low-cost Mg battery pack with high battery performance is still under development, and the industrialization of RMB requires more attention. Further improvement in the kinetics of hydrogen absorption and desorption of Mg based hydrogen materials is very important. The repeatability of high hydrogen storage performance needs to be improved, massive production of Mg based hydrogen materials as well as the integrated storage devices should be further developed.

5. Processing technologies

As stated in Section 2.3, the mechanical properties and microstructure of Mg alloys have attracted much attention in both 2020 and 2021, indicating the significance of such research areas. Processing technologies play a vital role in the mechanical properties and microstructural development. Thus, cast technology, plastic processing technology, as well as the newly emerged additive manufacturing technology were developed in 2021. In addition, China produces over 80% primary Mg in the world. The development of technology to produce ultra-high purity Mg is of great importance. Furthermore, welding and joining of Mg alloy parts are essential for their actual application.

5.1. Preparation technology of high-purity Mg

The purity of magnesium significantly affects the performance of the alloys, such as the biocompatibility, corrosion resistance and mechanical properties. Therefore, many researchers devoted to produce high purity magnesium, much progress was made. Several innovative processes were developed to produce magnesium with super high purity of 99.999 wt.%.

Lee et al. [197] developed a novel electrolytic process to produce high-purity (99.999 wt.%) magnesium. The electrolysis of MgO was conducted using liquid tin (Sn) cathode and carbon (C) anode. The Mg-Sn alloys were obtained with a current efficiency of 86.6% at 1053 K. The high-purity Mg (99.999 wt.%) was produced from the Mg-Sn alloy by vacuum distillation at 1200 – 1300 K for a duration of 5 – 10 h. Liang et al. [198] developed one-step vacuum distillation technology to produce high purity magnesium. They designed a horizontal fractional condensing vacuum (HFCV) furnace to purify primary magnesium ingot, as shown in Fig. 9. Magnesium with purity higher than 99.999 wt.% (5 N) was collected in high temperature region and magnesium with purity higher than 99.99 wt.% (4 N) was collected in the low temperature region in one step. Yuan Tian et al. [199] investigated the distribution and evaporation principles of impurities in distilled magnesium metal using a low vacuum (8×10^4 Pa) distillation purification. The results show that the optimum preparation temperature for high-purity Mg (99.99 wt.%) is 750 °C.

5.2. Cast technology for high strength Mg alloys

In addition to the traditional permanent mold cast and sand cast, optimizing and developing the casting process is one of the important measures to obtain high-strength magnesium alloy products [200–202].

The traditional fabrication of seamless Mg-Gd-Y-Zn-Zr alloy ring parts needs to undergo complex large deformation processing, which is easy to cause cracking and the decrease of YS due to excessive strain. Ma et al. [203] prepared the ring-shaped Mg-8.5Gd-4Y-1Zn-0.4Zr (wt.%) alloy via centrifugal casting and ring-rolling process, as shown in Fig. 10. It is the first time to use centrifugal casting and ring rolling process to prepare rings for Mg-RE-Zn alloys. The outer diameter and thickness of the centrifugal cast ring are 380 mm and 21 mm, respectively. After an accumulative rolling reduction of 80% and peak aging, the UTS of this ring-rolled alloy is further enhanced, reaching 511 MPa, and the EL reaches 5.3%.

In the case of the as-cast Mg alloys, the cooling rate plays a key part in controlling the microstructure. Shaokang Guan's

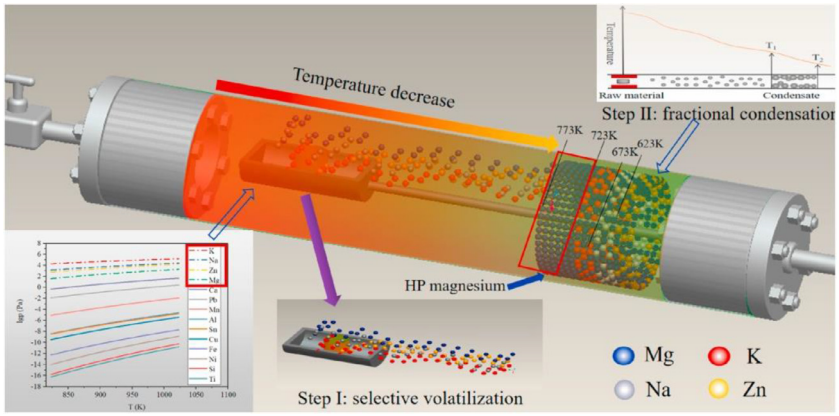

Fig. 9. The saturated vapor pressure of each element in magnesium ingot at different temperatures [198].

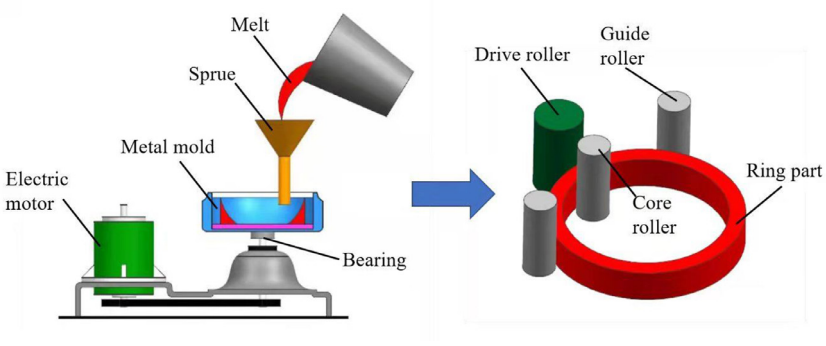

Fig. 10. Schematic diagram of centrifugal casting and ring rolling process [203].

group [204] prepared the sub-rapidly solidified Mg–Zn–Y–Nd alloy samples with diameters of 2–8 mm by step-copper mold casting. This result suggests that the sub-rapid solidification can significantly enhance the solid solubility limit of alloying elements, refine grains, and alter the type of precipitation phases. The sub-rapid solidification would be a promising technique to improve the mechanical properties of Mg alloys, which can be used as biodegradable mini-implants.

Yu et al. [205] prepared the vacuum die casting AZ91D alloy and studied the correlation of 3D defect-band morphologies and mechanical properties of the alloy. It is proved that the porosity became lower and the defect band became much less distinct with the introduction of vacuum. The average volume of porosity decreased from 8.1×10^{-6} mm^3 to 4.2×10^{-6} mm^3. The UTS and EL of vacuum-4 m/s castings continuously increased and reached 253 MPa and 7.6%, respectively.

5.3. Additive manufacturing technology of Mg alloys

Additive manufacturing (AM) technology has become significantly helpful in developing complex geometries and personalized products with a high customization freedom by computational modeling. In the past year, AM of magnesium has gained attention to overcome some issues in the processes and techniques in biomedical materials and structural materials [206–209].

5.3.1. Additive manufacturing technology of biomedical Mg alloys

Wang et al. [210] fabricated three different types of porous Mg-Nd-Zn-Zr alloy scaffolds by selective laser melting (SLM) process. The fabricated biomimetic, diamond, sheet-based gyroid scaffolds exhibit different pore structures with a unit cell size of 2 mm, 1.5 mm, 2.2 mm, respectively. By regulating the strut thickness, all scaffolds result in the same porosity of 75% and average pore size of 800 μm. Pou-Álvarez et al. [211] prepared open-porous scaffolds of WE43 Mg alloy with a body-center cubic cell pattern by laser powder bed fusion with different strut diameters. The scaffolds show excellent mechanical properties and the *in-vitro* biocompatibility tests suggest that PEO treatment is necessary to ensure cell proliferation.

Long et al. [212] reported the 3D-printed innovative multifunctional PLGA/Mg porous scaffolds for comprehensive postsurgical management of clinical treatment of Osteosarcoma (OS). The scaffolds have well interconnected macropores with a pore size around 415 ± 24 μm, and micropores ranging from 5 to 50 μm are also distributed on the strut surface of the scaffold frameworks. Dong et al. [213] developed 3D-printed customized Mg/PCL composite scaffolds with enhanced osteogenesis and biomineralization. The Mg/PCL scaffolds display a pore size of 480 ± 25 μm, a fiber diameter of 300 ± 25 μm, and a scaffold porosity of about 66%, which provide a compatible condition for tissue regen-

eration and bone healing. Marco Boi et al. [214] fabricated 3D PCL scaffolds reinforced with a novel Mg-doped bioactive glass (Mg-BG) and displayed good mechanical properties and biological reactivity. For the 50/50 composite, a fiber-fiber distance of 293 ± 14 μm and a fiber diameter of 331 ± 14 μm were obtained.

5.3.2. Additive manufacturing technology of structural Mg alloys

Salehi et al. [215] presented a detailed comparative analysis of the consolidation of as-printed Mg-5.06Zn-0.15Zr alloy parts by conventional (CT) and microwave (MW) sintering. This work enlightens the great potential of MW sintering as an attractive alternative to reduce energy consumption and shorten the lead time of the binder jetting technology. Julmi et al. [216] developed the high-quality WE43 components by laser powder bed fusion process (PBF-LB). The microstructure of the PBF-LB metal parts consisted of much more refined grains compared to as-cast parts.

Klein et al. [217] studied the microstructure and mechanical properties of a wire-arc additive manufactured AZ61A alloy. The mechanical properties lie in-between those of typical cast and wrought alloys, demonstrating the feasibility of processing Mg alloys by wire-arc additive manufacturing. Wang et al. [218] fabricated AZ31 magnesium alloy thin-wall component with 50 layers by the modified cold metal transfer-wire-arc additive manufacturing (CMT-WAAM). Compared with the as-forged and as-cast AZ31 alloy, the thin-wall component exhibits an UTS of 226 MPa and a high EL of 28.3% in the deposition direction. Liming Peng's group [219] investigated the influence of friction stir processing (FSP) and aging heat treatment on the microstructure and mechanical properties of selective laser melted (SLMed) Mg-Gd-Zr alloy. The results show that FSP can lead to porosity reduction from 0.78 to 0.015% as well as grain refinement. Wen et al. [220] reported a formation mechanism of hot cracking in laser powder bed fusion (LPBF) prepared ZK60 magnesium alloy. The hot cracking was attributed to a wide solidification temperature range, a low eutectic temperature as well as a high thermal stress. The serious solidification and liquation cracking hugely deteriorated the relative density of LPBF samples.

The 3DP (three dimensional printing) of Mg alloy is an additive manufacturing process in which bonded magnesium alloy powder by binder and then densified by sintering. This new manufacture process can rapidly produce parts with complex structures and shape. In the future this manufacture process is likely to replace some parts of the casting process. Compared with other additive manufacturing processes, the 3DP additive manufacturing process has high safety and low cost. Although this process has been relatively mature in other alloy systems, the sintering densification is still one of the difficulties in Mg alloys.

There are only 2 reports on 3DP Mg alloy in 2021, as listed in Table 18. Jingfeng Wang's group [221] developed a new sintering process which used high viscosity liquid Mg alloy to enhance the density and network-like of MgO framework structure to keep the original shape. The UCS of AZ91D Mg alloy prepared by the 3DP process can reach to 354 MPa. This means that the properties of 3DP Mg alloy can basically reach the properties of its as-cast alloy. Moreover, they introduced the two-step sintering process and combined it with the network-like of MgO framework structure [222], leading to an increased compressive strength to 393 MPa while the sintering time was significantly reduced. This proves that when the performance of 3DP magnesium alloy is close to that of as-cast magnesium alloy, and its production cost could be lower.

5.4. Plastic processing technologies of Mg alloys

5.4.1. Extrusion technology

In 2021, extrusion processes are modified to refine the microstructure and further improve the properties of magnesium alloys.

Zhou et al. [223] developed a new differential thermal equal channel angular extrusion process (DTECAP) for Mg-Sn-Zn-Zr (TZK) alloy. The TZK alloy exhibited an excellent balance of strength and ductility. Interestingly, Wang et al. [224] designated a constrained groove extrusion (CGP) process to fabricate Mg alloy sheets with improved texture, as shown in Fig. 11. A double-peak basal texture with the basal pole tilted from ND to RD appeared in the traditional CGP route, while an inclination of the basal pole from ND to TD was observed in cross-CGP routes. Dingfei Zhang's group [225] developed semi-solid extrusion (SSE) process to prepare AZ31 magnesium alloy sheets with uniform microstructure, fine grain size, weakened texture and improved mechanical properties.

5.4.2. Rolling technology

Huiyuan Wang's group [226] developed sub-rapid solidification (SRS) followed by hard plate rolling (HPR) to prepare Mg-6Zn-0.2Ca alloy sheet. Compared with the conventional solidification and combined with the HPR, it was observed that the fracture elongation increased from ~17% to ~23% without sacrificing the tensile strength (~290 MPa). This is mainly due to the refined $Ca_2Mg_6Zn_3$ eutectic phase which can effectively alleviate or avoid crack initiation. Wu et al. [227] prepared LA51/LA141 alloy composite plate with bimodal-grained microstructure by cumulative roll bonding (ARB). Due to the synergistic effect of bimodal grain microstructure and the activation of non-basal slip, the Mg-Li alloy composite sheet produced by ARB method presents a longer softening stage and thus maintains a high plasticity.

5.4.3. Forging technology

Forging processing has a wide application prospect because large samples can be readily deformed with conventional tools. Huang et al. [228] studied strain-controlled multi-pass multi-directional forging of Mg-Gd-Y-Zn-Ag-Zr alloy with dimensions of 460 mm × 260 mm × 160 mm. Zhimin Zhang's group [229] optimized the multi-directional forging (MDF) process of pre-solutionized Mg-13Gd-4Y-2Zn-0.5Zr alloy. Many plate-like Mg_5RE phases are present in 4 passes

Table 18
Sintering process and properties of the Mg alloys prepared by 3DP in 2021.

Alloys	Sintering process	Relative density%	Compressive strength MPa	Ref.
AZ91D	620 °C × 12 h	97.8	354 ± 29.7	[221]
AZ91D	680 °C × 0.5 *h* + 610 °C × 6 h	98.6	393 ± 15.8	[222]

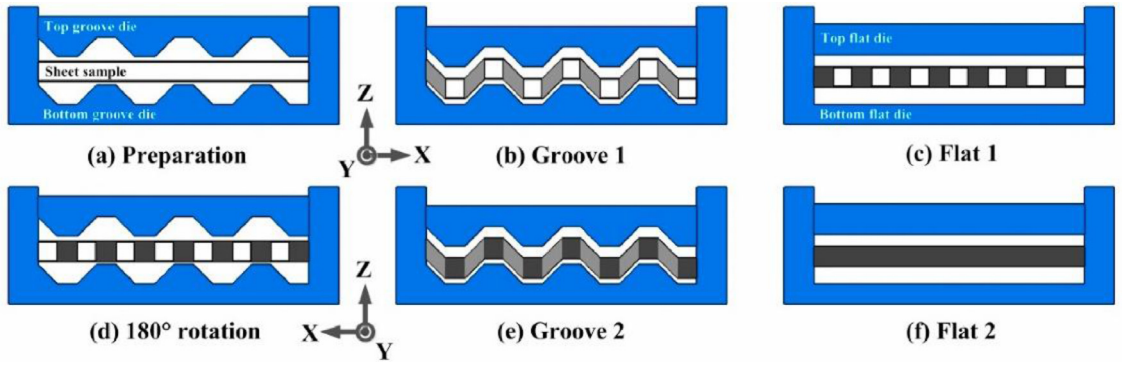

Fig. 11. Schematic illustration of CGP process [224].

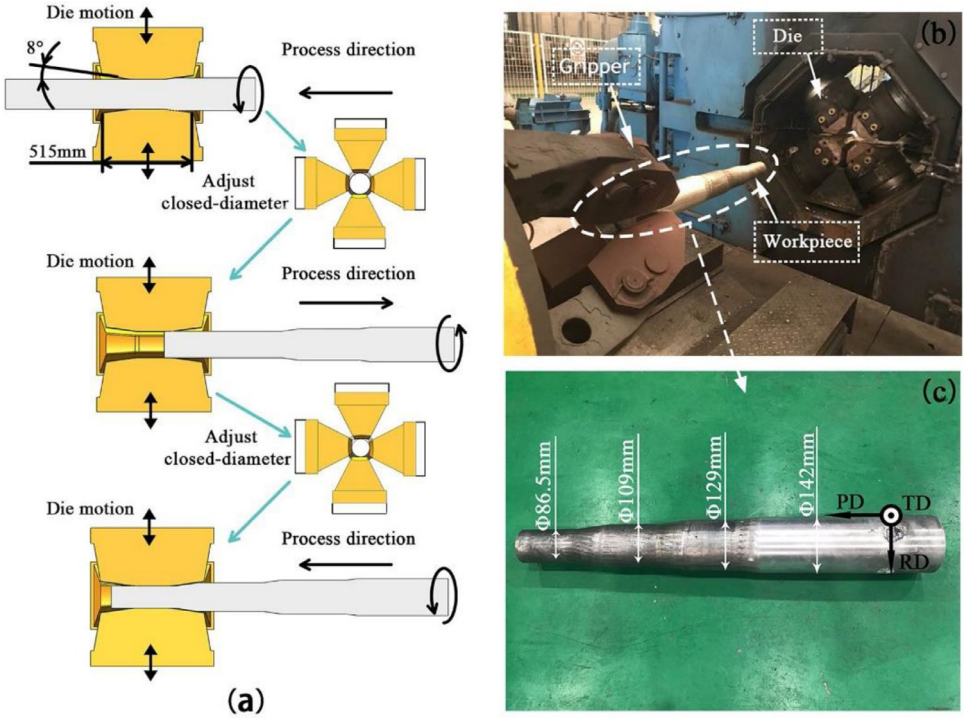

Fig. 12. Schematics of the step-ladder radial forging experiment (a), experimental equipment (b), and macroscopic morphology of the step-ladder specimen after three passes (c), where RD, PD, and TD represent the radial, processing, and tangential directions in this study, respectively [36].

in the MDFed sample. Chen et al. [230] successfully prepared high-strength Mg-Li alloy by cold rotary swaging process. The results show that nano-grains are formed in the central region of the alloy bar after five passes of swaging.

Zou et al. [36] utilized radial forging (RF) to prepare ZK60 magnesium alloy bar with step-shaft, as shown in Fig. 12. The results show that by increasing RF passes, the grains in different radial sections are gradually refined to form a bi-modal microstructure composed of coarse (~14.1 μm) and fine (~2.3 μm) grains. Besides, with increasing RF passes, the initial micro-sized β-phase is gradually broken and dissolved into the matrix, and finally evolving to form a larger area of nano-sized Zn_2Zr spherical particles, which are uniformly distributed in the grain interior. Excellent mechanical properties including higher tensile strength and ductility were obtained after three RFed passes.

5.4.4. Friction stir processing technology

Friction stir processing (FSP) is also regarded as an effective technology to improve the microstructure and enhance the

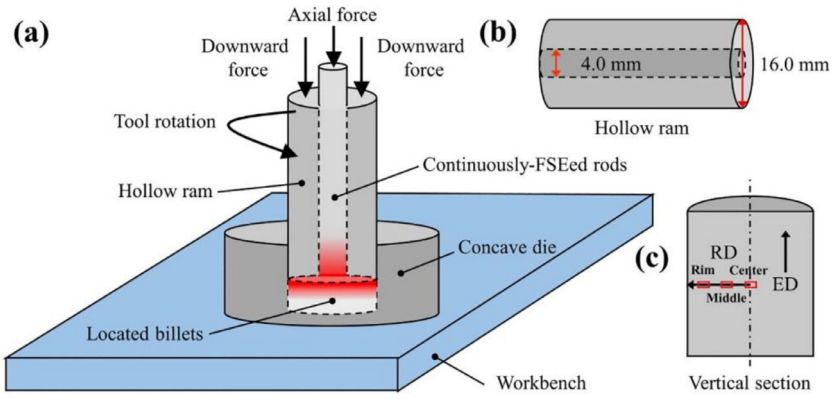

Fig. 13. Illustrations of (a) the FSE procedure, (b) the hollow ram and (c) the vertical section and sampling position. Here, ED and RD refers to the extrusion direction and the radial direction of the fabricated Mg-RE rods, respectively [234].

mechanical properties. FSP is a type of severe plastic deformation technology with high potential to be commercialized.

Xu et al. [231] modified the microstructure and mechanical properties of die-casting AZ91D by low-temperature FSP. They found that the microstructure was greatly refined by friction stirring due to continuous dynamic recrystallization, twin induced dynamic recrystallization and particle stimulated nucleation recrystallization. Luo et al. [232] improved the stretch formability of AZ61 alloy sheet by multi-pass friction stir processing (M-FSP) to an Erichsen value of 3.7 mm. This is mainly due to the grain refinement produced by M-FSP and the existence of extension twins to accommodate the deformation during Erichsen cupping test. Banglong Fu et al. [233] proposed a novel differential rotation refill friction stir spot welding (DR-refill FSSW) to improve the mechanical properties of cast Mg alloy welds. A bimodal microstructure with weakened texture compared to conventional refill FSSW was obtained, and the deformation incompatibility between the stir zone (SZ) and thermal mechanically affected zone (TMAZ) was avoided, leading to a significant increase in the tensile lap shear strength (TLSS) of the welded cast alloy. The welds have 50% higher TLSS than that of standard refill FSSW welds.

Li et al. [234] proposed a friction stir extrusion to fabricate rare-earth magnesium alloy rods with high strength and ductility, as shown in Fig. 13. In their study, the refined grains and uniform dispersion of the second phase were obtained under the coupled thermo-mechanical effect, resulting in the yield strength, ultimate strength and compression strain of the alloy increasing by 42.5%, 63.6% and 35.5%, respectively.

5.5. Welding and joining technology of Mg alloys

Welding and joining technology of magnesium alloys is a key to their engineering applications. The welding process optimization of magnesium alloys and the welding of dissimilar materials were developed in the past year.

5.5.1. Welding process

The optimization and development of welding methods and processes aim to improve the welding manufacturing efficiency, enhance product quality, and reduce the welding energy consumption and cost.

Chen et al. [235] found that the pulse current makes the microstructure transition from the SZ to the heat-affected zone (HAZ) smoother and improves the UTS and EL of EFSW joints of AZ31B Mg alloy. When the pulse current is 400A, the UTS are 286 MPa, reaching 96.4% of the base material and EL is 12.1%. Xu et al. introduced high frequency ultrasonic vibration (UV) to the arc welding of MB3 Mg alloy to reduce defects, improve weld microstructure and joint strength. The UTS of the optimized butt joint by UV treatment reached 239 MPa, which is equivalent to 93% of base metal [236]. Chang et al. [237] optimized the parameters of TIG welding with an alternating cusp-shaped magnetic field of AZ91 alloy. With an excitation current of 2 A and an excitation frequency of 80 Hz, the arc was compressed, and thus obtain a smooth weld with the largest depth-to-width ratio and fine-grained microstructure.

5.5.2. Welding of dissimilar materials

Joining of magnesium alloys with other materials such as Al alloys, steel, polymer or even different Mg alloys is quite important for the application of Mg alloy components. Thus, research was carried out on the dissimilar welding.

Fu et al. [238] utilized a novel refill friction stir spot welding (refill FSSW) to weld AZ31 Mg alloy and galvanized DP600 steel. The defect-free welds with high strength were successfully obtained in a wide window of parameters. Dileep Singh et al. [239] prepared the magnesium-steel welds by impact welding, and revealed that Fe-rich particles getting deep into the Mg matrix is conducive to the dissimilar metal joining. Liu et al. [240] studied laser welding of AZ31B magnesium alloy and DP590 dual-phase steel with concave groove joint. The mechanical property of magnesium/steel joints is improved due to the meshing effect of the concave groove and the metallurgical effect of adding Sn powders. In addition, the resistance rivet welding (RRW) was used to join Mg alloy to steel, and a metallurgical-mechanical hybrid joint was formed among the semi-tubular rivet [241].

Welding of Mg and Al were extensively investigated in the past year. Wu et al. [242,243] found that ultrasonic vibration could reduce the thickness of intermetallic compounds in the whole weld and improve the tensile strength of each part of the Al/Mg alloy welds by FSW. Acarer et al. [244] prepared Mg-Al composite by explosive welding and found that the UTS of the AZ31-Al5005 composite is 178 MPa, which is lower than that of the individual components owing to the formation of cracks. Galvanic corrosion was also observed in the joints. Kumar et al. [245] eliminated intermetallic compounds via Ni interlayer during friction stir welding of dissimilar Mg/Al alloys. The Ni can drastically cease the atomic diffusion of Mg and Al across their interfaces, eliminate typical intermetallic compounds Al_3Mg_2 and $Al_{12}Mg_{17}$, leading to the formation of Al_3Ni and Mg_2Ni compounds. In addition, Paidar et al. [246] used the modified friction stir clinching-brazing (MFSC-B) and probe-less friction stir spot brazing (PFSSB) processes to weld AA2024-T3 and AZ31 Mg alloys. The tensile shear failure load in the MFSC-B joint (4369 N) is improved due to improved material flow and intense dislocation density.

The newly developed friction stir-arc welding method was applied by Jiang et al. [247] to prepare dissimilar AM60/AZ31 joints. After the TIG arc heating, the UTS and YS of the two joints were similar, and the EL of the FSW-ARC joint was improved from 9.0 to 14.1%, which is attributed to the increase of Schmid factor for the basal slip and extension twinning caused by the weakening of the texture, the growth of the grain size and the annihilation of the residual dislocations in the NZ-middle.

Wang et al. [248] obtained AZ31–carbon fiber reinforced polymer (CFRP) joint by friction stir interlocking technique (FSI). Wang et al. [249] provided a new method for the control of welding quality in the process of riveting-welding hybrid bonding for magnesium and CFRP. The weld joints obtained by the reverse model operation have a favorable appearance, high tensile shear load and favorable plasticity.

To sum up, the centrifugal casting and the sub-rapid solidification by step-copper mold casting for high-strength Mg alloys were developed in the past year. Both bio-Mg alloys and structural Mg alloys with complex pore structure were successfully produced. However, the number of reports on 3DP Mg alloys is still far below the traditional additive manufacturing process like SLM. In addition, the commercialization of AM to prepare Mg alloy parts is still in its infancy. Current public reports mainly focused on AM of Mg alloy test coupons instead of real components. Several plastic processing technologies were reported to either improve the mechanical properties or weaken the textures. However, the commercialization and cost control of the plastic processing technologies remain a big challenge. In the aspect of joining and welding, publications are mainly seen on friction stir welding, which are used to weld Mg alloy parts with relatively simple geometry. However, argon arc welding of Mg alloys was seldom reported, although argon arc welding was extensively used in industries to repair some casting defects of large and complex Mg alloy parts.

In the future, the vacuum die casting might become the development trend for high strength Mg alloys. The 3DP Mg alloy still needs more attention and development. Special attention should be paid to additive manufacturing of large and complex Mg alloy parts with low cost and high safety. Plastic processing technologies of Mg alloys with low cost and industrialization potential are still in need. More attention is suggested to be paid to the welding of Mg alloy castings with complex morphology, since Mg alloy castings occupy over 80% market of Mg alloy parts.

6. Corrosion and protection of Mg alloy

Due to the extremely low electrode potential of Mg (−2.363 V), Mg alloys are believed to have a poor corrosion resistance and tend to have galvanic corrosion when joining with other metals. Researchers mainly attempt to understand the corrosion mechanism and explore possible ways to improve corrosion resistance of magnesium alloys. Recently, environmental corrosion of Mg alloys has been investigated to reveal the practical corrosion behavior in various service conditions, which is vital for industrialization of Mg alloys. In addition, bio-magnesium alloys have attracted increasing attention, the bio-corrosion of Mg alloys is also summarized.

6.1. Corrosion behavior of Mg alloys

6.1.1. Environmental corrosion of Mg alloys

The corrosion behavior of magnesium alloys in atmospheric environment is very different from that in laboratory accelerated tests. The atmospheric gasses, temperature, humidity and ultra-violet radiation have a significant effect on the corrosion behavior of magnesium alloys. As reviewed in the past, corrosion data of AZ31 in marine, haze and desert environments were well documented [106,107].

Jiang et al. [127] studied the corrosion behavior of Mg-Nd alloys in the South China Sea environment, and observed that NaCl deposited on the surface of Mg-Nd alloys after exposed in the marine environment, then the NaCl dissolved in high humidity environment. The electrochemical reaction between iron and magnesium alloys occurred severely and rapidly. The corrosion process can be divided into 4 steps: (1) adsorption of water vapor, (2) dissolution of NaCl and corrosive gas in water film, (3) the electrochemical reaction on the surface of specimens, and (4) surface drying-wetting alternating action. Song et al. [97] analyzed the corrosion behavior of AM60 magnesium alloy in Shenyang industrial atmospheric environment. The corrosion pitting and sediment were formed on the surface after exposure for 1 month. When the exposure time increased to 6 months, the corrosion sites greatly increased, and obvious microcracks were observed. The corrosion products of AM60 after exposure for 6 months were MgO, $Mg(OH)_2$, $MgSO_4$ and $MgCO_3$. Liu et al. [92] developed a superamphiphobic coating to improve the environmental corrosion resistance of magnesium alloys. The coating can remain superamphiphobic after ultraviolet irradiation (λ = 254 nm, 672 h), abrasion (50 cycles,1.0 kPa), sand

impact (≥10 cycles), strong acid/alkaline solution, organic solvents immersion (n-hexane, ethylene glycol, ≥48 h), high temperature (200 °C, 72 h) and acidic industrial atmosphere (Ph = 4.6, 40 d).

6.1.2. Corrosion mechanism of Mg alloys

Second phase has a complex influence on the corrosion behavior of magnesium alloy matrix. Liu et al. [250] found that the small dispersed LPSO phase of MgY3.6Zn1.2Zr0.16 alloy accelerated the micro-galvanic corrosion between the second phase and magnesium matrix and increased the hydrogen evolution rate. On the contrary, the large dominant LPSO phase of MgY2.8Zn1.9Zr0.16 alloy could provide a barrier for the magnesium matrix during corrosion and block the corrosion expansion. Zhang et al. [251] reported the Al–Si eutectic of Mg–4Li–6(Al–Si) alloy deteriorated the corrosion resistance of Mg–4Li alloy. The poor corrosion resistance was attributed to the increased micro-galvanic corrosion of the precipitates and the texture change from a basal texture to non-basal texture.

The mechanism of Mn on inhibiting magnesium alloy corrosion caused by Fe was clarified by Yang et al. [252]. The element of Fe in Mg-6Mn alloy was incorporated into Mn to form Mn (Fe) phase. With the corrosion time increased, a dense Mn-rich corrosion product film was formed on the partial surface, which can isolate the second phase and corrosive solution. Then the corrosion rate of Mg-6Mn alloy was decreased.

Merson et al. [253] studied the influence of corrosion products on stress corrosion cracking of Mg-Zn-Zr alloy in NaCl-based solutions. The embrittlement of Mg-Zn-Zr alloy after pre-exposure was related to the thickness, weight and hiding power of corrosion products. The more corrosion products deposited on the surface, the more serious the embrittlement of the specimen, which was attributed to the large volume of hydrogen in the product layer. Therefore, the removal of corrosion products from the surface of specimen pre-exposed to corrosion solution can inhibit the stress corrosion cracking of magnesium alloys.

Jia et al. [6] proposed a corrosion mechanism of AZ80 magnesium alloy with phosphate conversion coating after impaction. The corrosion occurred first at indentation areas because of the cracks and damage on the coating. With increasing immersion time to 24 h, the coating in the indentation area dropped and fell off. The coating without damage disappeared completely after immersion for 48 h.

Mg alloys have great potential to be used as biomedical materials, thus the bio-corrosion behavior in the simulated body fluid (SBF) and Dulbecco's modified eagle's medium (DMEM), etc. were extensively studied.

Sun et al. [254] studied the corrosion behavior of ZK60 magnesium alloy in SBF with different pH values. A lot of pitting occurred in the solution with a pH value of 5.2. The corrosion mechanism changed from filiform corrosion to uniform corrosion with the pH value of SBF increased from 7.4 to 9.0.Chen et al. [255] analyzed the protection capability of biodegradation product layer on Mg-1 Zn alloy. In SBF, the corrosion resistance of Mg-1 Zn decreased during dynamic strain, due to the damage of the corrosion product $Mg(OH)_2$ layer. In SBF-containing protein, the protein was spontaneously adsorbed to the degradation product layer. A stable and flexible composite anticorrosive film was formed, resulting in the improvement of corrosion resistance of magnesium alloy.

Norbert Hort's group [256] studied the degradation behavior of Mg-Nd alloys with different amounts of intermetallics in DMEM and 10% fetal bovine serum (FBS) solution. The intermetallic $Mg_{41}Nd_5$ particles in the Mg-Nd alloy affected the degradation of alloy in two opposite ways. The positive effect was related to the compact and protective corrosion product layer, the negative effect was attributed the micro-galvanic corrosion between $Mg_{41}Nd_5$ and matrix. In the early stage of degradation, the negative effect was predominant, while in the later stage of degradation, both negative and positive effects were present and jointly determined the corrosion performance. Azzeddine et al. [257] compared the corrosion behavior of binary magnesium-rare earth alloys of Mg–1.44Nd, Mg–0.3Ce, Mg–0.41Dy and Mg–0.63Gd in 2 mL DMEM with 10% FBS solution. The results show that the existence of sulfur can improve the corrosion resistance of Mg–RE alloys.

6.2. Corrosion resistance improvement of Mg alloys

Magnesium alloys are easily corroded because of the high reactivity, and the loose and porous self-corrosion products on the surface, which cannot effectively protect the matrix. Therefore, many researchers have been working on the development of new methods, materials and technologies that can delay the corrosion of magnesium alloys.

6.2.1. High-efficiency corrosion inhibitors of Mg alloys

Addition of corrosion inhibitor is one of the most effective methods to keep the Mg alloys away from the corrosion, which has the advantage of low-cost and easy operation. In 2021, corrosion inhibitors including 1-n–butyl–2-decylpyrazole bistrifluoromethanesulfonimide ([BDePz][NTf2]) [258], 1-n–butyl–2-octylpyrazole bis(trifluoromethylsulfonyl)amide ([BOPz][NTf_2]) [254], commercial corrosion inhibitors (LPS3 [259], LPS2 [259], AMLGuard [259] and Ardrox 3961 [259]), tri(bis(2-ethylhexyl)phosphate) ($Ce(DEHP)_3$) [260], Na_2MoO_4 [261], etc., were applied and the corrosion inhibition efficiencies are summarized in Table 19.

Wang et al. [262] investigated the synergistic corrosion inhibition of organic corrosion inhibitor L-Phenylalanine (L-Phe) and inorganic corrosion inhibitor ($Zn(NO_3)_2$) of AZ31B alloy in a 0.05 wt.% NaCl solution, and found that the highest inhibitory efficiency is 93.2%, which is much better than the single L-Phe-or $Zn(NO_3)_2$. The dense film containing Zn^{2+}-L-Phe-complex on the surface of magnesium alloy suppresses the corrosion of the alloy. Gao et al. [258] reported that the maximum inhibition efficiency of [BDePz][NTf_2] for AZ91D

Table 19
Corrosion inhibition efficiency of Mg alloys with different corrosion inhibitors in 2021.

Alloys	Corrosion inhibitor	Solution	Corrosion inhibition efficiency/%	Ref.
AZ31B	0.30 mM L-Phe + 0.07 mM $Zn(NO_3)_2$	0.05 wt.% NaCl	93.2	[262]
WE43	100 mM Na_2MoO_4	0.05 M NaCl	92.0	[261]
	150 mM Na_2MoO_4	0.05 M NaCl	91.0	[261]
	50 mM Na_2MoO_4	0.05 M NaCl	77.0	[261]
AZ91D	[BDePz][NTf_2]	0.05 wt.% NaCl	90.4	[258]
	[BOPz][NTf_2]	0.05 wt.% NaCl	86.0	[254]
	[BHPz][NTf_2]	0.05 wt.% NaCl	83.1	[254]
	[BDePz][NTf_2]	ASTM D1384–87	82.0	[258]

Table 20
Corrosion rates of Mg alloys in different conditions reported in 2021.

Alloys	Condition	Solution	Immersion duration/h	Corrosion rate /mm•y^{-1}	Ref.
AE42Sr1	–	3.5 wt.% NaCl + $Mg(OH)_2$	7	0.56	[271, 272]
AE42	–	3.5 wt.% NaCl+$Mg(OH)_2$	7	0.66	[271, 272]
AZ31–1.5Ca	As-cast	artificial seawater	168	0.72	[263]
AZ31	As-cast	artificial seawater	168	5.33	[263]
AZ63–0.1Y	As-cast	3.5 wt.% NaCl	5	1.49	[97, 267]
AZ63	As-cast	3.5 wt.% NaCl	5	3.67	[97, 267]
TAZE8110	hot-rolled	0.6 M NaCl	72	2.70	[273]
TAZ811	hot-rolled	0.6 M NaCl	72	19 .0	[273]
Mg-20Gd	As-cast	3.5 wt.% NaCl	24	14.97	[269]
Mg-0Gd	As-cast	3.5 wt.% NaCl	24	22.76	[269]
Mg-0.5Bi-0.5Sn-0.5Mn	As-cast	SBF	384	0.46	[266]
Mg-0.5Bi-0.5Sn	As-cast	SBF	384	7.18	[266]

in the 0.05 wt.% NaCl solution was 90.4%, which was attributed to the coverage of corrosion inhibitor to reduce the exposure area of magnesium alloy, where the insoluble small molecules reacted with corrosion products along with the hydrophobic effect of corrosion inhibitor. Aqueous molybdate provided effective corrosion inhibition of WE43 magnesium alloy in a 0.05 M NaCl solution [261]. When the concentration at and above 100 mM, the competitive adsorption of molybdate anions on the surface with the formation of a Mo(VI)-Mo(V) mixed-valence protective layer suppresses further corrosion attack.

6.2.2. Microalloying for Mg alloys

Alloying is an important way to improve the corrosion properties of magnesium alloys. In 2021, a large number of studies have been carried out to improve the corrosion resistance of Mg alloys by alloying, such as Ca [263], Mn [264–266], Y [97,267,268], Gd [269,270], Sr [271,272], Sm [273], and other alloying elements [20]. The corrosion rates are summarized in Table 20.

Adding an appropriate amount of calcium can improve the corrosion resistance of magnesium alloy. The corrosion rate of AZ31–0.5Ca was ~0.72 mm•y^{-1}, about 7.4 times lower than AZ31 alloy [263]. Chen et al. [97] improved the corrosion resistance of AZ63 alloy in 3.5 wt.% NaCl solution by adding Y and explored the mechanism as follows: (1) improving the content of Al_2O_3 in the oxide layer; (2) facilitating the intermetallic phase transformation from continuous $Mg_{17}Al_{12}$ to discrete Al_2Y phase and efficiently alleviating the micro-galvanic corrosion; (3) forming relatively continuous and dense layers. Dargusch et al. [271] found that the addition of Sr introduced a Sr-containing intermetallic phase (Mg_8Al_4Sr) into the AE42 alloy, increasing the volume fraction and continuity of the intermetallic network. The corrosion rate of the Sr-containing alloy was ~0.56 mm•y^{-1}, which is comparable to that of high-purity Mg. In addition, Sung Soo Park et al. reduced the corrosion property of hot-rolled Mg–8Sn–1Al–1 Zn alloy by S_m microalloying [273] from 19.0 to 2.7 mm•y^{-1}.

Furthermore, alloying is also utilized to improve the high-temperature oxidation resistance of magnesium alloys. Le et al. [268] investigated the effect of Y addition on high-temperature oxidation behavior and product of AZ80 alloy. The alloying element Y facilitated the transformation of loose flocculent shape oxide layer (MgO) on AZ80 surface into dense granular oxide layer ($MgCO_3$), which can prevent alloy matrix from further oxidation. High content of Gd is conducive to the formation of multi-layer films composed of Gd_2O_3-ZrO_2-MgO-cubic phases on the surface of the alloy from the inner to outside, and significantly increases the high-temperature oxidation resistance [269]. Yuan et al. [270] studied the effects of co-alloying of Ca and Gd on the high temperature oxidation of Mg alloys. They concluded that with an addition of ~0.5 wt.% Ca, Mg-3.5Gd-0.5Ca alloy is with the finest microstructure, lowest roughness and good high temperature oxidation resistance.

6.2.3. Surface treatment for Mg alloys

To suppress the corrosion of Mg alloys, many surface treatment procedures and coatings have been proposed to enhance

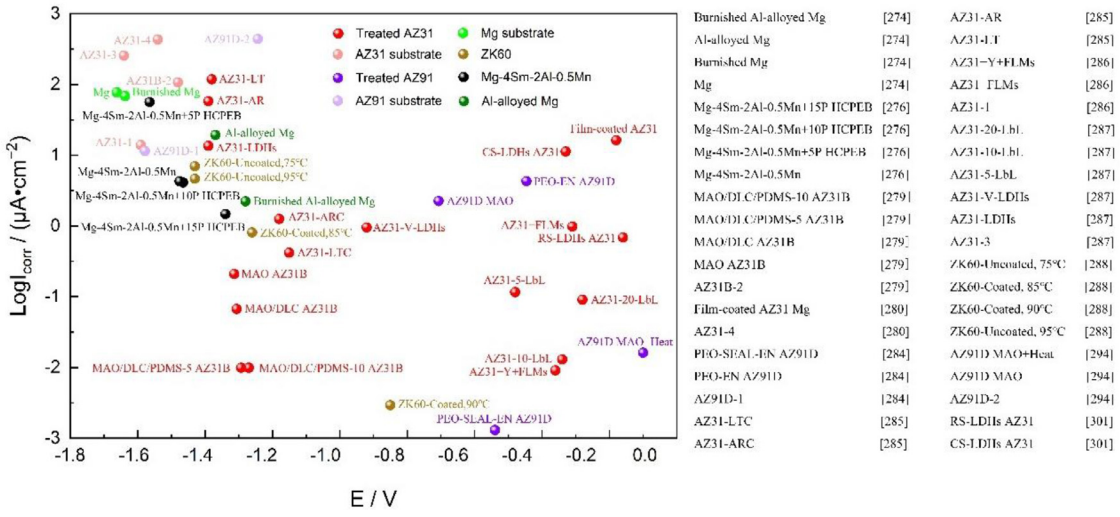

Burnished Al-alloyed Mg	[274]	AZ31-AR	[285]
Al-alloyed Mg	[274]	AZ31-LT	[285]
Burnished Mg	[274]	AZ31-Y+FLMs	[286]
Mg	[274]	AZ31-FLMs	[286]
Mg-4Sm-2Al-0.5Mn+15P HCPEB	[276]	AZ31-1	[286]
Mg-4Sm-2Al-0.5Mn+10P HCPEB	[276]	AZ31-20-LbL	[287]
Mg-4Sm-2Al-0.5Mn+5P HCPEB	[276]	AZ31-10-LbL	[287]
Mg-4Sm-2Al-0.5Mn	[276]	AZ31-5-LbL	[287]
MAO/DLC/PDMS-10 AZ31B	[279]	AZ31-V-LDHs	[287]
MAO/DLC/PDMS-5 AZ31B	[279]	AZ31-LDHs	[287]
MAO/DLC AZ31B	[279]	AZ31-3	[287]
MAO AZ31B	[279]	ZK60-Uncoated, 75°C	[288]
AZ31B-2	[279]	ZK60-Coated, 85°C	[288]
Film-coated AZ31 Mg	[280]	ZK60-Coated, 90°C	[288]
AZ31-4	[280]	ZK60-Uncoated, 95°C	[288]
PEO-SEAL-EN AZ91D	[284]	AZ91D MAO+Heat	[294]
PEO-EN AZ91D	[284]	AZ91D MAO	[294]
AZ91D-1	[284]	AZ91D-2	[294]
AZ31-LTC	[285]	RS-LDHs AZ31	[301]
AZ31-ARC	[285]	CS-LDHs AZ31	[301]

Fig. 14. Corrosion rate of magnesium alloys with different surface treatment conditions in 3.5 wt.% NaCl reported in 2021.

Table 21
Corrosion rate of magnesium alloys in different surface treatment conditions reported in 2021.

Alloys	Solution	E_{corr}/V	I_{corr}/μA•cm^{-2}	Ref.
Wrought MA8 with composite coating	MEM	– 0.180	7.60×10^{-4}	[289]
Wrought MA8 with PEO-coating	MEM	– 1.570	5.40	[289]
Bare wrought MA8	MEM	– 1.670	9.20	[289]
MgCa treated with 24 h/55 °C/pH 11	Hank's solution	–1.530	4.73	[290]
MgCa alloy	Hank's solution	–1.670	43.10	[290]
Rolled AZ31	SBF	−1.294	6.50	[278]
Rolled AZ91	SBF	−1.436	18.70	[278]
Superhydrophobic AZ91	SBF	−1.568	61.10	[278]
Superhydrophobic AZ31	SBF	−1.538	1.26×10^{2}	[278]

the corrosion resistance of Mg alloys, including surface alloying [274,275], high pulsed electron beam treatments (HCPEB) [276], laser surface melting (LSM) [277], superhydrophobic surface [5,278,279], organic coatings [280–282], nickel coating [283,284], conversion film [285–288], etc. The corrosion rate of magnesium alloys with different surface treatments in 3.5 wt.% NaCl is summarized in Fig. 14, and the bio corrosion rate is listed in Table 20. Among the developed coatings, the PEO-Seal and Ni-P composite coating on AZ91D alloy exhibited an excellent corrosion resistance of 0.001304 ± 0.000110 μA•cm^{-2} in 3.5 wt.% NaCl.

Surface alloying via thermal diffusion is a cost-effective technique to produce a Surface alloying via thermal diffusion is a cost-effective technique to produce a corrosion-resistant layer for Mg alloys. The aluminizing is the most promising approach to enhance the corrosion resistance. Song et al. [274] prepared an Al-alloyed layer through thermal diffusion on Mg surface with the passive current density of 19.4 ± 9.7 μA/cm^2, which acted as an effective barrier to protect the substrate Mg from scratching and corrosion attack. In addition, Hou et al. [275] constructed the double-layer protective film on Mg-In alloy. The formation of In-rich layer and compact $Mg(OH)_2$ film retarded the dissolution, and greatly improved the corrosion resistance of the alloy (Table 21).

Surface modification is another effective way to improve the corrosion resistance of magnesium alloys. Zhang et al. [276] modified surface of Mg-4Sm-2Al-0.5Mn alloy with HCPEB, and found that corrosion current density (I_{corr}) of the alloy treated by 15 pulses was the lowest (1.48×10^{-6} A•cm^{-2}). Besides, the effects of LSM on the microstructure and surface topography evolution in AZ31B magnesium alloy were explored by Dahotre et al. [277], and the corrosion rate of LSM AZ31B Mg samples (0.5 mm/year) was significantly lower than the untreated AZ31B (8 mm•y^{-1}). Compared with the traditional method, chemical methods have gradually become a research hotspot. Wang et al. [278] prepared superhydrophobic surfaces with tunable water adhesion on rolled Mg-3Al-1 Zn (AZ31) and Mg-9Al-1 Zn (AZ91) alloy sheets through simple chemical etching and surface modification, which is beneficial for durable anti-corrosion ability. Besides, preparing super-hydrophobic coating by homemade spraying suspension composed of the mixture of poly(methyl methacrylate) (PMMA), acetone, and stearic acid (SA)-modified ZnO nanoparticles was also a simple method [5]. Cui et al. [279] improved the performance of microarc oxidation/diamond-like carbon coating (MAO/DLC) by polydimethylsiloxane (PDMS) on AZ31B Mg alloy, with espe-

Table 22
Newly published ISO standards on magnesium and magnesium alloys in 2021.

No.	Standard No.	Name	Valid since
1	ISO 23,694:2021	Wrought Magnesium and Magnesium alloys – Extruded Rods, Bars and Tubes	2021–01–05
2	ISO 23,700:2021	Wrought Magnesium and Magnesium alloys – Rolled Plates and Sheets	2021–03–23
3	ISO 8287:2021	Magnesium and magnesium alloys — Unalloyed magnesium — Chemical composition	2021–06–09

cially high superhydrophobicity (CA = 110.5°) and corrosion resistance (i_{corr}= 9.93 × 10^{-3} μA cm^{-2}).

As one of the simplest and most economical methods to improve the corrosion resistance of magnesium, coatings including organic coating (chitosan-based [281]), inorganic coating (electrophoretic deposition film [282], Ni coating [283,284]) and conversion coating (phosphate conversion coating (PCC) [285,288], trivalent chromium conversion coating (TCC) [291], layered double hydroxide coating (LDH) [286,290,292–296], plasma electrolytic oxidation coating (PEO) [297–300]) etc., have made some progress in 2021. Yuansheng Yang's group [288] developed a PCC free of fluorine, chromium and nitrite, which showed perfect morphology and corrosion resistance. Li et al. [294] investigated the corrosion resistance of micro-arc oxidized AZ91D magnesium alloy by hydrothermal treatment, leading a decrease of corrosion rate by three orders of magnitude (3.54 × 10^{-4} mm/y). In addition, Wu et al. conducted an in-depth study on LDHs grown *in-situ* on the surface of rolled AZ31 [301] and Mg−Ca alloys [302], the LDH conversion film greatly improved the corrosion resistance of the magnesium alloys. The rare earth Ce [293], graphene oxide [303], corrosion inhibitor [304] and MXene [287] were successfully doped with LDHs, which can effectively protect the magnesium substrate from corrosion.

To meet the strict demand for corrosion resistance, the research also focuses on composite coatings. Zhou et al. [284] prepared a Ni-P composite coating on Mg alloys, and the coating with sealing treatment had excellent corrosion resistance (0.001304 $\mu A \cdot cm^{-2}$). Besides, Gnedenkov et al. [289] prepared the composite calcium-phosphate coating on MA8 Mg alloy, and the corrosion current density is 7.6 × 10^{-10} A cm^{-2}, which decreased by four orders of magnitude. In addition, Liang Wu et al. have been devoted to endow LDHs coatings with self-healing properties in order to further improve the corrosion resistance of composite coatings [305]. The yttrium-doped Mg-Al LDHs film was prepared on a magnesium alloy by a hydrothermal method. The ternary Mg-Al-Y LDHs coating was emphatically constructed, which can trap chloride ions into the interlayer in a corrosive environment, thereby triggering the stable precipitation of Y element, and had a certain self-healing ability [301].

In brief, the atmospheric temperature, gasses, humidity and ultra-violet radiation have a significant influence on the corrosion behavior of magnesium alloys. Magnesium alloys show unique corrosion behavior in South China Sea, Shenyang industrial atmosphere and high temperature environments. In addition, the second phase, intermetallic, pH values of corrosive solution and corrosion product layer have a great effect on the corrosion behavior of magnesium alloys. Corrosion resistance of magnesium alloys can be significantly improved by adding corrosion inhibitors and alloying elements or performing surface treatment. As one of the simple and efficient methods, coating has a remarkable protective effect on magnesium alloy surface. Among them, superhydrophobic coating, self-healing coating and composite coating are widely concerned by researchers, and are expected to promote the wide applications of magnesium alloys.

In the future, more studies and analyses on the corrosion behavior of magnesium alloys in different atmosphere environments are still needed. Special attention should be paid to the corrosion mechanisms of magnesium alloys. The corrosion protection technique via coatings should be further developed towards functionalization and commercialization.

7. Other progresses

7.1. Standards

In 2021, three standards are newly published which are all proposed by China, as listed in Table 22. ISO 23,694:2021, ISO 23,700:2021, and ISO 8287:2021 focused on extruded rods, bars and tubes, the rolled plates and sheets, and primary magnesium, respectively. All the three ISO standards were equally settled as British standards, which are BS ISO 23,694:2021, BS ISO 23,700:2021, BS ISO 8287:2021. The standard settlement indicates that the quality of ISO standards on magnesium is highly recognized by the Great Britain. It is anticipated that the establishment of these important international standards will pave the way for the further development and applications of magnesium and magnesium alloys in a variety of industrial sectors.

In 2021, all the five standards proposed by China were still under development and have been proceeded from CD (committee draft) stage to DIS (draft of International Standard), as listed in Table 23. ISO/CD 4155, ISO/WD 4177, ISO/CD 4181, ISO/CD 4188 and ISO/CD 4189 were proposed to measure the content of Ni, Cr, Sr, As, and Na with inductively coupled plasma atomic emission spectrometry, respectively. However, due to the current COVID situation, the interlaboratory tests of these elements in other countries were quite challenging.

7.2. Patents

The granted Mg-related patents in 2021 were searched in SooPAT with "Mg or magnesium alloy" as keyword. After

Table 23
ISO standards on magnesium and magnesium alloys under development in 2021.

No.	Standard No.	Name	New Project approved at
1	ISO/DIS 4155	Magnesium and magnesium alloys—Determination of nickel— inductively couple plasma atomic emission spectrometry	2020–02–21
2	ISO/DIS 4177	Magnesium and magnesium alloys—Determination of chromium— inductively couple plasma atomic emission spectrometry	2020–02–21
3	ISO/DIS 4181	Magnesium and magnesium alloys—Determination of Strontium— inductively couple plasma atomic emission spectrometry	2020–02–21
4	ISO/DIS 4188	Magnesium and magnesium alloys—Determination of Arsenic— inductively couple plasma atomic emission spectrometry	2020–02–21
5	ISO/DIS 4189	Magnesium and magnesium alloys—Determination of sodium— inductively couple plasma atomic emission spectrometry	2020–02–21

Note: DIS- draft of International Standard.

Table 24
Distribution of granted patents on magnesium and magnesium alloys in different countries and regions in 2021.

Countries and regions	Number
China	543
Japan	42
USA	36
South Korea	23
European patent	19
Russia	14
Canada	9
Australia	5
UK	4
Morocco	2
Other countries and regions	10

manually eliminating the irrelevant data, 707 granted patents in total were found.

According to the number of Mg-related granted patents published in 2021, the top 10 countries and regions of the granted patens are listed in Table 24. China granted the most patents on Mg and Mg alloys, followed by Japan, the United States, South Korea and Europe. In addition, many papers on magnesium and magnesium alloys have been published in these countries, indicating that they value the academic and industrial development of magnesium and magnesium alloys.

7.3. International awards

In 2021, both International Mg Society (IMS) and International Magnesium (IMA) Association issued awards on magnesium and magnesium alloys. Both awards are of great importance to the R&D and application of magnesium and magnesium alloys.

IMS issued the 2021 International Mg Science and Technology Award (Annual Award). Eight types of awards were conferred to 27 winners who have made significant contributions to the magnesium R&D and application. These awards covered many aspects including magnesium smelting, Mg-based structural materials, Mg-based functional materials and so on. The award effectively promoted the discussion and communication between scientists, young researchers, and students, stimulated the interaction and cooperation between universities, research institutes and enterprises, boosted the development and application of magnesium and magnesium alloy science and technology, and provided a long-term platform for international communication and cooperation.

IMA issued five types of awards, which are Automotive Cast Product/Process, Commercial Cast Product/Process, Process, Wrought Product, and Environmental Responsibility. The award effectively boosted the application and industrial development of magnesium and magnesium alloys.

7.4. Other industrial progress

Magnesium and magnesium alloy industry have attracted much attention in 2021. Many mega enterprises are very interested in joining in the Mg industry, indicating that Mg and Mg alloys have great application potential. Baosteel Metal Co., Ltd. plans to invest 18.2 billion Yuan to promote the R&D and industrilization of Mg and Mg alloys. In additon, Baosteel and Chongqing University co-established a 'Joint Research and Development Center for Advanced Magnesium Technology', with the aim to promote the high-quality development of China's magnesium industry. Guangdong National Technology Co., Ltd plans to invest 500 million Yuan in 5 years in total to the 'Development and Application of Solid-State Magnesium-Based Hydrogen Storage Materials and Technology' as well as R&D of magnesium-ion-based batteries. Western Magnesium Corporation in the United States plans to invest 1 billion dollors to build a primary Mg production base, which aims to produce 100,000 ton primary Mg. In 2021, the location of the production base is chosen as Harrison in the Ohio State.

8. Summary and outlook

The publications on magnesium and magnesium alloys continue to increase in the past 20 years, indicating that research and development of magnesium alloys have attracted more and more attention. According to the bibliometric analysis, microstructures, mechanical properties, and corrosion of magnesium alloys are the main research focus. The emerging research hot spots involve mainly energy storage magnesium materials, such as Mg ion batteries, hydrogen storage Mg materials.

In the structural Mg alloys, some new progress are made in cast and wrought Mg alloys. In the case of cast Mg alloys, a Mg-3Nd-4.5Gd-0.2Zn-0.5Zr alloy with an UTS of 343 MPa, and an EL of 5.4% was developed. In the case of wrought alloys, an UTS of 448 MPa, and EL of 15% can be achieved in commercial AZ61 alloy via 'ECAP+EPT' technology. It is of great importance to commercialize such a technology for the industrialization of Mg and Mg alloys. Furthermore, a new spinodal decomposition strengthening mechanism was reported in ultralight Mg-Li-Al alloys.

Functional magnesium materials such as bio-magnsium alloys and energy storage Mg materials have made some new progress. In the case of bio-magnesium alloys, a new Resoloy rare earth Mg–Dy alloy for biodegradable cardiovascular stents application is developed, which is a good alternative to CE approved WE43 alloy. In the case of Mg batteries, a family of methoxyethyl-amine chelants has been developed, which could tune solvation structure of simple $Mg(TFSI)_2$/DME electrolyte, improving the interfacial charge transfer kinetics and suppressing the passivation reaction. Additionally, rechargeable magnesium soft-pack cells were successfully assembled. In the case of hydrogen strorage materials, ultrafine MgH_2 nanoparticles were successfully synthesized, which reached 6.7 wt.% reversible storage of hydrogen at 30 °C. A lot of catalysts, such as TiFe, Ti_3C_2, Ni/ Ti_3C_2 and so on, were found to improve the thermodynamic and kinetic properties of MgH_2.

Although much progress has been made on the research and development of magnesium alloys, there are still some challenges limiting the massive application of magnesium and magnesium alloys. In the case of Mg materials development, mechanical properties of structual magnesium alloys at both room temperature and elevated temperature, and the industrialization of Mg batteries, hydrogen storage Mg materials need to be improved. In the aspact of processing technologies, the microstructual evolution and heat treatment of vacuum die castings, the cost and safety of additive manufacturing of large complex Mg alloy parts, plastic processing technologies with low cost and industrialization potential, and welding of castings with complex morphology requires extentive invesitigation. In the case of corrosion and protection of Mg alloys, the high corrosion-resistant magnesium alloys and effective surface treatment of magnesium alloys should be further developed to meet the application requirements on most occasions, the environmental corrosion behavior of Mg alloys needs more attention.

Acknowledgments

The authors would like to thank the experts worldwide (including Dr. Liang Wu, Dr. Jia She, Dr. Jianbo Li, and Dr. Shuangshuang Tan, etc.) who have contributed to this review by providing important information and commenting on the preparation. The financial support from the Guangdong Major Project of Basic and Applied Basic Research (2020B0301030006), National Natural Science Foundation of China (NSFC) (No. 52071036), Key Research and Development Program of Zhejiang Province (No. 2021C01086), and the Fundamental Research Funds for the Central Universities Project (Nos. 2021CDJCGJ009, SKLMT-ZZKT-2021M11) is also gratefully acknowledged.

References

[1] N.A. Ali, M. Ismail, Advanced hydrogen storage of the Mg–Na–Al system: a review, J. Magnes. Alloys 9 (4) (2021) 1111–1122.
[2] R. Chaharmahali, A. Fattah-Alhosseini, K. Babaei, Surface characterization and corrosion behavior of calcium phosphate (Ca-P) base composite layer on Mg and its alloys using plasma electrolytic oxidation (PEO): a review, J. Magnes. Alloys 9 (1) (2021) 21–40.
[3] S. Farshid, M. Kharaziha, Micro and nano-enabled approaches to improve the performance of plasma electrolytic oxidation coated magnesium alloys, J. Magnes. Alloys 9 (5) (2021) 1487–1504.
[4] A. Javaid, F. Czerwinski, Progress in twin roll casting of magnesium alloys: a review, J. Magnes. Alloys 9 (2) (2021) 362–391.
[5] Q. Li, Y. Lu, Q. Luo, et al., Thermodynamics and kinetics of hydriding and dehydriding reactions in Mg-based hydrogen storage materials, J. Magnes. Alloys 9 (6) (2021) 1922–1941.
[6] X. Jia, J. Song, B. Xiao, et al., Influence of indentation size on the corrosion behaviour of a phosphate conversion coated AZ80 magnesium alloy, J. Mater. Res. Technol. 14 (2021) 1739–1753.
[7] A. Malik, Y. Wang, C. Huanwu, et al., Post deformation analysis of the ballistic impacted magnesium alloys, a short-review, J. Magnes. Alloys 9 (5) (2021) 1505–1520.
[8] M. Molaei, K. Babaei, A. Fattah-Alhosseini, Improving the wear resistance of plasma electrolytic oxidation (PEO) coatings applied on Mg and its alloys under the addition of nano- and micro-sized additives into the electrolytes: a review, J. Magnes. Alloys 9 (4) (2021) 1164–1186.
[9] K.B. Nie, X.J. Wang, K.K. Deng, et al., Magnesium matrix composite reinforced by nanoparticles – a review, J. Magnes. Alloys 9 (1) (2021) 57–77.
[10] Y. Nie, J. Dai, X. Li, et al., Recent developments on corrosion behaviors of Mg alloys with stacking fault or long period stacking ordered structures, J. Magnes. Alloys 9 (4) (2021) 1123–1146.
[11] F. Peng, D. Zhang, X. Liu, et al., Recent progress in superhydrophobic coating on Mg alloys: a general review, J. Magnes. Alloys 9 (5) (2021) 1471–1486.
[12] P. Sekar, N. S, V. Desai, Recent progress in in vivo studies and clinical applications of magnesium based biodegradable implants – a review, J. Magnes. Alloys 9 (4) (2021) 1147–1163.
[13] N. Sezer, Z. Evis, M. Koç, Additive manufacturing of biodegradable magnesium implants and scaffolds: review of the recent advances and research trends, J. Magnes. Alloys 9 (2) (2021) 392–415.
[14] Y. Shang, C. Pistidda, G. Gizer, et al., Mg-based materials for hydrogen storage, J. Magnes. Alloys 9 (6) (2021) 1837–1860.
[15] Z.Z. Shi, H.T. Chen, K. Zhang, et al., Crystallography of precipitates in Mg alloys, J. Magnes. Alloys 9 (2) (2021) 416–431.
[16] Y. Sun, H. Helmholz, R. Willumeit-Römer, Preclinical in vivo research of magnesium-based implants for fracture treatment: a systematic review of animal model selection and study design, J. Magnes. Alloys 9 (2) (2021) 351–361.
[17] F. Tong, S. Wei, X. Chen, et al., Magnesium alloys as anodes for neutral aqueous magnesium-air batteries, J. Magnes. Alloys 9 (6) (2021) 1861–1883.
[18] V. Tsakiris, C. Tardei, F.M Clicinschi, Biodegradable Mg alloys for orthopedic implants – a review, J. Magnes. Alloys 9 (6) (2021) 1884–1905.
[19] G. Wu, C. Wang, M. Sun, et al., Recent developments and applications on high-performance cast magnesium rare-earth alloys, J. Magnes. Alloys 9 (1) (2021) 1–20.
[20] J. Xie, J. Zhang, Z. You, et al., Towards developing Mg alloys with simultaneously improved strength and corrosion resistance via RE alloying, J. Magnes. Alloys 9 (1) (2021) 41–56.

[21] H. Xie, G. Wu, X. Zhang, et al., The role of Gd on the microstructural evolution and mechanical properties of Mg-3Nd-0.2Zn-0.5Zr alloy, Mater. Charact. 175 (2021) 111076–111094.
[22] F. Qi, X. Zhang, G. Wu, et al., High cycle fatigue behavior and mechanical performance of a novel sand-cast Mg-Nd-Gd alloy: effect of heat treatment, Mater. Sci. Eng. A 813 (2021) 141172–1411187.
[23] H. Xie, G. Wu, X. Zhang, et al., Microstructural Characteristics and Mechanical Properties of Cast Mg–3Nd–3Gd–xZn–0.5Zr Alloys, Acta Metall. Sin. (2021) 1–19 (English Letters).
[24] S. Zhu, T.B. Abbott, J.F. Nie, et al., *Re*-evaluation of the mechanical properties and creep resistance of commercial magnesium die-casting alloy AE44, J. Magnes. Alloys 9 (5) (2021) 1537–1545.
[25] H. Xie, G. Wu, X. Zhang, et al., The role of Yb content on the microstructural evolution and mechanical characteristics of cast Mg-9Gd-0.5Zn-0.2Zr alloy, Mater. Sci. Eng. A 817 (2021) 1–16.
[26] Y. Bai, B. Ye, L. Wang, et al., A novel die-casting Mg alloy with superior performance: study of microstructure and mechanical behavior, Mater. Sci. Eng. A 802 (2021) 1–10.
[27] P.F. Qin, Q. Yang, Y.Y. He, et al., Microstructure and mechanical properties of high-strength high-pressure die-cast Mg–4Al–3La–1Ca–0.3Mn alloy, Rare Met. 40 (10) (2021) 2956–2963.
[28] X. Zhao, Z. Li, W. Zhou, et al., Effect of Al content on microstructure, thermal conductivity, and mechanical properties of Mg–La–Al–Mn alloys, J. Mater. Res. 36 (15) (2021) 3145–3154.
[29] J. Cui, T. Luo, Y. Li, et al., Fluidity, Microstructure, and Tensile Properties of Sub-rapidly Solidified Mg-6Al-4Zn-xSn (x = 0, 0.6, 1.2, 1.8) Alloy, Acta Metall. Sin. 34 (9) (2021) 1265–1276 (English Letters).
[30] A. Gungor, A. Incesu, Effects of alloying elements and thermomechanical process on the mechanical and corrosion properties of biodegradable Mg alloys, J. Magnes. Alloys 9 (1) (2021) 241–253.
[31] S. Sanyal, M. Paliwal, T.K. Bandyopadhyay, et al., Evolution of microstructure, phases and mechanical properties in lean as-cast Mg–Al—Ca–Mn alloys under the influence of a wide range of Ca/Al ratio, Mater. Sci. Eng. A 800 (2021) 1–16.
[32] X. Dong, L. Feng, S. Wang, et al., A new die-cast magnesium alloy for applications at higher elevated temperatures of 200–300 °C, J. Magnes. Alloys, 9 (1) (2021) 90–101.
[33] Y.G. Jung, W. Yang, Y.J. Kim, et al., Effect of Ca addition on the microstructure and mechanical properties of heat-treated Mg-6.0Zn-1.2Y-0.7Zr alloy, J. Magnes. Alloys 9 (5) (2021) 1619–1631.
[34] J. Yang, W. Wang, M. Zhang, et al., Effects of Gd/Nd ratio on the microstructures and tensile creep behavior of Mg–8Al–Gd–Nd alloys crept at 423K, J. Mater. Res. Technol., 14 (2021) 2522–2533.
[35] L. Guo, J. Yuan, J. Pei, et al., Study of the microstructure, bonding evolution and mechanical properties of continuously extruded magnesium AZ31 sheet, Mater. Sci. Eng. A (2021) 141456–141465.
[36] J. Zou, L. Ma, W. Jia, et al., Microstructural and mechanical response of ZK60 magnesium alloy subjected to radial forging, J. Mater. Sci. Technol. 83 (2021) 228–238.
[37] X. Zhang, S. Li, X. Guo, et al., Effects of texture and twinning on the torsional behavior of magnesium alloy solid rod: a crystal plasticity approach in comparison with uniaxial tension/compression, Int. J. Mech. Sci. 191 (2021) 106062–106071.
[38] Z. Shan, J. Yang, J. Fan, et al., Extraordinary mechanical properties of AZ61 alloy processed by ECAP with 160° channel angle and EPT, J. Magnes. Alloys 9 (2) (2021) 548–559.
[39] Z.HA.M. Li Y K, J. Rong, et al., Effect of large thickness-reduction on microstructure evolution and tensile properties of Mg-9Al-1Zn alloy processed by hard-plate rolling, J. Mater. Sci. Technol. 88 (2021) 215–225.
[40] Z. Zhang, L. Yuan, D. Shan, et al., The quantitative effects of temperature and cumulative strain on the mechanical properties of hot-extruded AZ80 Mg alloy during multi-directional forging, Mater. Sci. Eng. A 827 (2021) 142036–142047.
[41] L.I.S Zhao X, Y. Zheng, et al., The microstructure evolution, texture weakening mechanism and mechanical properties of AZ80 Mg alloy processed by repetitive upsetting-extrusion with reduced deformation temperature, J. Alloys Compd. 883 (2021) 160871–160885.
[42] J. Zou, L. Ma, Y. Zhu, et al., Deformation mechanism of ZK60 magnesium bars during radial forging: mathematical modeling and experimental investigation, Mater. Charact. 179 (2021) 111321–111333.
[43] R. Ma, S. Lv, Z. Xie, et al., Achieving high strength-ductility in a wrought Mg–9Gd–3Y–0.5 Zr alloy by modifying with minor La addition, J. Alloys Compd. 884 (2021) 161062–161074.
[44] N. Su, Y. Wu, Q. Deng, et al., Synergic effects of Gd and Y contents on the age-hardening response and elevated-temperature mechanical properties of extruded Mg–Gd (-Y)-Zn-Mn alloys, Mater. Sci. Eng. A, 810 (2021) 141019–141031.
[45] Y. Zhuang, Y. Zhang, Q. Zeng, et al., Coupling the semi-solid treatment and hot extrusion to strengthen a Mg-Zn-Gd alloy containing I-phase, Mater. Lett. 287 (2021) 129294–129298.
[46] J. Zheng, Z. Chen, Z. Yan, et al., An alternating ageing-annealing process for enhancing strength and ductility of a Mg-Gd-Y-Zn-Zr alloy, Mater. Sci. Eng. A 828 (2021) 142103–142117.
[47] L. Tong, J. Chu, W. Sun, et al., Achieving an ultra-high strength and moderate ductility in Mg–Gd–Y–Zn–Zr alloy via a decreased-temperature multi-directional forging, Mater. Charact. 171 (2021) 110804–110814.
[48] R.G. Li, Y.Q. Dai, P.F. Song, et al., Simultaneous enhancement of strength and ductility by aging treatment in fine-grained Mg-13Gd alloy, Mater. Sci. Eng. A 818 (2021) 141441–141449.
[49] Z. Yang, A. Ma, B. Xu, et al., Development of a high-strength Mg–11Gd–2Ag (wt.%) alloy sheet with extra-low anisotropy, Mater. Sci. Eng. A, 811 (2021) 141084–141094.
[50] Z. Yang, C. Xu, T. Nakata, et al., Effect of extrusion ratio and temperature on microstructures and tensile properties of extruded Mg-Gd-Y-Mn-*Sc* alloy, Mater. Sci. Eng. A 800 (2021) 140330–140340.
[51] G.L. Bi, Y. Wang, J. Jiang, et al., Microstructure and mechanical properties of extruded Mg-Y-Zn (Ni) alloys, J. Alloys Compd. 881 (2021) 160577–160588.
[52] B. Dong, X. Che, Z. Zhang, et al., Comparison of the microstructure evolution and mechanical properties via MDF and ITMT methods, J. Alloys Compd. 881 (2021) 160561–160570.
[53] L. Zheng, X. Zhang, H. Wang, et al., Synergistic effect of LPSO and eutectic phase on mechanical properties of Mg-Gd-Nd-Zn-Zr alloy during equal channel angular pressing, J. Mater. Res. Technol. 15 (2021) 2459–2470.
[54] B. Du, Z. Hu, L. Sheng, et al., Microstructural characteristics and mechanical properties of the hot extruded Mg-Zn-Y-Nd alloys, J. Mater. Sci. Technol. 60 (2021) 44–55.
[55] H. Pan, L.I.J Xie D, et al., Development of novel lightweight and cost-effective Mg–Ce–Al wrought alloy with high strength, Mater. Res. Lett. 9 (8) (2021) 329–335.
[56] J. Zong, J. Zhao, X. Wang, et al., Local atomic structures of Gd and Zn atoms in extruded Mg-Gd-Zn alloys, Scr. Mater. 195 (2021) 113720–113725.
[57] X. Huang, M. Bian, I. Nakatsugawa, et al., Simultaneously achieving excellent mechanical properties and high thermal conductivity in a high Mn-containing Mg-Zn-Ca-Al-Mn sheet alloy, J. Alloys Compd. 887 (2021) 161394–161402.
[58] Y. Gui, Y. Cui, H. Bian, et al., Deformation behavior of Mg-5Y-2Nd-0.5Zr alloys with different Sm additions, J. Alloys Compd. 856 (2020) 158201 150213.
[59] M. Li, D. Xie, J. Li, et al., Realizing ultra-fine grains and ultra--high strength in conventionally extruded Mg-Ca-Al-Zn-Mn alloys: the multiple roles of nano-precipitations, Mater. Charact. 175 (2021) 111049–111056.
[60] X. Chen, D. Zhang, J. Xu, et al., Improvement of mechanical properties of hot extruded and age treated Mg–Zn–Mn–Ca alloy through Sn addition, J. Alloys Compd. 850 (2021) 156711–156724.
[61] D. Zhang, D. Zhang, T. Xu, et al., Achieving high-strength in Mg-0.8Zn-0.2Zr (wt.%) alloy extruded at low temperature, Mater. Sci. Eng. A 822 (6374) (2021) 141657–141663.
[62] H. Yan, X. Gong, J. Chen, et al., Microstructure, texture characteristics, mechanical and bio-corrosion properties of high strain rate rolled Mg–Zn–Sr alloys, Met. Mater. Int. 27 (7) (2021) 2249–2263.

[63] P.Y. Wang, J.G. Wang, H.L. Jia, et al., Development of high strength and formability Mg-6Zn-0.2 Ca alloy via multi-pass warm rolling and aging treatment, Mater. Sci. Eng. A 819 (2021) 141452–141459.
[64] H.Z. Liu, C.L. Lu, X.C. Wang, et al., Combinations of V2C and Ti3C2 MXenes for boosting the hydrogen storage performances of MgH2, ACS Appl. Mater. Interfaces 13 (11) (2021) 13235–13247.
[65] B.J. Lv, S. Wang, T.W. Xu, et al., Effects of minor Nd and Er additions on the precipitation evolution and dynamic recrystallization behavior of Mg–6.0 Zn–0.5 Mn alloy, J. Magnes. Alloys 9 (3) (2021) 840–852.
[66] M. Bian, X. Huang, Y. Chino, Substantial improvement in cold formability of concentrated Mg–Al–Zn–Ca alloy sheets by high temperature final rolling, Acta Mater. 220 (2021) 117328–117340.
[67] J. Wang, G. Zhu, L. Wang, et al., Origins of high ductility exhibited by an extruded magnesium alloy Mg-1.8Zn-0.2 Ca: experiments and crystal plasticity modeling, J. Mater. Sci. Technol. 84 (2021) 27–42.
[68] J. Wang, L. Xu, R. Wu, et al., Simultaneous achievement of high electromagnetic shielding effectiveness (X-band) and strength in Mg-Li-Zn-Gd/MWCNTs composite, J. Alloy Compd. 882 (2021) 160524–160539.
[69] T. Zhou, Q. Zhang, Q. Li, et al., A simultaneous enhancement of both strength and ductility by a novel differential-thermal ECAP process in Mg-Sn-Zn-Zr alloy, J. Alloys Compd. 889 (2021) 161653–161665.
[70] B. Lei, B. Jiang, H. Yang, et al., Effect of Nd addition on the microstructure and mechanical properties of extruded Mg-Gd-Zr alloy, Mater. Sci. Eng. A 816 (7) (2021) 141320–141330.
[71] M. Sabbaghian, R. Mahmudi, K.S Shin, Microstructural evolution, mechanical properties, and biodegradability of a Gd-containing Mg-Zn alloy, Metall. Mater. Trans. A Phys. Metall. Mater. Sci. 52 (4) (2021) 1269–1281.
[72] J. Zhao, B. Jiang, Q. Wang, et al., Influence of Ce content on the microstructures and tensile properties of Mg-1Gd-0.5Zn alloys, Mater. Sci. Eng. A 823 (2021) 141675–141684.
[73] J. Wang, G. Zhu, L. Wang, et al., Origins of high ductility exhibited by an extruded magnesium alloy Mg-1.8Zn-0.2Ca: experiments and crystal plasticity modeling, J. Mater. Sci. Technol. 84 (C) (2021) 27–42.
[74] C. Liu, X. Chen, J. Chen, et al., The effects of Ca and Mn on the microstructure, texture and mechanical properties of Mg-4Zn alloy, J. Magnes. Alloys 9 (3) (2021) 1084–1097.
[75] D. Zhao, R. Shi, P. Evans, et al., On the exceptionally high ductility of Mg–2Zn-0.3Ca-0.2Ce-0.1Mn alloy, Mater. Sci. Eng. A 819 (12) (2021) 141484–141490.
[76] D. Zhao, G. Li, P. Li, et al., A comparative study on the microstructures and mechanical properties of the Mg-xCa/Mn/Ce alloys and pure Mg, Mater. Sci. Eng. A (2020) 140508–140517.
[77] L. Tong, J. Chu, W. Sun, et al., Development of a high-strength Mg alloy with superior ductility through a unique texture modification from equal channel angular pressing, J. Magnes. Alloys 9 (3) (2021) 1007–1018.
[78] L.I.Y He D, Y. Zheng, et al., Effects of Ga content on the microstructure and mechanical properties of as-extruded Mg-xGa alloys, J. Alloys Compd. (2021) 161317–161330.
[79] W.J. Ma K, J. Ren, et al., Enhanced degradation properties of Mg-Y-Ni alloys by tailoring the LPSO morphology for fracturing tools applications, Mater. Charact. 181 (2021) 111489–111500.
[80] X. Wang, Z. Chen, X. Liu, et al., The role of Ga in the microstructure, corrosion behavior and mechanical properties of as-extruded Mg–5Sn–xGa alloys, J. Alloys Compd. 863 (7) (2021) 158762–158773.
[81] Z.M. Hua, B.Y. Wang, C. Wang, et al., Development of low-alloyed Mg–Zn–Ca–Sn–Mn alloy with high strength-ductility synergy by sub-rapid solidification and hot rolling, J. Alloys Compd. 855 (2021) 157317–157327.
[82] Y. Luo, Y. Chen, L. Ran, et al., Effects of Zn/Al mass ratio on microstructure evolution and mechanical properties of Mg-Sn based alloys, Mater. Sci. Eng. A 815 (6) (2021) 141307–141320.
[83] C. Sun, H. Liu, X. Wang, et al., Microstructure evolution during superplastic deformation process and its impact on superplastic behavior of a Mg-Gd-Y-Zn-Zr alloy, Mater. Charact. 172 (2021) 110879–110894.
[84] A. Malik, Y. Wang, C. Huanwu, et al., Superplastic behavior of fine-grained extruded ZK61 Mg alloy, Results Phys. 20 (2021) 103731–103738.
[85] Z. Liu, X. Zhao, K. Chen, et al., Microstructural Evolution and Anisotropic Weakening Mechanism of ZK60 Magnesium Alloy Processed by Isothermal Repetitive Upsetting Extrusion, Acta Metall. Sin. (2021) 1–14 (English Letters).
[86] D. Chen, J. Kong, Z. Gui, et al., High-temperature superplastic behavior and ECAP deformation mechanism of two-phase Mg-Li alloy, Mater. Lett. 301 (2021) 130358–130362.
[87] T. Xin, Y. Zhao, R. Mahjoub, et al., Ultrahigh specific strength in a magnesium alloy strengthened by spinodal decomposition, Sci. Adv. 7 (23) (2021) 1–10.
[88] Y. Yang, X. Chen, J. Nie, et al., Achieving ultra-strong Magnesium-lithium alloys by low-strain rotary swaging, Mater. Res. Lett. 9 (6) (2021) 255–262.
[89] F. Cao, C. Sun, H. Shang, et al., Microstructure evolution and mechanical properties in an ultralight Mg-2.76 Li–3Al-2.6Zn-0.39 Y alloy, Mater. Sci. Eng. A, 822 (2021) 141680–141693.
[90] S. Zhang, X. Ma, R. Wu, et al., Effect of Sn alloying and cold rolling on microstructure and mechanical properties of Mg14Li alloy, Mater. Charact. 182 (2021) 111491 111399.
[91] P. Wang, Z. Chen, H. Huang, et al., Fabrication of Ti/Al/Mg laminated composites by hot roll bonding and their microstructures and mechanical properties, Chin. J. Aeronaut. 34 (8) (2021) 192–201.
[92] L.I.X Liu L, J. Lei, et al., Superamphiphobic Magnesium Alloys with Extraordinary Environmental Adaptability, Langmuir 37 (14) (2021) 4267–4275.
[93] M. Guo, S. Li, J. Han, et al., Effect of temperature on interface microstructure and mechanical properties of corrugated rolled Mg /Al composite plate, J. Plasticity Eng. 28 (05) (2021) 234–241.
[94] M. Bian, X. Huang, N. Saito, et al., Improving mechanical properties of an explosive-welded magnesium/aluminum clad plate by subsequent hot-rolling, J. Alloys Compd. 898 (2022) 162957–162967.
[95] H.W. Wang, C.J. Wang, K.K. Deng, et al., Microstructure and mechanical properties of Al/Mg/Al composite sheets containing trapezoidal shaped intermediate layer, Mater. Sci. Eng. A 811 (2021) 1–11.
[96] Q. Jiang, D. Lu, N. Wang, et al., The corrosion behavior of Mg–Nd binary alloys in the harsh marine environment, J. Magnes. Alloys 9 (1) (2021) 292–304.
[97] Y. Song, D. Liu, W. Tang, et al., Comparison of the corrosion behavior of AM60 Mg alloy with and without self-healing coating in atmospheric environment, J. Magnes. Alloys 9 (4) (2021) 1220–1232.
[98] X. Chen, W.Z. Wang, J.L. Zhang, et al., Tailoring AZ91 laminates for combination of strength and ductility, Trans. Nonferr. Met. Soc. Chin. 31 (12) (2021) 3703–3718.
[99] S. Bai, G. Fang, B. Jiang, et al., Investigation into atomic diffusion at the interface during extrusion welding of magnesium and magnesium alloys, Metall. Mater. Trans. A 52 (9) (2021) 422242 33.
[100] X. Tong, G. Wu, L. Zhang, et al., Achieving low-temperature Zr alloying for microstructural refinement of sand-cast Mg-Gd-Y alloy by employing zirconium tetrachloride, Mater. Charact. 171 (2021).
[101] S.Q. Yang, C.B. Li, G. Luo, et al., Mg adsorption on MgAl2O4 surfaces and the effect of additive Ca: a combined experimental and theoretical study, J. Alloys Compd. 861 (2021) 158564–158573.
[102] J. Cui, T. Luo, C. Wang, et al., Evolution of the microstructure and microsegregation in subrapidly solidified Mg–6Al–4Zn–1.2Sn magnesium alloy, Adv. Eng. Mater. 23 (2) (2021) 1–8.
[103] J. Cui, T. Luo, Y. Li, et al., Fluidity, Microstructure, and tensile properties of sub-rapidly solidified Mg-6Al-4Zn-xSn (x = 0, 0.6, 1.2, 1.8) alloy, Acta Metall. Sin. 34 (9) (2021) 1265–1276 English letters.
[104] H. Xie, G. Wu, X. Zhang, et al., The role of Yb content on the microstructural evolution and mechanical characteristics of cast Mg-9Gd-0.5Zn-0.2Zr alloy, Mater. Sci. Eng. A 817 (2021) 1–16.

[105] M. Bian, X. Huang, Y. Chino, Solute segregation assisted grain boundary precipitation and its impact to ductility of a precipitation-hardenable magnesium alloy, Mater. Sci. Eng. A 819 (2021) 141481–141487.
[106] Y. Yang, X. Xiong, J. Chen, et al., Research advances in magnesium and magnesium alloys worldwide in 2020, J. Magnes. Alloys 9 (3) (2021) 705–747.
[107] J. Song, J. She, D. Chen, et al., Latest research advances on magnesium and magnesium alloys worldwide, J. Magnes. Alloys 8 (1) (2020) 1–41.
[108] J. Zhang, Z. Chang, Z. Zhang, et al., Current design strategies for rechargeable magnesium-based batteries, ACS Nano 15 (10) (2021) 15594–15624.
[109] L. Han, Z. Zhang, J. Dai, et al., The influence of alternating cyclic dynamic loads with different low frequencies on the bio-corrosion behaviors of AZ31B magnesium alloy in vitro, Bioact. Mater. 7 (2022) 263–274.
[110] G. Uppal, A. Thakur, A. Chauhan, et al., Magnesium based implants for functional bone tissue regeneration – a review, J. Magnes. Alloys, (2021) 1–11.
[111] I. Antoniac, R. Adam, A. Biță, et al., Comparative assessment of *in vitro* and *in vivo* biodegradation of Mg-1Ca magnesium alloys for orthopedic applications, Materials 14 (1) (2021) 1–20 (Basel).
[112] Y. Hu, D. Dong, X. Wang, et al., Synthesis and properties of Mg-Mn-Zn alloys for medical applications, Materials 14 (8) (2021) 1–18 (Basel).
[113] B.S. Liu, M.M. Cao, Y.Z. Zhang, et al., Microstructure, anticorrosion, biocompatibility and antibacterial activities of extruded Mg−Zn−Mn strengthened with Ca, Trans. Nonferr. Met. Soc. Chin. 31 (2) (2021) 358–370.
[114] M. Rahmati, S. Stötzel, T.E. Khassawna, et al., Early osteoimmunomodulatory effects of magnesium–calcium–zinc alloys, J. Tissue Eng. 12 (2021) 1–19.
[115] X. Wang, Y. Zhang, E. Guo, et al., In vitro investigation on microstructure, bio-corrosion properties and cytotoxicity of as-extruded Mg–5Sn–xIn alloys, J. Alloys Compd. 877 (2021) 160294–160306.
[116] K. Saksl, I. Pethes, P. Jóvári, et al., Atomic structure of the Mg66Zn30Ca4 metallic glass, J. Non Cryst. Solids 558 (2021) 120660–120669.
[117] W. Weng, A. Biesiekierski, Y. Li, et al., A review of the physiological impact of rare earth elements and their uses in biomedical Mg alloys, Acta Biomater. 130 (2021) 80–97.
[118] J. Dou, J. Wang, Y. Lu, et al., Bioactive MAO/CS composite coatings on Mg-Zn-Ca alloy for orthopedic applications, Prog. Org. Coat. 152 (2021) 106112–106123.
[119] M. Zarka, B. Dikici, M. Niinomi, et al., A systematic study of β-type Ti-based PVD coatings on magnesium for biomedical application, Vacuum 183 (2021) 109850–109860.
[120] H. Helmholz, O. Will, T. Penate-Medina, et al., Tissue responses after implantation of biodegradable Mg alloys evaluated by multimodality 3D micro-bioimaging *in vivo*, J. Biomed. Mater. Res. Part A 109 (8) (2021) 1521–1529.
[121] R. Menze, E. Wittchow, *In vitro* and *in vivo* evaluation of a novel bioresorbable magnesium scaffold with different surface modifications, J. Biomed. Mater. Res. Part B Appl. Biomater. 109 (9) (2021) 1292–1302.
[122] J. Lötscher, A.A. Martí I Líndez, N. Kirchhammer, et al., Magnesium sensing via LFA-1 regulates CD8+ T cell effector function, Cell (2021) 1–11.
[123] H. Yang, L. Wu, B. Jiang, et al., Clarifying the roles of grain boundary and grain orientation on the corrosion and discharge processes of α-Mg based Mg-Li alloys for primary Mg-air batteries, J. Mater. Sci. Technol. 62 (2021) 128–138.
[124] Y.H. Chen, W.L. Cheng, X.J. Gu, et al., Discharge performance of extruded Mg-Bi binary alloys as anodes for primary Mg-air batteries, J. Alloys Compd. 886 (2021) 161271–161283.
[125] X.R. Chen, H.N. Wang, Q. Zou, et al., The influence of heat treatment on discharge and electrochemical properties of Mg-Gd-Zn magnesium anode with long period stacking ordered structure for Mg-air battery, Electrochim. Acta (2021) 367–376.
[126] H.B. Yang, L. Wu, B. Jiang, et al., Discharge properties of Mg-Sn-Y alloys as anodes for Mg-air batteries, Int. J. Miner. Metall. Mater. 28 (10) (2021) 1705–1715.
[127] Q. Jiang, D. Lu, N. Wang, et al., The corrosion behavior of Mg–Nd binary alloys in the harsh marine environment, J. Magnes. Alloys 9 (1) (2021) 292–304.
[128] X.Y. Dong, J.X. Wang, J.D. Yang, et al., $CuMnO_2$ nanoflakes as cathode catalyst for oxygen reduction reaction in magnesium-air battery, J. Electrochem. Soc. 168 (10) (2021) 1–7.
[129] H. Liu, J.X. Zhang, H.J. Fang, et al., Synthesis of delta-MnO2/reduced graphene oxide hybrid *in situ* and application in Mg-air battery, J. Electrochem. Soc. 168 (8) (2021) 1–14.
[130] K.W. Leong, Y.F. Wang, W.D. Pan, et al., Doubling the power output of a Mg-air battery with an acid-salt dual-electrolyte configuration, J. Power Sources 506 (2021) 1–9.
[131] L.H. Li, H. Chen, E. He, et al., High-energy-density magnesium-air battery based on dual-layer gel electrolyte, Angew. Chem. Int. Ed. 60 (28) (2021) 15317–15322.
[132] R. Mohtadi, O. Tutusaus, T.S. Arthur, et al., The metamorphosis of rechargeable magnesium batteries, Joule 5 (3) (2021) 581–617.
[133] S. Tan, F. Xiong, J. Wang, et al., Crystal regulation towards rechargeable magnesium battery cathode materials, Mater. Horiz. 7 (8) (2020) 1971–1995.
[134] Q. Guo, W. Zeng, S.L. Liu, et al., Recent developments on anode materials for magnesium-ion batteries: a review, Rare Met. 40 (2) (2021) 290–308.
[135] Y. Zhao, A. Du, S. Dong, et al., A Bismuth-based protective layer for magnesium metal anode in noncorrosive electrolytes, ACS Energy Lett. 6 (7) (2021) 2594–2601.
[136] R. Zhang, C. Cui, R. Li, et al., An artificial interphase enables the use of Mg (TFSI) 2-based electrolytes in magnesium metal batteries, Chem. Eng. J. (2021) 130751–130759.
[137] H. Dou, X. Zhao, Y. Zhang, et al., Revisiting the degradation of solid/electrolyte interfaces of magnesium metal anodes: decisive role of interfacial composition, Nano Energy 86 (2021) 106087–106098.
[138] X. Wen, Z. Yu, Y. Zhao, et al., Enabling magnesium anodes by tuning the electrode/electrolyte interfacial structure, ACS Appl. Mater. Interfaces 13 (44) (2021) 52461–52468.
[139] Z. Li, T. Diemant, Z. Meng, et al., Establishing a stable anode–electrolyte interface in Mg batteries by electrolyte additive, in: ACS Appl. Mater. Interfaces, 13, 2021, pp. 33123–33132.
[140] J.H. Kwak, Y. Jeoun, S.H. Oh, et al., Operando visualization of morphological evolution in Mg metal anode: insight into dendrite suppression for stable Mg metal batteries, ACS Energy Lett.s 7 (2020) 162–170.
[141] J. Bae, H. Park, X. Guo, et al., High-performance magnesium metal battery via switching passivation film into solid electrolyte interphase, Energy Environ. Sci. (2021) 4391–4399.
[142] Z. Song, Z. Zhang, A. Du, et al., Uniform magnesium electrodeposition via synergistic coupling of current homogenization, geometric confinement, and chemisorption effect, Adv. Mater. 33 (24) (2021) 2100224–2100235.
[143] M. Song, J. Niu, W. Cui, et al., Self-healing liquid Ga-based anodes with regulated wetting and working temperatures for advanced Mg ion batteries, J. Mater. Chem. A 9 (31) (2021) 17019–17029.
[144] C. Pei, F. Xiong, Y. Yin, et al., Recent progress and challenges in the optimization of electrode materials for rechargeable magnesium batteries, Small 17 (3) (2021) 2004108–2004138.
[145] X. Yang, C. Du, Y. Zhu, et al., Constructing defect-rich unconventional phase Cu7. 2S4 nanotubes via microwave-induced selective etching for ultra-stable rechargeable magnesium batteries, Chem. Eng. J. 430 (2022) 133108–133117.
[146] Y. Shen, Q. Zhang, Y. Wang, et al., A pyrite iron disulfide cathode with a copper current collector for high-energy reversible magnesium-ion storage, Adv. Mater. 33 (41) (2021) 2103881–2103890.
[147] J. Huang, Y. Zhu, C. Du, et al., Hierarchical nanosheet-assembled copper sulfide microspheres as the cathode materials for rechargeable magnesium batteries, Electrochim. Acta 388 (2021) 138619–138627.

[148] Q. Zhang, Y. Hu, J. Wang, et al., CuCo2S4/CuS@ MWCNTs composite as a cathode for rechargeable magnesium-ion batteries with long cycle life, J. Phys. Chem. C 125 (36) (2021) 19673–19681.
[149] S. Ding, Z. Li, X. Dai, et al., Mo-doped VS4 with interlayer-expanded and engineering sulfur vacancies as cathode for advanced magnesium storage, Chem. Eng. J. 417 (2021) 129328–129338.
[150] Y. Zhang, Y. Zhu, Z. Wang, et al., Pulverization-tolerant CuSe nanoflakes with high (110) planar orientation for high-performance magnesium storage, Adv. Funct. Mater. 31 (46) (2021) 2104730–2104744.
[151] K. Shimokawa, T. Atsumi, N.L. Okamoto, et al., Structure design of long-life spinel-oxide cathode materials for magnesium rechargeable batteries, Adv. Mater. 33 (7) (2021) 2007539–2007548.
[152] C. Zuo, W. Tang, B. Lan, et al., Unexpected discovery of magnesium–vanadium spinel oxide containing extractable Mg^{2+} as a high-capacity cathode material for magnesium ion batteries, Chem. Eng. J. 405 (2021) 127005–127013.
[153] C. Zuo, Y. Xiao, X. Pan, et al., Organic-inorganic superlattices of vanadium oxide@ polyaniline for high-performance magnesium-ion batteries, ChemSusChem 14 (9) (2021) 2093–2099.
[154] S. Rubio, Z. Liang, X. Liu, et al., Reversible multi-electron storage enabled by Na5V (PO4) 2F2 for rechargeable magnesium batteries, Energy Storage Mater. 38 (2021) 462–472.
[155] J. Wang, S. Tan, G. Zhang, et al., Fast and stable Mg 2+ intercalation in a high voltage NaV 2 O 2 (PO 4) 2 F/rGO cathode material for magnesium-ion batteries, Sci. Chin. Mater. 63 (9) (2020) 1651–1662.
[156] Y. Sun, Q. Zou, W. Wang, et al., Non-passivating anion adsorption enables reversible magnesium redox in simple non-nucleophilic electrolytes, ACS Energy Lett. 6 (10) (2021) 3607–3613.
[157] R. Horia, D.T Nguyen, A.Y.S. Eng, et al., Using a chloride-free magnesium battery electrolyte to form a robust anode–electrolyte nanointerface, Nano Lett. 21 (19) (2021) 8220–8228.
[158] S. Hou, X. Ji, K. Gaskell, et al., Solvation sheath reorganization enables divalent metal batteries with fast interfacial charge transfer kinetics, Science 374 (6564) (2021) 172–178.
[159] P. Jankowski, Z. Li, Z. Zhao-Karger, et al., Development of magnesium borate electrolytes: explaining the success of Mg [B (hfip) 4] 2 salt, Energy Storage Mater. (2021) 1–12.
[160] W. Ren, D. Wu, Y. Nuli, et al., An efficient Bulky Mg [B (Otfe) 4] 2 electrolyte and its derivatively general design strategy for rechargeable magnesium batteries, ACS Energy Lett. 6 (9) (2021) 3212–3220.
[156] L. Ma, Y. Lv, J. Wu, et al., Recent advances in emerging non-lithium metal–sulfur batteries: a review, Adv. Energy Mater. (2021) 2100770–2100798.
[162] D.T Nguyen, R. Horia, A.Y.S. Eng, et al., Material design strategies to improve the performance of rechargeable magnesium–sulfur batteries, Mater. Horiz. 8 (3) (2021) 830–853.
[163] Y. Xu, Y. Zhao, S. Zhao, et al., Reversible function switching of Ag catalyst in Mg/S battery with chloride-containing electrolyte, Energy Storage Mater. 42 (2021) 513–516.
[164] Q. Zhao, R. Wang, Y. Zhang, et al., The design of Co3S4@ MXene heterostructure as sulfur host to promote the electrochemical kinetics for reversible magnesium-sulfur batteries, J. Magnes. Alloys 9 (1) (2021) 78–89.
[165] Q. Zou, Y. Sun, Z. Liang, et al., Achieving efficient magnesium–sulfur battery chemistry via polysulfide mediation, Adv. Energy Mater. 11 (31) (2021) 2101552–2101560.
[166] H.O. Ford, E.S. Doyle, P. He, et al., Self-discharge of magnesium–sulfur batteries leads to active material loss and poor shelf life, Energy Environ. Sci. 14 (2) (2021) 890–899.
[167] X. Ding, R.R. Chen, X.Y. Chen, et al., Study on the eutectic formation and its correlation with the hydrogen storage properties of Mg98Ni2-xLax alloys, Int. J. Hydrog. Energy 46 (34) (2021) 17814–17826.
[168] Y.H. Zhang, H.F. Sun, W. Zhang, et al., A comparison study of hydrogen storage performances of as-cast La10-xRExMg80Ni10 (x=0 or 3; RE = Sm or Ce) alloys, J. Alloy Compd. 884 (2021) 1–13.
[169] J.H. He, J. Zhang, X.J. Zhou, et al., Hydrogen storage properties of Mg98.5Gd1Zn0.5 and Mg98.5Gd0.5Y0.5Zn0.5 alloys containing LPSO phases, Int. J. Hydrog. Energy 46 (65) (2021) 32949–32961.
[170] J.W. Mao, T.P. Huang, S. Panda, et al., Direct observations of diffusion controlled microstructure transition in Mg-In/Mg-Ag ultrafine particles with enhanced hydrogen storage and hydrolysis properties, Chem. Eng. J. 418 (2021) 129301–129311.
[171] M. Peska, K. Smektalska, J. Dworecka-Wojcik, et al., Hydrogen sorption behavior of mechanically synthesized Mg-Ag alloys, Int. J. Hydrog. Energy 46 (66) (2021) 33152–33163.
[172] L.J. Huang, H. Wang, L.Z. Ouyang, et al., Achieving fast hydrogenation by hydrogen-induced phase separation in Mg-based amorphous alloys, J. Alloy Compd. 887 (2021) 161476–161484.
[173] X. Zhang, Y.F. Liu, Z.H. Ren, et al., Realizing 6.7 wt% reversible storage of hydrogen at ambient temperature with non-confined ultrafine magnesium hydrides, Energy Environ. Sci. 14 (4) (2021) 2302–2313.
[174] D.J. Han, S. Kim, E.S Cho, Revealing the role of defects in graphene oxide in the evolution of magnesium nanocrystals and the resulting effects on hydrogen storage, J. Mater. Chem. A 9 (15) (2021) 9875–9881.
[175] S.S. Samantaray, P. Anees, V.B. Parambath, et al., Graphene supported MgNi alloy nanocomposite as a room temperature hydrogen storage material - Experiments and theoretical insights, Acta Mater. 215 (2021) 117040–117052.
[176] C.X. Zhu, M. Chen, M.M. Hu, et al., Hydrogen storage properties of Mg-Nb@C nanocomposite: effects of Nb nanocatalyst and carbon nanoconfinement, Int. J. Hydrog. Energy 46 (14) (2021) 9443–9451.
[177] X. Lu, L.T. Zhang, H.J. Yu, et al., Achieving superior hydrogen storage properties of MgH2 by the effect of TiFe and carbon nanotubes, Chem. Eng. J. 422 (2021) 130101–130123.
[178] X.J. Hou, L. Yang, K.M. Hou, et al., Hydrolysis hydrogen generation medium regulated by alkali metal cations for Mg-based alloy–Green seawater modification strategy, J. Power Sources 509 (2021) 230364–230374.
[179] J. Zhang, S. Yan, G.L. Xia, et al., Stabilization of low-valence transition metal towards advanced catalytic effects on the hydrogen storage performance of magnesium hydride, J. Magnes. Alloys 9 (2) (2021) 647–657.
[180] Z.H. Tian, Z.X. Wang, P.F. Yao, et al., Hydrogen storage behaviors of magnesium hydride catalyzed by transition metal carbides, Int. J. Hydrog. Energy 46 (80) (2021) 40203–40216.
[181] H.G. Gao, R. Shi, J.L. Zhu, et al., Interface effect in sandwich like Ni/Ti3C2 catalysts on hydrogen storage performance of MgH2, Appl. Surf. Sci. 564 (2021) 150302–150310.
[182] M.B. Pang, S.I. Hong, S.I. Ri, et al., Effects of different substitution concentration and configuration on some properties of magnesium hydrides substituted with titanium; Ab initio study, Int. J. Hydrog. Energy 46 (21) (2021) 11824–11831.
[183] G. Liu, L. Wang, Y. Hu, et al., Enhanced catalytic effect of TiO2@rGO synthesized by one-pot ethylene glycol-assisted solvothermal method for MgH2, J. Alloy Compd. 881 (2021) 160644–160656.
[184] Y. Guo, Y. Shi, R. Yuan, et al., Inhibition mechanism of capacity degradation in Mg-substituted LaY2-xMgxNi9 hydrogen storage alloys, J. Alloy Compd. 873 (2021) 1–8.
[185] X. Lin, W. Xie, Q. Zhu, et al., Rational optimization of metal hydride tank with LaNi4.25Al0.75 as hydrogen storage medium, Chem. Eng. J. 421 (2021) 127844–127854.
[186] D. Wang, S. Liu, R. Wu, et al., Synergistically improved damping, elastic modulus and mechanical properties of rolled Mg-8Li-4Y-2Er-2Zn-0.6 Zr alloy with twins and long-period stacking ordered phase, J. Alloys Compd. (2021) 160663–160671.
[187] T. Tu, X. Chen, T. Chen, et al., New high-modulus and high--strength Mg-Gd-Ag-Mn-Ge alloys, Mater. Sci. Eng. A 805 (2021) 140559–140567.
[188] D. Zhao, X. Chen, J. Li, et al., Microstructure, texture and mechanical properties of the rolled high modulus Mg-Y-Zn-Al-Li alloy, Mater. Sci. Eng. A 831 (2022) 142242–142254.

[189] L. Liu, S. Yu, E. Liu, et al., Effect of Ni addition on the mechanical and degradation properties of hollow glass microsphere/Mg alloy composites, J. Alloy Compd. 853 (2021) 157125–157136.
[190] J. Wang, T. Li, H.X. Li, et al., Effect of trace Ni addition on microstructure, mechanical and corrosion properties of the extruded Mg–Gd–Y–Zr–Ni alloys for dissoluble fracturing tools, J. Magnes. Alloys 9 (5) (2021) 1632–1643.
[191] W.J. Ma K, J. Ren, et al., Enhanced degradation properties of Mg-Y-Ni alloys by tailoring the LPSO morphology for fracturing tools applications, Mater. Charact. 181 (2021) 111489–111500.
[192] K. Ma, S. Liu, C. Dai, et al., Effect of Ni on the microstructure, mechanical properties and corrosion behavior of MgGd1Nix alloys for fracturing ball applications, J. Mater. Sci. Technol. 91 (2021) 121–133.
[193] J. Wang, S. Gao, X. Liu, et al., Enhanced mechanical properties and degradation rate of Mg–Ni–Y alloy by introducing LPSO phase for degradable fracturing ball applications, J. Magnes. Alloys 8 (1) (2020) 127–133.
[194] J. Wang, K. Ma, S. Liu, et al., Effect of Ni on the microstructure, mechanical properties and corrosion behavior of MgGd1Nix alloys for fracturing ball applications, J. Mater. Sci. Technol. 91 (2020) 121–133.
[195] J. Ye, X. Chen, Z. Luo, et al., Improving strength and electromagnetic shielding effectiveness of Mg–Sn–Zn–Ca–Ce Alloy by Sn addition, Adv. Eng. Mater. 23 (9) (2021) 1–7.
[196] G. Zhang, S. Qin, L. Yan, et al., Simultaneous improvement of electromagnetic shielding effectiveness and corrosion resistance in magnesium alloys by electropulsing, Mater. Charact. 174 (2021) 111042–111054.
[197] T.H. Lee, T.H. Okabe, J.Y. Lee, et al., Development of a novel electrolytic process for producing high-purity magnesium metal from magnesium oxide using a liquid tin cathode, J. Magnes. Alloys 9 (5) (2021) 1644–1655.
[198] D. Liang, Y. Tian, B. Yang, et al., One-step preparation of high purity magnesium by vacuum distillation technology, Vacuum 192 (2021) 160464–160469.
[199] Y. Tian, X. Zhang, T. Qu, et al., Technical research on vacuum distillation to purify magnesium to 99.99% purity, Mater. Res. Express 8 (5) (2021) 1–11.
[200] P. Emadi, B. Andilab, C. Ravindran, Preparation and characterization of AZ91E/Al2O3 composites using hybrid mechanical and ultrasonic particle dispersion, Mater. Sci. Eng. A Struct. Mater. Prop. Microstruct. Process 819 (2021) 141505–141516.
[201] F. Wen, J. Zhao, M. Yuan, et al., Influence of Ni interlayer on interfacial microstructure and mechanical properties of Ti-6Al-4V/AZ91D bimetals fabricated by a solid-liquid compound casting process, J. Magnes. Alloy 9 (4) (2021) 1382–1395.
[201] S. Kandemir, S. Gavras, H. Dieringa, High temperature tensile, compression and creep behavior of recycled short carbon fibre reinforced AZ91 magnesium alloy fabricated by a high shearing dispersion technique, J. Magnes. Alloys 9 (5) (2021) 1753–1767.
[203] Z. Ma, G. Li, Q. Peng, et al., Microstructural evolution and enhanced mechanical properties of Mg–Gd–Y–Zn–Zr alloy via centrifugal casting, ring-rolling and aging, J. Magnes. Alloy (2021) 1–10.
[204] Z.W. Gong, J.F. Wang, Y.F. Sun, et al., Microstructure and mechanical properties of the sub-rapidly solidified Mg-Zn-Y-Nd alloy prepared by step-copper mold casting, Mater. Today Commun. 27 (2021) 102308–102317.
[205] W. Yu, C. Ma, Y. Ma, et al., Correlation of 3D defect-band morphologies and mechanical properties in high pressure die casting magnesium alloy, J. Mater. Process. Technol. 288 (2021) 116853–116862.
[206] R. Allavikutty, P. Gupta, T.S. Santra, et al., Additive manufacturing of Mg alloys for biomedical applications: current status and challenges, Curr. Opin. Biomed. Eng. 18 (2021) 1–9.
[207] N. Sezer, Z. Evis, M. Koc, Additive manufacturing of biodegradable magnesium implants and scaffolds: review of the recent advances and research trends, J. Magnes. Alloy 9 (2) (2021) 392–415.
[208] N. Madhuri, V. Jayakumar, M. Sathishkumar, Recent developments and challenges accompanying with wire arc additive manufacturing of Mg alloys: a review, in: Proceedings of the 3rd International Conference on Materials, Manufacturing and Modelling (ICMMM), 46, Vellore, INDIA, Elsevier, 2021, pp. 8573–8577. F Mar 19-21[C]AMSTERDAM2021.
[209] V. Herber, B. Okutan, G. Antonoglou, et al., Bioresorbable magnesium-based alloys as novel biomaterials in oral bone regeneration: general review and clinical perspectives, J. Clin. Med. 10 (9) (2021) 1–19.
[210] Y.C. Wang, H. Huang, G.Z. Jia, et al., Fatigue and dynamic biodegradation behavior of additively manufactured Mg scaffolds, Acta Biomater. 135 (2021) 705–722.
[211] P. Pou-Álvarez, A. Riveiro, X.R. Nóvoa, et al., Corrosion control: laser-guided corrosion control: a new approach to tailor the degradation of Mg-alloys, Small 17 (18) (2021) 2170080–2170090.
[212] J. Long, W. Zhang, Y.Q. Chen, et al., Multifunctional magnesium incorporated scaffolds by 3D-printing for comprehensive post-surgical management of osteosarcoma, Biomaterials 275 (2021) 120950–120963.
[213] Q.S. Dong, M. Zhang, X.X. Zhou, et al., 3D-printed Mg-incorporated PCL-based scaffolds: a promising approach for bone healing, Mater. Sci. Eng. C Mater. Biol. Appl. 129 (2021) 112443–112445.
[214] M. Petretta, A. Gambardella, M. Boi, et al., Composite scaffolds for bone tissue regeneration based on PCL and Mg-containing bioactive glasses, Biology 10 (5) (2021) 398–416 Basel.
[215] M. Salehi, S.H. Li, M. Gupta, et al., Rapid densification of additive manufactured magnesium alloys via microwave sintering, Addit. Manuf. 37 (2021) 101655–101666.
[216] S. Julmi, A. Abel, N. Gerdes, et al., Development of a laser powder bed fusion process tailored for the additive manufacturing of high--quality components made of the commercial magnesium alloy WE43, Materials 14 (4) (2021) 1–19 (Basel).
[217] T. Klein, A. Arnoldt, M. Schnall, et al., Microstructure formation and mechanical properties of a wire-arc additive manufactured magnesium alloy, JOM 73 (4) (2021) 1126–1134.
[218] P. Wang, H.Z. Zhang, H. Zhu, et al., Wire-arc additive manufacturing of AZ31 magnesium alloy fabricated by cold metal transfer heat source: processing, microstructure, and mechanical behavior, J. Mater. Process. Technol. 288 (2021) 116895–116907.
[219] Q.C. Deng, Y.J. Wu, N. Su, et al., Influence of friction stir processing and aging heat treatment on microstructure and mechanical properties of selective laser melted Mg-Gd-Zr alloy, Addit. Manuf. 44 (2021) 102036–102049.
[220] J.G. Liu, B.Z. Yin, Z.R. Sun, et al., Hot cracking in ZK60 magnesium alloy produced by laser powder bed fusion process, Mater. Lett. 301 (2021) 130283–130287.
[221] C. Su, J. Wang, J. Li, et al., Mechanical and corrosion performance of Mg alloy via 3DP by full liquid phase sintering, Powder Technol. (2022) 117138–117148.
[222] C. Su, J. Wang, H. Li, et al., Binder-jetting additive manufacturing of Mg alloy densified by two-step sintering process, J. Manuf. Process 72 (2021) 71–79.
[223] T. Zhou, F. Guo, Q. Zhang, et al., Offsetting strength-ductility tradeoff in Mg-Sn-Zn-Zr alloy by a novel differential-thermal ECAP process, Mater. Lett. 305 (2021) 130764–130768.
[224] W.T. Wang Z, Y. Guan, et al., Effect of strain path on microstructure and mechanical properties of AZ31 magnesium alloy sheets processed by constrained groove pressing, Mater. Sci. Eng. A 804 (2021) 140794–140812.
[225] J. Feng, D. Zhang, H. Hu, et al., Improved microstructures of AZ31 magnesium alloy by semi-solid extrusion, Mater. Sci. Eng. A 800 (2021) 140204–140212.
[226] Z.Z. Jin, M. Zha, H.L. Jia, et al., Balancing the strength and ductility of Mg-6Zn-0.2Ca alloy via sub-rapid solidification combined with hard-plate rolling, J. Mater. Sci. Technol. 81 (2021) 219–228.
[227] H. Wu, Y. Wang, R. Wu, et al., Microstructure, Mechanical Properties and Strain Hardening Behavior of Alternative α/β Mg-Li Composite Sheets Prepared by Accumulative Roll Bonding, Met. Mater. Int. (2021) 1–13.
[228] C. Huang, C. Liu, S. Jiang, et al., Inhomogeneous microstructure and mechanical anisotropy of multi-directional forged Mg-Gd-Y-Zn-Ag-Zr alloy, Mater. Sci. Eng. A 807 (2021) 140853–140863.

[229] B. Dong, X. Che, Z. Zhang, et al., Microstructure evolution and microhardness of Mg-13Gd-4Y–2Zn-0.5Zr alloy via pre-solution and multi-directional forging (MDF) process, J. Alloys Compd. 853 (2021) 157066–157078.
[230] X. Chen, C. Liu, S. Jiang, et al., Fabrication of nanocrystalline high--strength magnesium−lithium alloy by rotary swaging, Adv. Eng. Mater. (2021) 1–7.
[231] N. Xu, R.N. Feng, Q.N. Song, et al., Influence of heterogeneous microstructures on the mechanical properties of low-temperature friction stir processed AZ91D Mg alloy, Mater. Sci. Eng. A 809 (2021) 141004–141015.
[232] X. Luo, H. Liu, L. Kang, et al., Stretch formability of an AZ61 alloy plate prepared by multi-pass friction stir processing, Materials 14 (12) (2021) 3168–3179 (Basel).
[233] B. Fu, J. Shen, U.F.H.R. Suhuddin, et al., Revealing joining mechanism in refill friction stir spot welding of AZ31 magnesium alloy to galvanized DP600 steel, Mater. Des. 209 (2021) 109997–110005.
[234] J. Li, X. Meng, Y. Li, et al., Friction stir extrusion for fabricating Mg-RE alloys with high strength and ductility, Mater. Lett. 289 (2021) 116912–116921.
[235] S.J. Chen, L. Wang, X.Q. Jiang, et al., Microstructure and mechanical properties of AZ31B Mg alloy fabricated by friction stir welding with pulse current, J. Manuf. Process. 71 (2021) 3173 -28.
[236] C. Xu, X.J Yuan, Effect of ultrasonic field parameters on interfacial characteristics and mechanical properties of Mg alloy welding joint, Mater. Lett. 306 (2022) 130962–130966.
[237] H. Wu, Y. Chang, Z. Guan, et al., Arc shape and microstructural analysis of TIG welding with an alternating cusp-shaped magnetic field, J. Mater. Process. Technol. 289 (2021) 116912–116921.
[238] B. Fu, J. Shen, U.F.H.R. Suhuddin, et al., Revealing joining mechanism in refill friction stir spot welding of AZ31 magnesium alloy to galvanized DP600 steel, Mater. Des. 209 (2021) 109997–110005.
[239] L.H. Xiong, J.H. Cheng, A.C. Chuang, et al., Synchrotron experiment and simulation studies of magnesium-steel interface manufactured by impact welding, Mater. Sci. Eng. A Struct. Mater. Prop. Microstruct. Process. 813 (2021) 141023–141034.
[240] T. Tao, J. Liu, D. Zhou, et al., Microstructure and mechanical properties of laser welding of AZ31B magnesium alloy and DP590 dual-phase steel with concave groove joint, J. Manuf. Process. 72 (2021) 227–239.
[241] S. Niu, M. Lou, Y. Ma, et al., Resistance rivet welding of magnesium/steel dissimilar materials, Mater. Lett. 282 (2021) 1–4.
[242] J. Zhao, C.S. Wu, H. Su, Ultrasonic effect on thickness variations of intermetallic compound layers in friction stir welding of aluminium/magnesium alloys, J. Manuf. Process. 62 (2021) 388–402.
[243] J.J. Zhao, C.S. Wu, H. Su, Acoustic effect on the tensile properties and metallurgical structures of dissimilar friction stir welding joints of Al/Mg alloys, J. Manuf. Process. 65 (2021) 328–341.
[244] M. Acarer, B. Demir, B. Dikici, et al., Microstructure, mechanical properties, and corrosion resistance of an explosively welded Mg–Al composite, J. Magnes. Alloy (2021) 43–50.
[245] S. Kumar, C.S Wu, Eliminating intermetallic compounds via Ni interlayer during friction stir welding of dissimilar Mg/Al alloys, J. Mater. Res. Technol. JMRT 15 (2021) 4353–4369.
[246] M. Paidar, A. Kazemi, S. Mehrez, et al., Investigation of modified friction stir clinching-brazing process of AA2024 Al/AZ31 Mg: metallurgical and mechanical properties, Arch. Civ. Mech. Eng. 21 (3) (2021) 1–17.
[247] J.L. Zhang, Y. Huang, J. Xiang, et al., Characterization of newly developed friction stir-arc welding method for AM60/AZ31 dissimilar Mg alloy, Mater. Sci. Eng. A Struct. Mater. Prop. Microstruct. Process. 800 (2021) 1–16.
[248] T. Wang, L. Li, M.R. Pallaka, et al., Mechanical and microstructural characterization of AZ31 magnesium - carbon fi ber reinforced polymer joint obtained by friction stir interlocking technique, Mater. Des. 198 (2021) 1–12.
[249] H.Y. Wang, J.Z. Li, L.M Liu, Process optimization and weld forming control based on GA-BP algorithm for riveting-welding hybrid bonding between magnesium and CFRP, J Manuf. Process. 70 (2021) 97–107.
[250] X. Liu, Z. Zhu, J. Xue, Electrochemical and corrosion behaviors of the wrought Mg–Y–Zn based alloys with high Y/Zn mole ratios, J. Magnes. Alloys 9 (4) (2021) 1419–1427.
[251] C. Zhang, L. Wu, Z. Zhao, et al., Effect of the Al–Si eutectic on the microstructure and corrosion behavior of the single-phase Mg alloy Mg–4Li, J. Magnes. Alloys, 9 (4) (2021) 1339–1348.
[252] L. Yang, S. He, C. Yang, et al., Mechanism of Mn on inhibiting Fe–caused magnesium corrosion, J. Magnes. Alloys 9 (2) (2021) 676–685.
[253] E. Merson, V. Poluyanov, P. Myagkikh, et al., Inhibiting stress corrosion cracking by removing corrosion products from the Mg-Zn-Zr alloy pre-exposed to corrosion solutions, Acta Mater. 205 (2021) 116570–116585.
[254] K. Sun, H. Gao, J. Hu, et al., Effect of pH on the corrosion and crack growth behavior of the ZK60 magnesium alloy, Corros. Sci. 179 (2021) 109135–109146.
[255] L. Chen, C. Guo, C. Blawert, et al., Evaluation of the biodegradation product layer on Mg-1Zn alloy during dynamical strain, J. Magnes. Alloys 9 (5) (2021) 1820–1833.
[256] Y. Zhang, Y. Huang, F. Feyerabend, et al., Influence of the amount of intermetallics on the degradation of Mg-Nd alloys under physiological conditions, Acta Biomater. 121 (2021) 695–712.
[257] H. Azzeddine, A. Hanna, A. Dakhouche, et al., Corrosion behaviour and cytocompatibility of selected binary magnesium-rare earth alloys, J. Magnes. Alloys 9 (2) (2021) 581–591.
[258] X. Gao, Q. Huang, D. Ma, et al., Improving environmental adaptability and long-term corrosion resistance of Mg alloys by pyrazole ionic liquids: experimental and theoretical studies, J. Mol. Liq. 333 (2021) 115964–115983.
[259] A. Soltan, M.S. Dargusch, Z. Shi, et al., Effect of corrosion inhibiting compounds on the corrosion behaviour of pure magnesium and the magnesium alloys EV31A, WE43B and ZE41A, J. Magnes. Alloys 9 (2) (2021) 432–455.
[260] L.M. Calado, M.G. Taryba, Y. Morozov, et al., Cerium phosphate-based inhibitor for smart corrosion protection of WE43 magnesium alloy, Electrochim. Acta 365 (2021) 1–13.
[261] D.S. Kharitonov, M. Zimowska, J. Ryl, et al., Aqueous molybdate provides effective corrosion inhibition of WE43 magnesium alloy in sodium chloride solutions, Corros. Sci. 190 (2021) 109664–109678.
[262] Y. Zhang, Y. Wu, N. Li, et al., Synergistic inhibition effect of L-Phenylalanine and zinc salts on chloride-induced corrosion of magnesium alloy: experimental and theoretical investigation, J. Taiwan Inst. Chem. Eng. 121 (2021) 48–60.
[263] Q. Xie, A. Ma, J. Jiang, et al., Tailoring the corrosion behavior and mechanism of AZ31 magnesium alloys by different Ca contents for marine application, Corros. Sci. 192 (2021) 109842–109857.
[264] V.E. Bazhenov, A.V. Li, A.A. Komissarov, et al., Microstructure and mechanical and corrosion properties of hot-extruded Mg–Zn–Ca–(Mn) biodegradable alloys, J. Magnes. Alloys 9 (4) (2021) 1428–1442.
[265] X. Li, S. Liu, Y. Du, Investigation on the corrosion resistance of the Mg-10Al-xMn alloys based on thermodynamic calculations, Corros. Sci. 189 (2021) 109631–109647.
[266] Y. Liu, W.L. Cheng, X.J. Gu, et al., Tailoring the microstructural characteristic and improving the corrosion resistance of extruded dilute Mg–0.5Bi–0.5Sn alloy by microalloying with Mn, J. Magnes. Alloys, 9 (5) (2021) 1656–1668.
[267] S.M. Baek, S.Y. Lee, J.C. Kim, et al., Role of trace additions of Mn and Y in improving the corrosion resistance of Mg–3Al–1Zn alloy, Corros. Sci. 178 (2021) 1–10.
[268] C. Cheng, Q. Le, D. Li, et al., Effect of Y on high-temperature oxidation behavior and products of AZ80 alloy, Mater. Chem. Phys. 269 (2021) 124732–124749.
[269] Y. Cai, H. Yan, M. Zhu, et al., High-temperature oxidation behavior and corrosion behavior of high strength Mg-xGd alloys with high Gd content, Corros. Sci. 193 (2021) 109872–109884.

[270] J. Wu, Y. Yuan, X. Yu, et al., The high-temperature oxidation resistance properties of magnesium alloys alloyed with Gd and Ca, J. Mater. Sci. 56 (14) (2021) 8745–8761.
[271] M.S. Dargusch, Z. Shi, H. Zhu, et al., Microstructure modification and corrosion resistance enhancement of die-cast Mg-Al-*Re* alloy by Sr alloying, J. Magnes. Alloys 9 (3) (2021) 950–963.
[272] Y. Wen, Q. Liu, J. Wang, et al., Improving *in vitro* and *in vivo* corrosion resistance and biocompatibility of Mg-1Zn-1Sn alloys by microalloying with Sr, Bioact. Mater. 6 (12) (2021) 4654–4669.
[273] J. Kwon, S.M. Baek, H. Jung, et al., Role of microalloyed Sm in enhancing the corrosion resistance of hot-rolled Mg–8Sn–1Al–1Zn alloy, Corros. Sci. 185 (2021) 109425–109437.
[274] Y.X. Zhu, G.L. Song, P.P. Wu, et al., A burnished and Al-alloyed magnesium surface with improved mechanical and corrosion properties, Corros. Sci. 184 (2021) 109395–109404.
[275] M. Yin, L. Hou, Z. Wang, et al., Self-generating construction of applicable corrosion-resistant surface structure of magnesium alloy, Corros. Sci. 184 (2021) 109378–109385.
[276] Y. Liu, K. Zhang, J. Zou, et al., Microstructure and property modifications in surface layers of a Mg-4Sm-2Al-0.5Mn alloy induced by pulsed electron beam treatments, J. Magnes. Alloys 9 (1) (2021) 216–224.
[277] T.C. Wu, S.S. Joshi, Y.H. Ho, et al., Microstructure and surface texture driven improvement in *in-vitro* response of laser surface processed AZ31B magnesium alloy, J. Magnes. Alloys 9 (4) (2021) 1406–1418.
[278] D. Wei, J. Wang, Y. Liu, et al., Controllable superhydrophobic surfaces with tunable adhesion on Mg alloys by a simple etching method and its corrosion inhibition performance, Chem. Eng. J. 404 (2021) 126444–126457.
[279] X.J. Cui, C.M. Ning, G.A. Zhang, et al., Properties of polydimethylsiloxane hydrophobic modified duplex microarc oxidation/diamond-like carbon coatings on AZ31B Mg alloy, J. Magnes. Alloys 9 (4) (2021) 1285–1296.
[280] C. Tang, X. Zhao, J. Lei, et al., Brome-like rare-earth film for durable protection of magnesium alloy, J. Taiwan Inst. Chem. Eng. 128 (2021) 409–416.
[281] I. Kozina, H. Krawiec, M. Starowicz, et al., Corrosion resistance of MgZn alloy covered by chitosan-based coatings, Int. J. Mol. Sci. 22 (15) (2021) 8301–8317.
[282] V.S Saji, Electrophoretic (EPD) coatings for magnesium alloys, J. Ind. Eng. Chem. 103 (2021) 358–372.
[283] Y.K. Wei, X.T. Luo, X. Chu, et al., Ni coatings for corrosion protection of Mg alloys prepared by an *in-situ* micro-forging assisted cold spray: effect of powder feedstock characteristics, Corros. Sci. 184 (2021) 109397–109408.
[284] L. Guo, B. Yu, P. Zhou, et al., Fabrication of low-cost Ni-P composite coating on Mg alloys with a significant improvement of corrosion resistance: critical role of mitigating the galvanic contact between the substrate and the coating, Corros. Sci. 183 (2021) 109329–109346.
[285] H. Liu, Z. Tong, Y. Yang, et al., Preparation of phosphate conversion coating on laser surface textured surface to improve corrosion performance of magnesium alloy, J. Alloys Compd. 865 (2021) 158701–158712.
[286] Y. Wu, L. Wu, W. Yao, et al., Improved corrosion resistance of AZ31 Mg alloy coated with MXenes/MgAl-LDHs composite layer modified with yttrium, Electrochim. Acta 374 (2021) 137913–137924.
[287] Y. Wu, L. Wu, M.L. Zheludkevich, et al., MgAl-V2O7 4-LDHs/(PEI/MXene)10 composite film for magnesium alloy corrosion protection, J. Mater. Sci. Technol. 91 (2021) 28–39.
[288] T. Li, S. Wang, H. Liu, et al., Improved corrosion resistance of Mg alloy by a green phosphating: insights into pre-activation, temperature, and growth mechanism, J. Mater. Sci. 56 (1) (2020) 828–843.
[289] A.S. Gnedenkov, S.V. Lamaka, S.L. Sinebryukhov, et al., Control of the Mg alloy biodegradation via PEO and polymer-containing coatings, Corros. Sci. 182 (2021) 109254–109273.
[290] J. Chen, J. Feng, L. Yan, et al., *In situ* growth process of Mg–Fe layered double hydroxide conversion film on MgCa alloy, J. Magnes. Alloys 9 (3) (2021) 1019–1027.
[291] J. Qi, Z. Ye, N. Gong, et al., Formation of a trivalent chromium conversion coating on AZ91D magnesium alloy, Corros. Sci. 186 (2021) 109459–109470.
[292] H. Su, Y. Wu, Y. Zhang, et al., Enhancing the long-term anti-corrosion property of Mg alloy by quaternary phosphonium salt: integrated experimental and theoretical approaches, Corros. Sci. 178 (2021) 1–11.
[293] L. Wu, X. Ding, Z. Zheng, et al., Doublely-doped Mg-Al-Ce-V2O74-LDH composite film on magnesium alloy AZ31 for anticorrosion, J. Mater. Sci. Technol. 64 (2021) 66–72.
[294] J. Zhu, H. Jia, K. Liao, et al., Improvement on corrosion resistance of micro-arc oxidized AZ91D magnesium alloy by a pore-sealing coating, J. Alloys Compd. 889 (2021) 161460–161469.
[295] Y. Song, Y. Tang, L. Fang, et al., Enhancement of corrosion resistance of AZ31 Mg alloys by one-step in situ synthesis of ZnAl-LDH films intercalated with organic anions (ASP, La), J. Magnes. Alloys 9 (2) (2021) 658–667.
[296] J. Chen, L. Wu, X.X. Ding, et al., Effects of deformation processes on morphology, microstructure and corrosion resistance of LDHs films on magnesium alloy AZ31, J. Mater. Sci. Technol. 64 (2021) 10–20.
[297] C. Liu, X. Lu, Y. Li, et al., Influence of post-treatment process on corrosion and wear properties of PEO coatings on AM50 Mg alloy, J. Alloys Compd. 870 (2021) 159462–159471.
[298] N. Attarzadeh, A. Kazemi, M. Molaei, et al., Multipurpose surface modification of PEO coatings using tricalcium phosphate addition to improve the bedding for apatite compounds, J. Alloys Compd. 877 (2021) 160275–160291.
[299] R. Parichehr, C. Dehghanian, A. Nikbakht, Preparation of PEO/silane composite coating on AZ31 magnesium alloy and investigation of its properties, J. Alloys Compd. 876 (2021) 159995–170000.
[300] M. Ostapiuk, M.G. Taryba, L.M. Calado, et al., A study on the galvanic corrosion of a sol-gel coated PEO Mg-CFRP couple, Corros. Sci. 186 (2021) 109470–109479.
[301] J. Chen, L. Wu, X. Ding, et al., Effects of deformation processes on morphology, microstructure and corrosion resistance of LDHs films on magnesium alloy AZ31, J. Mater. Sci. Technol. 64 (2021) 10–20.
[302] Y. Xia, L. Wu, W.H. Yao, et al., *In-situ* layered double hydroxides on Mg−Ca alloy: role of calcium in magnesium alloy, Trans. Nonferr. Met. Soc. Chin. 31 (6) (2021) 1612–1627.
[303] Y. Chen, L. Wu, W. Yao, et al., One-step in situ synthesis of graphene oxide/MgAl-layered double hydroxide coating on a micro-arc oxidation coating for enhanced corrosion protection of magnesium alloys, Surf. Coat. Technol. 413 (2021) 127083–127095.
[304] G. Zhang, E. Jiang, L. Wu, et al., Corrosion protection properties of different inhibitors containing PEO/LDHs composite coating on magnesium alloy AZ31, Sci. Rep. 11 (1) (2021) 2774–2788.
[305] Y. Wu, L. Wu, W. Yao, et al., Improved corrosion resistance of AZ31 Mg alloy coated with MXenes/MgAl-LDHs composite layer modified with yttrium, Electrochim. Acta 374 (2021) 137913–137924.